Regulation of Multidirectional Communication within Tripartite Synapses in the Hippocampus

Pei-Yu Shih

Thesis submitted to University College London for the degree of Doctor of Philosophy
January 2012

Institute of Neurology
University College London

Declaration

I, Pei-Yu Shih, confirm that the work presented in this thesis is my own. Where information has been derived from other sources, I confirm that this has been indicated in the thesis. The simulation results presented in Fig. 18 were developed by Dr. L. Savtchenko in UCL, institute of Neurology. All other experiments were conducted by me.

Abstract

Tripartite synapses, a new concept in synaptic physiology, comprise active bidirectional communications between astrocytes, pre- and postsynaptic neurons. Although the postsynaptic neuron is often referred to as a listener due to lack of neurotransmitter release apparatus, recent studies of retrograde signals hint at its ability to transmit information back to the presynaptic neuron and astrocyte. In this thesis, I aim to provide an entry point for further exploration of this feedback regulation, focusing on the involvement of potassium ions. To this end, I used astrocytic recordings to monitor extracellular potassium changes in hippocampal slices. I found that 62.3 ± 8.0 % of astrocytic K^+ current can be blocked by AP5 (an NMDA receptor antagonist). Puff application of 1 mM NMDA also induced the AP5-sensitive K^+ current. Because astrocytes do not express functional NMDA receptors (Karavanova et al., 2007), this K^+ current should have a neuronal origin. In mice lacking NMDA receptors selectively in CA1 pyramidal neurons, stimulation of Schaffer collaterals led to impaired AP5-sensitive K^+ currents in CA1 astrocytes, pointing to the role of 'postsynaptic' NMDA receptors. Postsynaptic NMDA receptor activation can trigger either Ca^{2+}-sensitive K^+ channels or voltage-gated K^+ channels in these neurons. However, NMDA-puff induced K^+ currents in astrocytes was relatively insesnsitive to removal of extracellular Ca^{2+} or regional voltage change, implying the possibility of direct K^+ efflux through NMDA receptors. Intriguingly, this K^+ released from postsynaptic neurons was localized to active synapses and displayed activity-dependency. Releasing Mg^{2+} blockade of NMDA receptors by either repeated stimuli or pairing of pre- and postsynaptic activation produced supralinear increases in astrocytic K^+ currents. Such a retrograde K^+ signal is coupled to modulation of presynaptic Ca^{2+} signaling and paired-pulse ratio when sufficient fibers were stimulated. Glutamate uncaging results also revealed its potential role in modulating astrocytic glutamate transporters. My results clearly demonstrate a contribution of postsynaptic neurons via K^+ in shaping tripartite synaptic communication.

Contents

Figure and Table List

Publication arising from this thesis

Shih PY, Savtchenko L, Kamasawa N, McHugh TJ, Rusakov DA, Shigemoto R, Semyanov A (2012) Retrograde synaptic signaling through NMDA receptor mediated K^+ efflux (in preparation)

Afzalov R, Pryazhnikov E, Shih PY, Kondratskaya E, Khiroug L, Semyanov A (2012) Low micromolar Ba^{2+} potentiates glutamate transporter current in hippocampal astrocytes. *J. Neurosci.* (submitted)

Tanaka M, Gomi H, Nakai J, Lebedinskiy A, Shih PY, Ando R, Mikoshiba K, Semyanov A, Itohara S (2012) Astrocyte Ca^{2+} signals are required for the functional integrity of tripartite synapse. *Nature Neuroscience* (submitted)

Published abstracts

Shih PY, Savtchenko L, Kamasawa N, McHugh TJ, Rusakov DA, Shigemoto R, Semyanov A. (2011) K^+ efflux through postsynaptic NMDA receptors modulates presynaptic Ca^{2+} transients. *41th Annual Meeting of the society for Neuroscience*, Washington, USA

Shih PY, McHugh T, Semyanov A. (2010) NMDA receptor activation is a major source of potassium elevation during synaptic transmission. *40th Annual Meeting of the Society for Neuroscience*, San Diego, USA

Shih PY, McHugh T, Semyanov A. (2010) Postsynaptic NMDA receptors mediate main potassium efflux during synaptic activity. *29th Naito Conference*, Kanagawa, Japan

Shih PY, McHugh T, Semyanov A. (2010) Activation of postsynaptic NMDA receptors is responsible for the most potassium efflux during synaptic transmission. *7th Forum of European Neuroscience*, Amsterdam, Netherlands

Shih PY, Semyanov A. (2009) NMDA currents on hippocampal astrocytes. *International Congress of Physiological Sciences*, Kyoto, Japan

Acknowledgement

My PhD years and this thesis have had mentorship from numerous outstanding individuals both from within the university and outside of it. It is to these individuals that my heartfelt gratitude and thanks go out to, for without their help, this thesis would not have been possible.

First and foremost, I would like to express my sincere gratitude to my supervisors, Dr. Alexey Semyanov and Prof. Matthew Walker for the continuous support of my Ph.D. study and research, for their motivation, enthusiasm, and immense knowledge. Their guidance helped me in all the time of research. I am also thankful to them for encouraging the use of correct grammar and consistent notation in my writings and for carefully reading and commenting on countless revisions of this manuscript. I am indebted to Dr. Thomas McHugh for kindly providing the NR1 knockout mice. I am also thankful to Prof. Mark Farrant, Prof. Delia Belelli, Prof. Dimitri Kullmann, Prof. Dmitri Rusakov, Dr. Hajime Hirase and Dr. Andre Zeug for their encouragement and practical advice.

All my labmates in Semyanov Unit in RIKEN made it a convivial place to work. In particular, I would like to thank yu-wei for his friendship and help in the past five years. His insightful comments and criticisms at different stages of my research were thought-provoking and they helped me focus my ideas. His patience and support helped my overcome many crisis situations and finish this dissertation. I am grateful to Tanja Brenner and Alistair Jennings for reading and correcting my dissertation. Their practical advices help me enrich my ideas. I am also thankful to the following former or current lab members, for their various forms of support during my graduate study – Sylvain Rama, Sergei Grebenyuk, Inseon Song, Alexander Lebedinskiy, Vetrivel Lakshmanan, Xiaofang Tang, Ivan Pavlov, Christian Henneberger, Leonid Savtchenko, and Pi-shan Change. Many thanks go to Ms Akiko Ashikari for assisting me in complicated paper works, ordering and delivering. I feel she is the most patient and efficient secretary in the world.

Many friends have helped me overcome setbacks and stay focused on my graduate study throughout these years. I greatly value their friendship and warmly appreciate their belief in me. I will always look back with fondness and gratitude for the precious coffee time with Jaeyeon, Mishima-san, Yu-chen and Cynthia. My deepest gratitude goes to my family and Shu-hao for their unflagging love, concern and support throughout my life. This dissertation is dedicated to them.

Chapter 1: Introduction

1. Communication within Tripartite Synapses

Synaptic communication in the central nervous system (CNS) relies mainly on chemical mechanisms. Chemical synaptic transmission can be divided into two steps: a 'transmitting' step, in which the presynaptic cell releases a chemical messenger, and a 'receiving' step, in which the transmitter binds to the receptor molecules in the postsynaptic cell. A neuron usually communicates only with specific cells, the cells with which it forms synapses. The classical view of synaptic communication consists of a presynaptic neuron sending an action potential down its axon to the axon terminal, where the electrical signal triggers the focused release of the chemical transmitter. The transmitter then diffuses across a tiny cleft, binding to receptors on the target postsynaptic neuron, changing local permeability of the cell membrane, shunting ion conductance, and might change membrane potential. In this process, a chemical signal travels only a small distance to its target. Neuronal signaling, therefore, has two special features: it is both fast and precisely directed.

But this two-part picture may not tell the whole story. Central to a new view of the synapse is the concept of "tripartite synapse" (Araque et al., 1999). According to this new concept, reciprocal communications exist between three equally important parts: the presynaptic terminal, the postsynaptic neuronal membrane and a new member, the perisynaptic astrocytes. Astrocytes are a subtype of glial cells in the CNS. They have a close morphological relationship with synapses and they functionally express relevant receptors, enabling them to respond to neurotransmitter released from presynaptic terminals. However, their excitation is not encoded electrophysiologically, as in postsynaptic neurons, but by intracellular Ca^{2+} transients and oscillations (Perea et al., 2009; Wang et al., 2006). Activated astrocytes, in turn, release several

kinds of neuroactive molecules, called "gliotransmitters," such as glutamate, D-serine and adenosine triphosphate (ATP). Gliotransmitters released by astrocytes can evoke slow inward currents (SIC) through activation of *N*-methyl-D-aspartate (NMDA) receptors on the postsynaptic neurons and synchronously excite clusters of pyramidal neurons, operating as a nonsynaptic mechanism for neuronal synchronization (Angulo et al., 2004; Araque et al., 1998b; Fellin et al., 2004; Shigetomi et al., 2008). Gliotransmitters might also feed back onto the presynaptic terminal either to enhance or depress further release of neurotransmitter (Fiacco and McCarthy, 2004; Jourdain et al., 2007; Liu et al., 2004; Perea and Araque, 2007). Therefore, a single gliotransmitter can exert multiple effects depending on the sites of action and the activated receptor subtypes, providing a high degree of complexity to astrocyte-neuron communication.

In most studies of this complex tripartite scheme, the postsynaptic neurons are regarded as a signal receiver, rather than a signal producer, as they lack the necessary apparatus for transmitter release (Alger, 2002). However, postsynaptic neurons can provide retrograde signals another way by the release of diffusible molecules. Diffusible messengers do not require vesicles for storage or release, and indeed can be released from morphologically undifferentiated regions of the postsynaptic neurons. Several molecules have been suggested as candidates for diffusible messengers. The gases, nitric oxide and carbon monoxide, as well as the lipid, arachidonic acid, were the first proposed retrograde signals. Endocannabinoid release from postsynaptic neurons also functions as a rapid, retrograde signal that activates CB_1 cannabinoid receptors and inhibits transmitter release (Kreitzer and Regehr, 2001; Wilson and Nicoll, 2001). Apart from the diffusible messengers, the extracellular ionic environment is another postsynaptic induction signaling pathway. Depletion of extracellular Ca^{2+} during postsynaptic NMDA receptor

activation can be a fast retrograde synaptic signal that reduces the probability of consecutive synaptic release of presynaptic neurons. As postsynaptic neuronal potential changes are inevitably associated with ion influx (Na^+ and Ca^{2+}) and efflux (K^+), it is likely that the fluctuation of other ions in the extracellular space also act as a retrograde signal (Summary in Fig. 1).

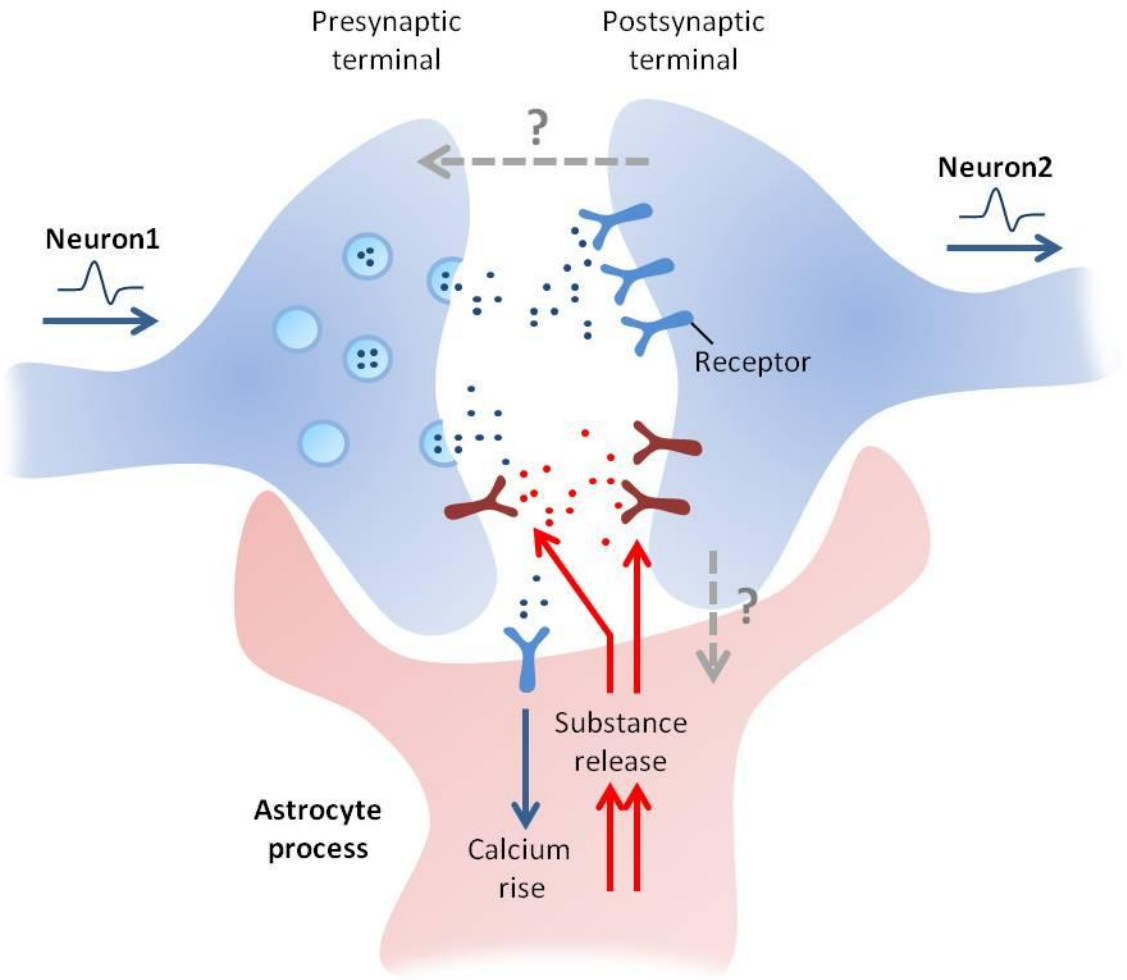

Figure 1. Question marks remain in the communication within the tripartite synapse. When an action potential arrives at the presynaptic axon, it causes the release of neurotransmitter that open ion channels in the postsynaptic neuron. The combined excitatory and inhibitory

postsynaptic potentials of such inputs can initiate a new action potential in the postsynaptic neuron. Astrocytic receptors are thought to be activated in this process as well, leading to a rise in calcium ions in the astrocyte and the release of various active substances, which act in turn on either side of neurons. However, whether the postsynaptic neuron can use extracellular ions as a kind of communicating signal with presynaptic neuron and astrocyte has yet to be determined.

The study of K^+ is of particular interest in this context. Potassium channels are the most abundant and diverse channel family in the brain. The diversity of potassium channels is, in fact, much greater than those of Na^+, Ca^{2+}, or Cl^- channels (Pongs, 2008; Sandhiya and Dkhar, 2009). It is possible that this diversity reflects the need for K^+ signal at various levels of complexity in space and time. Thus, neuronal signals, through voltage, calcium, pH change and neurotransmitter, can activate corresponding types of potassium channels and be translated to distinct patterns of K^+ release into the extracellular space (Kim and Hoffman, 2008). Considering the very narrow interstitial space between adjacent neurons and astrocytes and the low physiological content of extracellular K^+, efflux of small amounts of K^+ into this space can significantly alter extracellular K^+ concentration ($[K^+]_o$) (Nicholson, 1980), and potentially affect subsequent neuronal and astrocytic function.

2. Communication via K^+ in the Tripartite Synapse

If K^+ is an essential signal in the tripartite synapse, what is the usual range of its variation and how does it regulate and fine tune the receiving cells? Many studies have revealed that the interstitial accumulation of K^+ could act as a positive feedback signal and become a factor in the modulation of both normal and pathological brain.

2.1 Range of $[K^+]_o$ Variation in Physiological and Pathological Conditions

Estimates of bulk $[K^+]_o$ variation by potassium microelectrodes have shown that during intense (but still physiological) neuronal activity, the $[K^+]_o$ may almost double, from 2-2.5 mM to 4-4.2 mM (Krnjevic et al., 1982; Somjen, 2002); such an increase can be observed, for example, in the cat spinal cord during rhythmic and repetitive flexion/extension of the knee joint (Heinemann et al., 1990). As a rule, however, during regular physiological activity in the CNS, the $[K^+]_o$ rarely increases by more than 0.2 to 0.4 mM. Nonetheless, locally, in tiny microdomains such as the narrow clefts between neuronal and astroglial membranes in perisynaptic areas, $[K^+]_o$ may transiently attain much higher levels. During seizures, the accumulation of extracellular potassium is further enhanced, but again there seems to be a ceiling level of 12 mM (Heinemann and Lux, 1977; Moody et al., 1974). Only during injury (hypoxia/ischemia, trauma, hypoglycemia) is this ceiling level exceeded and concentrations of up to 25 mM are reached (Hansen, 1985). An extreme case is spreading depression waves which result in transient elevations of the $[K^+]_o$ to 30-80 mM in the intact nervous tissue (Somjen et al., 1992). The narrow range of $[K^+]_o$ variation in physiological condition suggests that K^+ may have a strong influence on receiving cells and needs to be regulated strictly.

2.2 K^+ Effects on Neurons

2.2.1 Modulation of Synaptic Transmission by K^+

Patterns of interstitial accumulation of $[K^+]_o$ can act as a positive feedback signal linked to all aspects of neuronal excitability (Balestrino et al., 1986; Chamberlin et al., 1990; Korn et al., 1987; Meeks and Mennerick, 2004). Superfusion of solutions containing elevated $[K^+]_o$ causes

neuronal depolarization that can lead to enhanced glutamate release from presynaptic cells and enhances NMDA receptor activation in the postsynaptic cell (Chamberlin et al., 1990; Poolos and Kocsis, 1990). The afferent volley amplitudes can also be biphasically modulated by $[K^+]_o$. Elevated $[K^+]_o$ up to 6 mM increased the peak amplitude, whereas $[K^+]_o$ above 6 mM decreased it (Poolos et al., 1987).

2.2.2 Modulation of Long-Term Plasticity by K^+

As well as the transient effects above, $[K^+]_o$ variation is also involved in long-term modulation of neuronal commmunication. Activity-dependent modulation of potassium channel properties or distribution generates plasticity of intrinsic excitability, perhaps contributing to some forms of memory storage (Zhang and Linden, 2003). Increasing the K^+ content in the extracellular perfusing medium resulted in facilitation of long-term potentiation (LTP) induction in weak excitatory postsynaptic potentials (EPSPs) in the hippocampal slice. Even locally increasing $[K^+]_o$ by ionophoresis was sufficient to facilitate LTP of weak EPSPs, suggesting that synaptic K^+ levels can influence cooperativity necessary for LTP induction (Ballyk and Goh, 1992). Janigro et al (1997) directly linked $[K^+]_o$ to modulation of synaptic strength by demonstrating that impairment of K^+ uptake prevents long-term depression (LTD) maintenance in hippocampus. They attributed this observation to the K^+-mediated depolarization of neighboring neurons, which results in potentiation of synaptic activity (Janigro et al., 1997).

2.2.3 Neuronal Oscillation & Seizure

Rhythmic oscillations, including those at gamma (30-80 Hz), beta (15-30 Hz) and ultrafast (>.80

Hz) frequencies, are thought to be important in a variety of cognitive processes. One mechanism that could contribute to network oscillations is a change in $[K^+]_o$ (Kaila et al., 1997). Kaila and colleagues started to link the activity-induced $[K^+]_o$ change under high frequency stimulation with the generation of gamma frequency activity (Kaila et al., 1997; Smirnov et al., 1999). This activity, studied in detail using brief and focal application of K^+ into *stratum radiatum* of either the CA1 or the CA3 regions *in vitro,* demonstrated the role of $[K^+]_o$ in inducing transient episodes of oscillatory network activity, mainly in the gamma range (LeBeau et al., 2002). In addition, Herreras et al., (1994) found that focal injection of K^+ into the CA1 region *in vivo* elicited what they termed 'sawtooth wavelets', a gamma frequency network oscillation, prior to the onset of spreading depression. This result suggested that changes in $[K^+]_o$ could be sufficient to propagate neuronal activity and synchronize epileptic neuronal populations (Lian et al., 2001). Actually, it is well documented that localized ventricular perfusion with high- K^+ saline induces recurring hippocampal seizures (Zuckermann and Glaser, 1968). Even *in vitro*, in rat hippocampal slices, raising the concentration of K^+ in the perfusate by a few millimolars can induce various types of epileptiform activity (Jensen and Yaari, 1988; Korn et al., 1987; Rutecki et al., 1985). Focal application of potassium is a protocol commonly used to evoke spreading depression (Herreras et al., 1994). These studies provide evidence for the role of $[K^+]_o$ in the initiation and spread of epileptiform events (Fertziger and Ranck, 1970; Konnerth et al., 1984; Yaari et al., 1986).

2.3 K^+ Effect on Astrocytes

2.3.1 Modulation of Glutamate Transporter by K^+

Changes in K^+ gradients and the associated membrane depolarization may affect the activity of ion gradient-dependent transporters. Indeed, cell depolarization and disturbance of ion gradients have been shown to inhibit glutamate transporter function and at times cause transporter reversal and glutamate release (Bordey and Sontheimer, 2003; D'Ambrosio, 2004; Mennerick et al., 1999; Otis and Kavanaugh, 2000). In mice lacking K^+ uptake, glutamate transporter currents were impaired, further supporting this concept (Djukic et al., 2007). Pathological rises in $[K^+]_o$ inhibit glutamate uptake by depolarizing glial cells and by weakening the electrochemical transmembrane gradients of K^+. This action facilitates the accumulation of extracellular glutamate to neurotoxic levels, which induces neuronal death observed in both brain anoxia and ischaemia (Barbour et al., 1988).

2.3.2 Modulation of Gap Junction Coupling by K^+

Interestingly, the gap junction coupling between astrocytes can also be enhanced by high levels of $[K^+]_o$ (Enkvist and McCarthy, 1994; Giaume and McCarthy, 1996). Although very little is known about the mechanisms by which high levels of K^+ induces the increase in astrocytic coupling, it has been proposed that it may be either related to a direct effect of membrane potential on gap junction conductance (Enkvist and McCarthy, 1994) or to the effect of intracellular pH shifts on junctional conductance resulting from depolarization-induced cytoplasmic alkalinization (Pappas and Ransom, 1994). Furthermore, alterations in junctional coupling attributable to Cx43 phosphorylation have been associated with activation of several

distinct protein kinases (Godwin et al., 1993; Moreno et al., 1994; Saez et al., 1997; Warn-Cramer et al., 1996); in this regard, it has been shown that Cx43 phosphorylation states could be altered in rat brain slices after exposure to high K^+ solution (Nagy and Li, 2000) and in spinal cord after sciatic nerve stimulation (Li and Nagy, 2000).

2.3.3 Modulation of Glycolysis by K^+

An acute fall in glucose concentration and a concurrent increase in lactate concentration can be observed with neural activation in brain tissue (Caesar et al., 2008; Hu and Wilson, 1997; Mangia et al., 2003; McNay et al., 2000; Silver and Erecinska, 1994). The lactate surge is thought to play roles in neurometabolic (Pellerin and Magistretti, 1994) and neurovascular coupling (Gordon et al., 2008). It has been proposed that $[K^+]_o$ stimulates astrocytic glycolysis (Brookes and Yarowsky, 1985). A recent study underscored that K^+ can stimulate astrocytic glycolysis in seconds, much faster than the glutamate-induced effect. This K^+-stimulated glycolysis can be detected even at low millimolar concentrations and was also present in organotypic hippocampal slices (Bittner et al., 2011).

2.4 High Contribution of Postsynaptic Neuron to $[K^+]_o$

2.4.1 Axonal and Dendritic Potassium Channels

Activity-evoked K^+ efflux might come from either afferent axons or pyramidal cell dendrites, via action potentials or synaptic potentials, respectively. Do both axon and dendrite express abundant potassium channels? In fact, it has been shown that the passage of a single action potential can increase local $[K^+]_o$ by 1 mM above the resting level of 3 mM (Adelman and Fitzhugh, 1975).

Several subtypes of voltage-gated potassium channels (K_V) can contribute to this depending on the activity state and brain regions. $K_v1.1$, $K_v1.2$, $K_v1.4$, $K_v3.1$ and $K_v3.4$ have been identified in mammalian axons (Cooper et al., 1998; Devaux et al., 2003; Dodson et al., 2003; Ishikawa et al., 2003; Sheng et al., 1993; Sheng et al., 1992; Veh et al., 1995; Wang et al., 1993; Wang et al., 1994). Amongst these K_V channels, high threshold types (such as K_v3) shape the action potential waveform and facilitate rapid repolarization (Rudy and McBain, 2001). Low threshold types which activate close to resting potentials (such as K_v1) regulate firing threshold and excitability (Brew and Forsythe, 1995). In addition, large-conductance calcium-dependent potassium channels (BK channels) are present in axons and presynaptic terminals (Bielefeldt and Jackson, 1993; Hu et al., 2001; Jonas et al., 1991; Krause et al., 1996). Certain conditions, by causing depolarization (Hansen et al., 1982; Rosen and Morris, 1991), may cause inactivation of voltage-gated potassium channels. The resulting depolarization-induced spike broadening (Cowan and Martin, 1992) results in BK channel activation which then repolarizes the membrane (Hu et al., 2001).

On the other hand, direct patch-clamp recordings from pyramidal neuron dendrites has also revealed the existence of a variety of potassium channels (Yuan and Chen, 2006). Most remarkably, non-uniform gradients in the distribution of dendritic K_v strongly correlates with the progressive decline of spike amplitude as action potentials generated in the soma/axon region back-propagate along the dendrites (Hoffman et al., 1997). Interestingly, a train of synaptic inputs can lead to a progressive inactivation of dendritic K_v such that temporal summation of subsequent inputs is facilitated and somatically initiated action potentials can propagate into more distal dendritic domains (Johnston et al., 2000; Magee and Johnston, 1997). Ca^{2+}-activated

potassium channels (K_{Ca}) participate in spike repolarization (Cai et al., 2004) and elicit a brief afterhyperpolarization following single action potentials. Reduction of K_{Ca} along the dendrites is at least one factor responsible for significantly broader dendritic action potentials (Johnston et al., 2000). The varied pattern of K^+ channels along the dendritic tree subserves the processing of signals in individual dendritic compartments.

2.4.2 Relative Contribution of Pre- and Postsynaptic Neurons to $[K^+]_o$

As both pre- and postsynaptic neurons contain abundant potassium channels, their relative contribution to $[K^+]_o$ has been the subject of intense interest. The increase in $[K^+]_o$ induced by repetitive stimulation was reduced to < 25% by blocking postsynaptic receptors (Poolos et al., 1987). Similar results have been demonstrated in several studies with different methods to inhibit postsynaptic activity (Bergles and Jahr, 1997; De Saint Jan and Westbrook, 2005), leading to the proposal that the postsynaptic neuron is the predominant contributor to activity-evoked $[K^+]_o$.

3. K^+ Signals Triggered by Glutamate Receptors on Postsynaptic Neurons

Because changes in $[K^+]_o$ can modify surrounding cellular activity, and since much of the K^+ release is derived from postsynaptic elements, it has been suggested that the increase in $[K^+]_o$ acts as a feedback signal. Indeed, the above observations lend support to the notion that the extracellar K^+ environment can mediate changes in both neuronal excitability and astrocytic function, and thus should be considered as a distinct mechanism for cellular communication in the nervous system. The next question is which receptors could trigger the release of K^+ from postsynaptic neurons?

Neurotransmitter receptors can broadly be classified into two categories: G-protein-coupled (metabotropic) receptors and ionotropic receptors. The binding of synaptic transmitters to G-protein-coupled receptors triggers a series of signal transduction cascades at postsynaptic neurons. Ionotropic receptors are specialized ion channels, which are gated by the binding of specific synaptic transmitters, and the flux of ions that occurs on activation of ionotropic receptors alters the polarization state of the postsynaptic neuron.

L-glutamate is the main excitatory neurotransmitter in the mammalian nervous system. Most fast glutamate signals are conveyed through ionotropic receptors, and the two main types on the postsynaptic side are α-amino-3-hydroxy-5-methyl-4-isoxazolepropionic acid (AMPA) and *N*-methyl-D-aspartic acid (NMDA) receptors (Ozawa et al., 1998). In most cases, AMPA and NMDA receptors often co-localize at synapses (He et al., 1998), and presumably experience the same pulse of glutamate release from the presynaptic terminal. However, their time course of activation is very different. AMPA receptors activate and deactivate within a few milliseconds of presynaptic glutamate release, whereas the open probability of NMDA receptors typically reaches a peak after 20-30 ms, and decays over hundreds of milliseconds (Stern et al., 1992), the difference resulting from the lower affinity of AMPA receptors for glutamate. Therefore, voltage-clamped glutamate excitatory postsynaptic currents appear biphasic, with a very fast AMPA transient, and a much slower NMDA tail. Based on their differing time scales, these two groups of glutamate receptors would be expected to trigger distinct potassium channels and produce patterns of K^+ release into the extracellular space in conjunction.

3.1 K^+ Signals Induced by AMPA Receptors

The transient depolarization mediated by AMPA receptor activation is sufficient to activate the

dendritic K_v, which acts transiently to counter dendritic depolarization. This dampening effect reduces the ability of dendrites to initiate action potentials, decreases the amplitude of back-propagating action potentials (bAPs), and reduces the magnitude of excitatory postsynaptic potentials (EPSPs). In addition, the AMPA receptor itself can conduct both Na^+ and K^+, serving as another way to change $[K^+]$ in the extracellular space.

3.2 K^+ Signals Induced by NMDA Receptors

NMDA receptors can be distinguished from other ionotropic glutamate receptors by their slower kinetics and high permeability to Ca^{2+}. NMDA receptors are 5-10 times more permeable to Ca^{2+} than to Na^+ and K^+ (Ascher and Nowak, 1988; Burnashev et al., 1995; Mayer and Westbrook, 1987). These properties may enable NMDA receptors to activate separate groups of potassium channels from those activated by AMPA receptors. NMDA application, under voltage-clamp conditions, results in a very slow outward current following the inward current in pyramidal neurons of several brain regions (Mistry and Hablitz, 1990; Yu et al., 1999; Zorumski et al., 1989). This outward current was abolished by potassium channel blockers, in agreement with the activation of K^+ currents (Shah and Haylett, 2002). Consistent with this finding, there is accumulating evidence that dendritic excitability can be regulated by NMDA receptor dependent potassium channels, including small-conductance of K_{Ca} (SK) channels and several kinds of K_v channels (A-type and M-type potassium channel) (Barish et al., 1996; Kim and Hoffman, 2008; Ngo-Anh et al., 2005; Shah and Haylett, 2002).

3.2.1 K_{Ca} Activated by NMDA Receptors

K_{Ca} channels can be simply divided into two types: large-conductance K_{Ca} (BK channel) and small-conductance K_{Ca} (SK channel). While BK channels are mostly expressed at presynaptic terminals, SK channels are located mainly on the postsynaptic side (Voglis and Tavernarakis, 2006).

The SK channel is the only class of K_{Ca} that is not voltage-gated but purely Ca^{2+}-activated (Kohler et al., 1996; Schumacher et al., 2001; Xia et al., 1998). Its Ca^{2+} gating is achieved by constitutive heteromeric assembly of the pore-forming channel subunits with calmodulin (CaM), which serves as the high-affinity Ca^{2+} sensor for the channel (Xia et al., 1998). Recent studies have revealed the intimate relation between SK channels and NMDA receptors (Faber et al., 2005; Ngo-Anh et al., 2005). Firstly, SK channels are colocalized with NMDA receptors in dendritic spine heads (Lin et al., 2008). In addition, activation of NMDA receptors leads to a compartmentalized rise in spine [Ca^{2+}] (Sabatini et al., 2002) that was shown to activate apamin-sensitive SK channels (Ngo-Anh et al., 2005). This activity repolarizes the spine membrane, and, in turn, increases NMDA receptor magnesium block, which limits further Ca^{2+} influx. Thus, SK channels functionally integrate with NMDA receptors to form a Ca^{2+}-mediated negative feedback loop in dendritic spines (Ngo-Anh et al., 2005). One consequence of blocking this negative feedback is the facilitation of long-term potentiation (LTP) at the Schaffer-collateral synapses, whereas SK overexpression diminishes LTP and impairs learning behaviors such as spatial learning and fear conditioning (Blank et al., 2003; Hammond et al., 2006; Stackman et al., 2002; Tzounopoulos and Stackman, 2003).

3.2.2 K_v Activated by NMDA Receptors

Activation of NMDA receptors results in membrane depolarization as well as Ca^{2+} influx. At least four types of K_v channels have been identified on dendrites, A-, D-, M-type, and delayed-rectifier potassium channels (Chen and Johnston, 2004). Within these types, the M-type potassium channels (K_v7/M) is a true non-inactivating current and can be activated only during prolonged membrane depolarization (Chen and Johnston, 2004). For other K_v channels, activation of either NMDA or AMPA receptors can induce enough depolarization to activate them. However, only the NMDA receptors, which deactivate with a much slower time course, can provide long enough depolarization to activate K_v7/M channels (Qiu et al., 2007). These features enable K_v7/M channels to exert a significant, often dominant influence on neuronal subthreshold excitability and to regulate spike generation. In the hippocampus, perisomatic K_v7/M channels are known to control the excitability of pyramidal neurons (Golomb et al., 2006; Gu et al., 2005; Yue and Yaari, 2006). Using dynamic clamp, it was shown that K_v7/M channels act to modulate gamma oscillations by regulating the phase coupling of action potential firing in pyramidal neurons (Leao et al., 2009). Blocking them promotes burst firing and even epileptiform seizures (Qiu et al., 2007; Vervaeke et al., 2006).

Besides K_v7/M channels, NMDARs are also involved in regulating a subtype of A-type potassium channel, $K_v4.2$. Hoffman and colleagues in 1997 suggested that A-type potassium channels might shape synaptic input (Hoffman et al., 1997). More recently, electron microscopy and enhanced green fluorescence protein (EGFP)- tagged $K_v4.2$ fluorescence showed the greater density of $K_v4.2$ in spines compared to dendritic shafts, suggesting its spine enrichment (Kim et al., 2007; Kim et al., 2005). This expression of $K_v4.2$ on spines is dynamic, displaying

redistribution and internalization depending on neuronal activity. Interestingly, NMDA receptor activation seems to be essential for this activity dependent $K_v4.2$ regulation (Kim et al., 2007).

4. Properties of NMDA Receptors

An overwhelming number of studies implicate all types of ionotropic receptors in learning and memory (Voglis and Tavernarakis, 2006). AMPA and NMDA receptors synergize at postsynaptic terminals to facilitate various forms of synaptic plasticity. An important feature of the NMDA receptor, which is particularly relevant to synaptic plasticity, is its high permeability to Ca^{2+}; in turn, Ca^{2+}, which is a central messenger molecule, orchestrates a battery of signaling pathways and responses that collectively elicit synaptic modification. However, K^+ flow following NMDA receptor activation might also be involved in the regulation of synaptic plasticity. Progress in the understanding of NMDA receptor properties provides a possible scheme of the $[K^+]_o$ pattern it can produce.

4.1 Subunit Composition of NMDA Receptors

The most structurally complex glutamatergic receptor is the NMDA receptor. It is an ion channel made up of different and variably assembled protein isoforms. Currently, three known families of NMDA receptor subunits have been identified – namely GluN1, a group of GluN2 subunits (GluN2A, -2B, -2C, -2D), and a pair of GluN3 subunits (GluN3A and GluN3B) (Cull-Candy and Leszkiewicz, 2004; Mori and Mishina, 1995; Nakanishi and Masu, 1994). Most native NMDA receptors appear to function as heterotetrameric assemblies composed of two glycine-binding GluN1 and two glutamate-binding GluN2 subunits. The GluN1 subunit is the only subunit that is

indispensable for the formation of a functional NMDA receptor; its elimination would abolish all functional NMDARs in a cell (Cull-Candy et al., 2001). The GluN2 subunits (GluN2A-GluN2D) are expressed in a cell-type specific manner, critically determining the biophysical and pharmacological properties of NMDA receptors (Cull-Candy and Leszkiewicz, 2004; Dingledine et al., 1999; Sheng and Kim, 2002). Although GluN3 is not essential for most native NMDA receptors, they can influence the surface expression and Ca^{2+} permeability of GluN1/GluN2 receptors (Perez-Otano et al., 2001). GluN1/GluN3 assemblies show impermeability to Ca^{2+} and resistance to Mg^{2+} block (Chatterton et al., 2002), and GluN3 acts as a regulatory subunit in some regions during early development (Ciabarra et al., 1995; Nishi et al., 2001).

4.2 Location: Synaptic & Extrasynaptic

Most NMDA receptors are found on the postsynaptic membrane at excitatory synapses. Through their carboxy-terminal tail they anchor to a multiprotein scaffold that forms a structure known as the 'postsynaptic density' (PSD) (Kornau et al., 1995; Sheng, 2001). The density of NMDA receptors in dendritic spines, within the PSD, is much higher than that in the dendritic shaft and somatic membrane. Although the proportion of synaptically located NMDARs increases with development, a small population of NMDA receptors remains extrasynaptic in adulthood (Cottrell et al., 2000; Petralia et al., 2010; Tovar and Westbrook, 1999). Around one-quarter of extrasynaptic NMDA receptors in adult hippocampal slices are classified as being perisynaptic (that is, within 100 nm of the PSD), the rest being localized on dendritic shafts and non-perisynaptic parts of the spine. The activation of perisynaptic NMDA receptors depends on the location and activity of neuronal and glial transporters and requires the access of glutamate diffusing from synaptic release sites, for example, during trains of stimulation (Huang and

Bergles, 2004; Kullmann and Asztely, 1998; Lozovaya et al., 2004). The subcellular localization of NMDA receptors, and hence Ca^{2+} influx into the cell at synaptic and extrasynaptic sites, is known to activate region-specific signal transduction mechanisms (Kohr, 2006), which can thus have distinct downstream signaling and physiological function (Ivanov et al., 2006; Vanhoutte and Bading, 2003).

4.3 Activation of NMDA Receptors by Removing Mg^{2+}

When NMDARs are activated, there is an influx of Na^{+} and Ca^{2+} ions and an efflux of K^{+} ions. The binding of Mg^{2+} ions to sites within the channel prevents the ion flow. Activation of the channel can occur only if there is simultaneous glutamate and glycine binding. Glycine is an 'obligate co-agonist' for glutamate, i.e. glutamate cannot act on the NMDA receptor in the absence of glycine (Johnson and Ascher, 1987; Matsui et al., 1995; Schell et al., 1997). The simultaneous binding of the two transmitters and partial depolarization permits Mg^{2+} displacement and channel opening. Thus, NMDARs are subject to voltage-dependent block by Mg^{2+}. This can be seen in the current-voltage (I-V) relationship presented in Fig. 2. I-V curves plotted from currents recorded in the presence of Mg^{2+} have a characteristic negative slope conductance for voltages more negative than -40 mV (Ascher and Nowak, 1988; Mayer and Westbrook, 1987; Nowak et al., 1984). Simply removing the physiological Mg^{2+} ion from the bathing solution potentiates NMDA currents and almost eliminates its voltage dependence. The voltage dependence of NMDA receptors has the effect of enhancing the depolarisation initiated by non-NMDA receptor channels. Ion flow through NMDA receptors can subsequently act as a second messenger and initiate a wide range of cellular responses that underlie a number of complex neurophysiological phenomena.

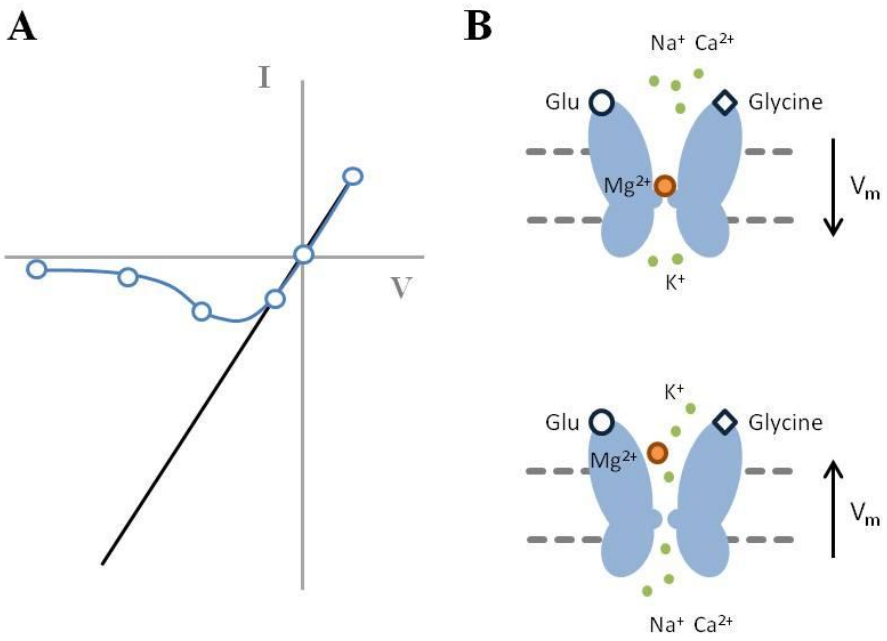

Figure 2. Mg^{2+} block of NMDA receptors. (A) Distinct I-V curve of AMPA (black line) and NMDA (blue line) currents in Mg^{2+} containing solution. (B) Schematic of the mechanism of the Mg^{2+} block. At resting potential, the pore of the NMDA receptor channel is blocked by Mg^{2+}. Upon depolarization, the Mg^{2+} is removed from the pore, and the channel can pass current.

The property of voltage-dependent block by Mg^{2+} enables NMDARs to serve as coincidence detectors. When glutamate is released at a synapse on a cell at their resting membrane potential, the NMDA receptors remain blocked by Mg^{2+}. But if the cell is already depolarized, NMDA receptor channels will open for tens of milliseconds and pass a stream of Ca^{2+} into the postsynaptic neuron. Thus they detect the coincidence of postsynaptic depolarization and glutamate released at the synapse. Entry of Ca^{2+} into the postsynapse via NMDAR permits coupling of electrical synaptic activity to biochemical signaling via activation of Ca^{2+}-dependent enzymes and downstream signaling pathways. This sequence of events is required for the

induction of LTP in the CA1 region of the hippocampus, a synaptic potentiation that can be induced with a few seconds of stimulation and that can last for days (Bliss and Lomo, 1973; Malenka and Nicoll, 1999).

4.4 Activation of NMDA Receptors by EPSP-bAP Pairing

The characteristics of the induction of long-term plasticity (LTP or LTD) resemble a model for memory storage previously suggested by Donald Hebb. This model was based on the idea that neurons that are active at the same time strengthen their synaptic connections (‘fire together wire together’) (Hebb, 1949). In recent years, a variation of this form of synaptic plasticity has been described that involves pairings of a few pre- and postsynaptic action potentials, in which the sign and magnitude of the change in synaptic strength are determined by the relative timing of spikes in the connected neurons (Fig. 3). This form of synaptic plasticity has been named spike-timing-dependent plasticity (STDP) (Abbott and Nelson, 2000; Bi and Poo, 1998). Typically, synapses that have transmitted an excitatory postsynaptic potential (EPSP) just before the generation of a postsynaptic action potential will be potentiated (positive timing), whereas EPSPs arriving after action potential generation undergo synaptic depression (negative timing). Given that most synaptic inputs are made onto dendrites, signaling to the synapse that the neuron has generated an output is thought to be mediated by backpropagating action potentials (bAPs) (Magee and Johnston, 1997). Action potentials once generated in the axon (Palmer and Stuart, 2006; Stuart et al., 1997), not only propagate along the axon towards presynaptic terminals, but are also capable of propagating backwards into the dendritic tree in many neurons (Stuart et al., 1997). There, they provide the necessary depolarization to relieve the Mg^{2+} block of the NMDA receptors (Kampa et al., 2004; Vargas-Caballero and Robinson, 2003), which is essential for

STDP induction (Bi and Poo, 1998; Debanne et al., 1998). The timing of backpropagating action potentials relative to glutamate binding to NMDA receptors determines the amount of NMDA receptor activation (Kampa et al., 2004; Kampa et al., 2006) and hence Ca^{2+} influx (Koester and Sakmann, 1998; Nevian and Sakmann, 2004, 2006). Different levels of postsynaptic Ca^{2+} are thought to activate different signaling cascades, thereby controlling the sign and magnitude of the induced synaptic change (Dan and Poo, 2004).

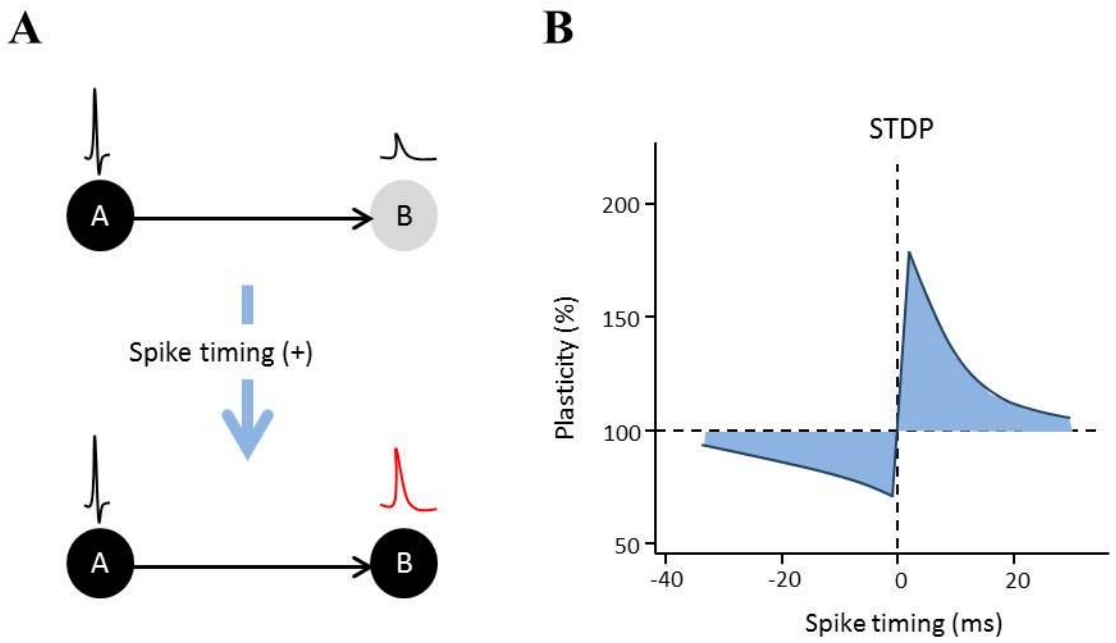

Figure 3. Classical view of STDP. (A) Schematic representation of Hebb's postulate (1949). (B) Classical STDP timing curve providing experimental support for Hebb's postulate by defining the time window in which correlated firing leads to LTP; whereas negative timings (uncorrelated events) cause depression.

Although K^+ represents another potential signaling mechanisms contingent on NMDA receptor activation, functional coupling of NMDA receptors and related K^+ channels to synaptic transmission has yet to be firmly established. To address this question, I studied the relationship between NMDA receptors and extracellular potassium signals in hippocampus slices with a sensitive and independent K^+ sensor: the astrocyte recordings.

5. Astrocytes as Potassium Detectors

Technological advances over the past decades have given us many novel techniques to study astrocytes. From the Golgi staining to immunostaining for GFAP, dye-filling techniques (e.g. sharp electrode, patch-clamp recordings, and now single cell electroporation), and transgenic approaches to visualize fluorescent astrocytes, our understanding of astrocyte characteristics has dramatically evolved over the past decades.

5.1 Astrocyte Identification

Astrocytes occupy 20-30 % of the cell population in rodent cerebral cortex (Nedergaard et al., 2003). Astrocytes have traditionally been described as forming a relatively homogeneous population characterized by a highly negative resting membrane potential, low input resistance and extensive intercellular coupling via gap junctions (Casullo and Krnjevic, 1987; Picker et al., 1981). In the last decade, the heterogeneity of the astrocyte population has become a matter of controversy (Matyash and Kettenmann, 2010; Walz, 2000). Whole cell recordings demonstrated the heterogeneity of membrane current patterns that were attributed to astrocytes. The two most common subtypes were termed “passive” and “complex” astrocytes.

5.1.1 Passive Astrocytes

Astrocytes can be distinguished by their morphology, cellular marker expression, and the corresponding patterns of membrane currents. Passive astrocytes have highly complex morphology, revealing the organization of the major processes and the distinctive spongiform ramifications. Wherever large branches extend outward from the soma, spongiform material consisting of very dense ramifications of fine processes was observed to extend ~2-10 μm out of these branches. These dainty branches either contact with blood vessels, forming so called 'perivascular' endfeet, or form multiple contacts with surrounding neurons (D'Ambrosio et al., 1998; Wang and Bordey, 2008). Another particular property of passive astrocytes is their high expression of glial fibrillary acidic protein (GFAP, the major component of glial fibrils) as well as glutamate transporters (Matthias et al., 2003; Steinhauser et al., 1992; Zhou et al., 2006). Whole-cell patch-clamp recordings also indicated several electrophysiological properties of these cells that contrast with those of neurons: linear current-voltage curve, more negative resting membrane potentials, lower input resistance, and larger membrane conductance. These electrophysiological properties can largely be attributed to the abundant expression of background potassium channels and inward rectifier potassium channels. Although passive astrocytes also express other types of potassium channels (transient potassium channels and delayed rectifier potassium channels), the ratio is relatively low after their maturation (Matthias et al., 2003).

5.1.2 Complex Astrocytes

On the basis of the presence of voltage-gated channels, the other population of astrocytes was named complex cells. They are considered to be a mixed population of both immature astrocytes

and a subpopulation that is immunoreactive for the chondroitin sulfate proteoglycan NG2 (Bergles et al., 2000). Complex astrocytes are S100β immunopositive with weak expression levels of GFAP (Matthias et al., 2003; Matyash and Kettenmann, 2010). Morphologically, the complex astrocyte has a relatively small cell body and numerous thin, filamentous processes that originate directly from the soma; these processes are punctuated with wider segments (varicosities) and are never seen in proximity of blood vessels, nor are there regions of contact with capillary endothelial cells. Fast application of glutamate to these cells evoked AMPA receptor-mediated currents, but not glutamate transporter currents (Zhang and Barres, 2010). The whole-cell current pattern of these cells was dominated by outward K^+ currents, whereas background or inward rectifier potassium channels were much less pronounced (Jabs et al., 2005; Matthias et al., 2003; Wallraff et al., 2004; Zhou et al., 2006).

5.1.3 Developmental Change of the Ratio Between Passive and Complex Astroctyes

The relative amounts of these two types of astrocytes vary depending on the age of the animal. Analysis based on glial electrophysiological phenotypes revealed the outline of this developmental variation (Zhou et al., 2006). Complex astrocytes are evident in newborn mice but their number decrease dramatically during the course of development. By contrast, passive astrocytes originate postnatally and in the adult brain. Starting from the fourth postnatal week, passive astrocytes become the dominant glial phenotype comprising 92% of total cells in the hippocampal area. The glial diversity therefore occurs predominantly in the developing brain, and the ratio of glial phenotypes becomes stabilized after the third postnatal week, suggesting that the maturation of the hippocampus starts from the fourth postnatal week (Kafitz et al., 2008; Zhou et al., 2006).

5.1.4 Identification of Passive Astrocyte by SR101

The analysis of astrocytes in the intact tissue with electrophysiological and high-resolution imaging techniques, however, was always hampered by the problem of reliable identification of this cell type. The identification of astrocytes based solely on morphological criteria, such as somatic size and cellular architecture, may lead to the mistaken inclusion of small-sized neurons (Kimelberg, 2004). Immunohistochemical identification of markers such as GFAP or the Ca^{2+}-binding protein S100B can only be performed after the experiment, are time-consuming and often do not allow certain identification of the cells analyzed in physiological experiments. To overcome this problem, transgenic mice, in which enhanced green fluorescent protein is expressed under the human GFAP promoter have been bred (Hirrlinger et al., 2006; Nolte et al., 2001). However, because astrocytes show very diverse levels of GFAP-expression (Kimelberg, 2004), this approach enables the identification of only a subset of astrocytes. Sulforhodamine 101 (SR101), as an amphoteric rhodamine, is a water-soluble red fluorescent dye that has been used extensively for investigating neuronal morphology (Ehinger et al., 1994; Kjaerulff et al., 1994; Miller et al., 2001), preparing fluorescent liposomes (Barish et al., 1996; Skopinskaia et al., 2000; VanderMeulen et al., 1992), monitoring exocytosis and endocytosis (Kjaerulff et al., 1994; McLaren et al., 1993; Wang and Goren, 1987), and quenching the fluorescence background of FM 1–43 in slice experiments (Pyle et al., 1999; Winterer et al., 2006). Recently, SR101 has been reported as a specific marker of astroglia *in vivo* (Nimmerjahn et al., 2004; Winship et al., 2007) and in slices (Kafitz et al., 2008). Characterizing the electrophysiological properties of SR101-positive and SR101-negative cells with glial morphology demonstrated that SR101 selectively labels the population of passive astrocytes (Kafitz et al., 2008). The mechanism of SR101 uptake by astrocytes is not clear. Based on the efficacy and rapid time course of SR101 loading into

neocortical astrocytes, a specific transporter system may act as the uptake mechanism (Ehinger et al., 1994). Owing to its reliability and uncomplicated handling, this SR101 staining method is now widely used in studies of passive astrocytes (Kafitz et al., 2008; Nimmerjahn et al., 2004; Zhou et al., 2006).

5.2 Astrocyte Response to Neuron

Because astrocytes lack axons and the ability to generate action potentials, they were traditionally thought to be mere "brain glue" that support neuronal activity. However, astrocytes have several critical functions including promoting neuronal maturation, synapse formation, neuronal survival during development, regulating angiogenesis, and maintaining a viable microenvironment for neurons. In particular, they are now regarded as important direct communication partners of neurons (Araque et al., 1998a; Bezzi et al., 1998; Grosche et al., 1999; Haydon, 2001; Kang et al., 1998).

5.2.1 Astrocytes are Intimately Associated with Synapses

In the grey matter, astrocytes are closely associated with neuronal compartments and specifically with synaptic regions, so that in many cases astroglial membranes completely or partially enwrap presynaptic terminals as well as postsynaptic spines. In the hippocampus, for example, around 60% of synapses are contacted by astrocytic processes at the synaptic cleft. These astrocyte-synapse contacts show peculiar specificity: while astroglial processes enwrap the vast majority of large perforated synapses (which are probably the most functionally active), only about half of small (known as macular) synapses have glial membranes coverage (Ventura and Harris, 1999).

In the cerebellum, glial-synaptic relations are even more intimate, as nearly all of the synapses formed by parallel fibres on the dendrites of Purkinje neuron are covered by the processes of Bergmann glial cells; a single Bergmann cell can form the sheaths from 2000 to 6000 synapses and the eight Bergmann glial cells surrounding a single Purkinje cell can provide perisynaptic coverage of all its 17000-51500 dendritic spine synapses (Reichenbach et al., 1995). The terminal structures of astrocytes, which cover the synaptic regions, have a rather complicated morphology: the main process of glial cells and their side branches, send numerous thin, convoluted cytoplasmic tongues, which appear to meander and branch randomly close to the neuropil and form a relatively independent functional unit (Grosche et al., 2002; Grosche et al., 1999). Functionally, the processes of astroglial cells have neurotransmitter receptors and transporters, and, most importantly, the receptors and transporters positioned on astroglial membranes correspond to the neurotransmitter released at the synapses they enwrap (Chaudhry et al., 1995; Kirischuk et al., 1996; Luque and Richards, 1995; Meguro et al., 1999). This anatomical feature allows astrocytes to sense neuronal activity with receptors specific for various neurotransmitters (Haydon, 2001).

5.2.2 Each Astrocyte Occupies its Own Domain

Dye-filling of single astrocytes, immunostaining against astrocytic processes or genetic labeling by mosaic Cre/loxP mediated recombination in Brainbow mice reveals distinct territories of single astrocytes (Bushong et al., 2002; Halassa et al., 2007; Ogata and Kosaka, 2002). It is intuitively evident from the regular spacing of telencephalic astrocytes that there is a spherical or ellipsoidal tissue compartment around every individual astrocyte soma which is occupied by only this astrocyte (Bushong et al., 2004). In immunocytochemical staining for astrocytic proteins

preferentially labeling thin processes (Derouiche and Frotscher, 2001), the approximate territorial boundaries and the tiling become obvious. Indeed, when two adjacent astrocytes are injected with different dyes, the very dense nature of the processes of the astrocytes imparted a rather distinct boundary to the extent of each astrocyte. Only small proportion (4-6 %) are overlapped (Ogata and Kosaka, 2002). These cellular domains appear to develop early postnatally by a competitive interaction between neighboring astrocytes (Bushong et al., 2004). Interestingly, glutamate released from astrocytes can synchronize closely spaced neurons through the generation of slow inward currents (SICs) (Angulo et al., 2004; Kozlov et al., 2006). In addition, Ca^{2+} elevation in astrocytes evoked by short stimulus trains could evoke a synchronous Ca^{2+} rise in an average of two to three pyramidal neurons, but up to twelve (Fellin and Carmignoto, 2004; Halassa et al., 2007). Thus, a given astrocyte has the potential to respond to small clusters of neurons and work together as a functional synaptic island (Halassa et al., 2007).

5.3 Astrocytic Currents Reflect Neuronal Activity

Removal of K^+ from the extracellular space (Amedee et al., 1997; Kofuji and Newman, 2004) and clearance of glutamate from the synaptic cleft (Danbolt, 2001) are two well-known functions of passive astrocytes in the brain. Both mechanisms produce currents that reflect neuronal activity. As the astrocyte forms a functional unit with limited numbers of neurons, the astrocytic currents produced by K^+ and glutamate uptake report the ensemble activity of a group of neurons behaving as a single unit (summary in Fig. 4).

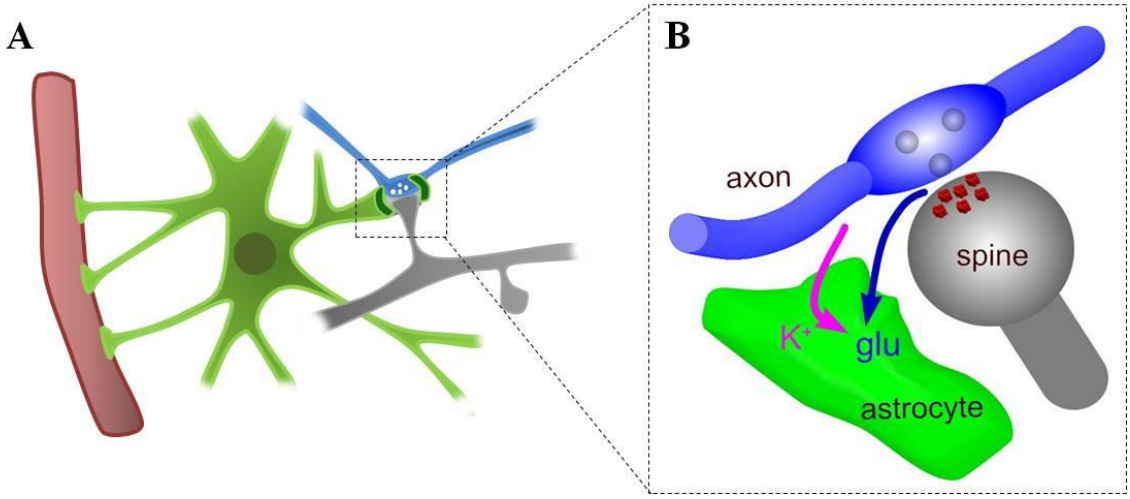

Figure 4. Interplay between astrocytes, neurons and the vasculature. (A) Astrocytes processes ensheath blood vessels, as well as synapses, interact with both parts to control cognitive functions. (B) Activation signals (glutamate and K^+) is manufactured by the neuron and presented to the astrocyte. Both molecules are then taken up by the astrocyte, thus protecting surrounding cells from excitotoxicity.

5.3.1 Estimate of Glutamate Release by Transporter Current (TC)

5.3.1.1 Astrocytic Glutamate Transporters

Astrocytes have long been known to take up and metabolize glutamate (Schousboe et al., 1992). Among the five cloned high affinity glutamate transporters (Palacin et al., 1998; Torres and Amara, 2007), two of the most abundant glutamate transporter subtypes, EAAT1 and EAAT2 (also called GLAST and GLT-1, respectively), are expressed primarily in astrocytes (Lehre et al., 1995; Minelli et al., 2001). The EAAT-type of transporters Glutamate transporters harness the energy stored in the electrochemical gradients for Na^+, H^+, and K^+ to force glutamate into cells against its concentration gradient (Danbolt, 2001). The density of glutamate transporter is highest in synaptic regions as opposed to regions of presumably lower demand for glutamate uptake, i.e. dendrites, pial surface, and apposed astrocytic membranes (Chaudhry et al., 1995). Astroglial

glutamate uptake is a major line of defence against excess glutamate accumulation, preventing epilepsy and excitotoxicity (Rothstein et al., 1996; Tanaka et al., 1997). Indeed, knocking out glial EAAT2 (Tanaka et al., 1997) results in lethal spontaneous seizures and increased susceptibility to acute forebrain injury. Mice deficient in glial EAAT1 have increased susceptibility to cerebellar injury as well as reduced motor coordination (Watase et al., 1998). In addition, astrocytic glutamate transporters were shown to be critical for limiting the extent to which transmitter spills over between synapses (Asztely et al., 1997), serving to decrease synaptic noise and improve the reliability of synaptic transmission. Notably, the fact that synaptic glutamate is taken up by astrocytes via a process that induces changes in membrane potential, intracellular Na^+ and pH suggests that glutamate transporters may translate information carried by excitatory transmission into a number of active signals for astrocytes.

5.3.1.2 Detecting Glutamate Time Course by Astrocyte Recording

A series of elegant studies showed that astrocyte glutamate transporters are activated by synaptically released glutamate in acute slices (Bergles and Jahr, 1997; Bordey and Sontheimer, 2003; Clark and Barbour, 1997). Astrocytic glutamate transporter currents were then used as an independent sensor to monitor synaptic transmitter release. It has been shown that astrocytic glutamate transporter currents report paired-pulse facilitation of synaptic transmission and have been suggested as a sensitive assay for measuring changes in release probability (Pr) under different types of manipulations (paired-pulse facilitation, changing Ca^{2+}/Mg^{2+} ratio, and high frequency stimulation) (Bergles and Jahr, 1997). In fact, the transporter currents were suggested to be even more sensitive than field potential to changes brought about by these manipulations of Pr (Diamond et al., 1998). This may result from the fact that field responses were contaminated

by significant postsynaptic depolarization that reduced the driving force on the synaptic conductance and thereby diminished the effect of increased transmission. Because astrocytes have low input resistances, they are depolarized only slightly during a synaptic response, causing little attenuation of the transporter currents due to reduction in driving force. Consequently, the astrocytic glutamate transporter current is a linear, fast indicator of the glutamate kinetics inside the cleft, offering significant analytic advantages to estimate glutamate clearance rate (Diamond, 2005).

5.3.2 Estimation of Extracellular Potassium from I_K

5.3.2.1 Astrocytic K^+ Uptake Mechanisms

Neuronal activity is dependent on the appropriate concentrations of ions in the extracellular and intracellular space. As mentioned previously, the $[K^+]_o$ increases with intense neuronal activity, resulting in an increase in neuronal excitability. Once released from neurons, $[K^+]_o$ must be cleared from the extracellular space. Clearing of excess $[K^+]_o$ is believed to occur by diffusion, active uptake by neurons and glia, or by passive uptake by glia. There is strong evidence that K^+ release would quickly overwhelm diffusion (Somjen, 1979), indicating a need for additional mechanisms for clearing potassium.

Astrocytes are postulated to maintain the correct baseline $[K^+]_o$ (Coles and Poulain, 1991; Gardner-Medwin and Nicholson, 1983). Having strongly negative resting membrane potential and selective membrane permeability to potassium, astrocytes are very sensitive to increases in $[K^+]_o$, more so than neurons. The resting membrane potential (V_m) of astrocytes is very close to

the K^+ equilibrium potential, E_k. Increases in extracellular K^+ would instantly shift the astrocytic E_k towards depolarized values, which would generate an inflow of K^+ ions (as the $V_m < E_k$).

The pioneering work by Kuffler's group showed that nerve impulses cause slow depolarization of glia attributable to K^+ influx in the amphibian optic nerve (Orkand et al., 1966), and they proposed a K^+ spatial buffering hypothesis, which states that astrocytes take up excess extracellular K^+ ions, distribute them through the gap junction-coupled astrocytic syncytium, and extrude the ions at sites of low extracellular K^+ level (Kuffler and Nicholls, 1966). This homeostatic function has been confirmed in astrocytes in rat neocortical slices (Holthoff and Witte, 2000). Astrocytes can also release K^+ directly into the blood stream by direct discharge into capillaries by their endfeet connections. This process, termed spatial siphoning, was first shown in the retina (Newman, 1986).

To achieve efficient K^+ uptake, astrocytes have both passive uptake (via channel and cotransporters) and active uptake (via Na^+/K^+ ATPases) capabilities. Passive transport of K^+ into astrocytes is achieved predominantly by inwardly rectifying potassium channels (K_{ir}) and to a lesser extent, Na^+/K^+ or K^+/Cl^- antiporters, based on pharmacological studies (Ballanyi et al., 1987; Karwoski et al., 1989). In the CNS, $K_{ir}4.1$ is specifically localized to astrocytes, oligodendrocytes, and retinal Muller cells (Li et al., 2001; Olsen et al., 2006; Poopalasundaram et al., 2000). K_{ir} channels are suitable for K^+ uptake because they retain high open probability at the resting potential and allow K^+ influx although impeding K^+ efflux (Djukic et al., 2007). Besides, they preferentially locate on astroglia processes ensheathing synapses and blood vessels (Higashi et al., 2001). Generation and study of $K_{ir}4.1^{-/-}$ mice confirmed the importance of $K_{ir}4.1$

in K^+ buffering by several cell types, including Muller glia and cochlear epithelium (Kofuji et al., 2000; Marcus et al., 2002). Consistent with the importance of glial $K_{ir}4.1$ in $[K^+]_o$ modulation, quantitative trait loci mapping identified its gene as a putative seizure susceptibility gene in mice (Ferraro et al., 2004), and a missense variation in this gene was linked to general seizure susceptibility in humans (Buono et al., 2004).

5.3.3 Detecting $[K^+]_o$ Change via Astrocyte Recording

Although neuronal recording and microelectrodes are usual ways to approach $[K^+]_o$ variation within a neural circuit, increasing number of studies use astrocyte recordings. There are a few reasons for this. Firstly, astrocyte recording is a much more independent method of $[K^+]_o$ measurement. Results of traditional neuronal recording (e.g. the relative amplitudes of NMDA and AMPA receptor mediated excitatory postsynaptic currents) are complicated, because the recorded postsynaptic response can be an integrated result of changes in both transmitter release and postsynaptic sensitivity. In contrast, astrocytic responses constitute only TC and I_K, which can be simply separated from neuronal changes by pharmacological tools. Secondly, astrocytes encroach upon the confined extracellular space (ECS) using their tiny processes, appropriate to detect the variation of extracellular neuroactive substances and ions in small space. Although potassium-sensitive double-barrel microelectrodes are often used to estimate increases of $[K^+]_o$, this method is accurate only for the estimation of wide-spread or massive K^+ release. Also, due to the creation of a dead space around the tip of the electrode that is several times the volume of the associated extracellular space, limited K^+ release will be greatly underestimated. Hence, astrocyte recording can provide a better spatial measurement of $[K^+]_o$.

6. Aims of This Study

The goals of the present study were to (1) examine the relative contribution of AMPA and NMDA receptors to K^+ signals during synaptic transmission, (2) identify and characterize the candidate potassium channels following the activation of the target receptor, (3) check if the K^+ signal can be adjusted depending on neuronal activity, and (4) determine how this K^+ signal can execute retrograde modulation of presynaptic and astrocytic partners within the tripartite synapse.

Chapter 2: Material & Methods

1. Chemicals & Equipment

Chemicals, dyes, antibodies and media were purchased from Sigma (St. Louis, MO, USA), Invitrogen / Molecular Probes (Carlsbad, CA, USA), Tocris Cookson (Bristol, UK), Wako Chemicals (Osaka, Japan), Nacalai Tesque (Kyoto, Japan), Alfa Aesar (Ward Hill, MA, USA), and Vector Labs (Burlingame, CA, USA). Deionized water (Purelab Ultra, Elga, High Wycombe, UK) was used to prepare all solutions.

1.1.Chemicals

Chemical	**Supplier**
ACSF/intracellular solution	
Sucrose	Wako Chemicals
NaCl	Wako Chemicals
KCl	Nacalai Tesque
$MgCl_2$	Wako Chemicals
NaH_2PO_4	Nacalai Tesque
$NaHCO_3$	Wako Chemicals
$CaCl_2$	Nacalai Tesque
$MgCl_2$	Wako Chemicals
Glucose	Wako Chemicals
K-gluconate	Sigma
K-methanesulfonate	Alfa Aesar
HEPES	Nacalai Tesque
Na_2-phosphocreatine	Nacalai Tesque
Na_2ATP	Sigma
MgATP	Sigma
NaGTP	Sigma
Na-ascorbate	Nacalai Tesque

Biocytin	Sigma
KOH	Nacalai Tesque
Agonist / Antagonist	
$BaCl_2$	Wako Chemicals
TBOA	Tocris Cookson
TTX	Tocris Cookson
NBQX	Tocris Cookson
AP5	Tocris Cookson
MCPG	Tocris Cookson
Picrotoxin	Tocris Cookson
CGP 52432	Tocris Cookson
MK-801	Tocris Cookson
NMDA	Tocris Cookson
Glutamate	Tocris Cookson
Other	
Na_2HPO_4	Wako Chemicals
Bovine serum albumin	Sigma
DMSO	Nacalai Tesque
Pluronic F127	Invitrogen
Paraformaldehyde 4% (PFA 4%)	Wako Chemicals
Triton X-100	Nacalai Tesque
ABC kit	Vector Labs
3,3'-diaminobenzidine (DAB)	Sigma
Agar	Wako Chemicals
2-bromo-2-chloro-1,1,1-trifluroethane	Sigma

1.2.Media

- **Cutting ACSF (cutting artificial cerebrospinal fluid)**

75 M Sucrose, 87 mM NaCl, 2.5 mM KCl, 0.5 mM $CaCl_2$, 7 mM $MgCl_2$, 1.25 mM

NaH_2PO_4, 25 mM $NaHCO_3$, and 4.4 mM glucose, 315-320 mOsm, pH 7.4

- **Storage ACSF (storage artificial cerebrospinal fluid)**

127 NaCl, 2.5 mM KCl, 1.25 mM NaH_2PO_4, 25 mM $NaHCO_3$, 1 mM $CaCl_2$, 1 mM $MgCl_2$, 11 mM glucose, 300 ± 3 mOsm, pH 7.4

- **Recording ACSF (recording artificial cerebrospinal fluid)**

127 NaCl, 2.5 mM KCl, 1.25 mM NaH_2PO_4, 25 mM $NaHCO_3$, 2 mM $CaCl_2$, 1 mM $MgCl_2$, 11 mM glucose, 300 ± 3 mOsm, pH 7.4

- **Intracellular solution for astrocyte**

135 K-methanesulfonate, 10 mM HEPES, 10 mM Na_2-phosphocreatine, 4 mM $MgCl_2$, 4 mM Na_2ATP, 0.4 mM NaGTP, 290 mOsm, pH 7.2

- **Intracellular solution for pyramidal neurons**

130 K-methanesulfonate, 8 mM NaCl, 10 mM HEPES, 10 mM Na_2-phosphocreatine, 0.4 mM Na_2GTP, 4 mM MgATP, 3 mM Na-ascorbate, 290 mOsm, pH 7.2

- **PBS (phosphate buffer saline)**

130mM NaCl, 7 mM Na_2HPO_4, 3 mM NaH_2PO_4, pH 7.4

1.3.Dyes

Dye	**Concentration (μM)**	**Supplier**
SR101	1	Invitrogen
OGB1-AM	500	Invitrogen
Fluo-5F	200-300	Invitrogen
Alexa Fluor 594	20-50	Invitrogen

1.4.Equipment

Instrument	**Supplier**

Two-Photon Laser-Scanning Microscope (TPLSM)	
Chameleon Ti-Sapphire laser	Coherent, CA, USA
Acousto-optic modulators (AOM)	AA Opto-Electronic, France
Refraction dichroic mirror RDM690/405	Olympus, Japan
Bandpass filter BA495-540HQ (green)	Olympus, Japan
Bandpass filter BA570-625HQ (red)	Olympus, Japan
Dichroic mirror DM570	Olympus, Japan
Photomultipler tubes	Olympus, Japan
Upright microscope BX61	Olympus, Japan
Water-immersion objective, 60x, NA 0.9	Olympus, Japan
Confocal Laser-Scanning Microscopy (CLSM)	
488 nm Argon laser	Melles Griot, CA, USA
Dichroic mirror 405/488	Olympus, Japan
Bandpass filter BA505IF	Olympus, Japan
Photomultipler tubes	Olympus, Japan
Upright microscope BX61	Olympus, Japan
Water-immersion objective, 60x, NA 0.9	Olympus, Japan
Electrophysiology	
A/D converter PCI-6221 (16 bit)	National Instruments, TX, USA
Multiclamp 700B amplifier	Axon Instruments, CA, USA
Motorized manipulator system	Luigs and Neumann, Germany
Borosilicate glass capillaries (outer diameter = 1.5 mm, inner diameter = 0.86 mm)	Harvard Apparatus, UK
Constant current stimulator	Digitimer, UK
Pneumatic picopump PV830	WPI, FL, USA
CCD camera IR-1000	Dage-MTI, IN, USA
Software	

ImageJ	NIH, MD, USA
Matlab	MathWorks, MA, USA
Origin 8	OriginLab Corp, MA, USA
Fluoview	Olympus, Japan
WinWCP	Strathclyde University
Clampfit 10.2	Axon Instruments, CA, USA
Other	
Vibrotome HM650V	Microm, Germany
Micropipette puller model P-97	Sutter Instruments, CA, USA
Temperature controller	Scientific Systems Design Inc. Canada
Perfusion pump	Masterflex, IL, USA

2. Model System: Hippocampal Slice

The *in vitro* slice preparation provides precise control over experimental conditions (compared to *in vivo*) and an intact cell circuitry (compared to cell cultures). Acute slice preparation was therefore chosen as the model system of this thesis.

2.1. Trisynaptic Circuit of Hippocampus

All experiments were carried out in the hippocampus region. The hippocampus is a major experimental system for studies of synaptic transmission in the context of putative information-storage structure in the brain. It comprises the dentate gyrus, Ammon's horn, and subiculum. Ammon's horn, routinely abbreviated CA (for cornu Ammonis), can be further divided into three zones, CA1 through 3, based on cytological architecture and synaptic connectivity. The superiorly arching CA1 is joined by CA2 to form the medial floor of the temporal horn of the

lateral ventricle. The dorsally situated CA2 is usually recognizable by the greater compactness of the pyramidal cell layer, as compared to CA1, and CA3 forms a descending medial arch that terminates in the hilus of the dentate gyrus (summary in Fig. 5, left).

An apparently important feature of the intrinsic circuit of the hippocampus is its connection selectivity and unidirectional projections. The major pathways of signal flow through the hippocampus combine to form “trisynaptic circuit” (summary in Fig. 5, right). The first synapse is made by neurons from the layer II of the entorhinal cortex onto granule cells of the dentate gyrus, through the perforant pathway. The second synapse is made by granule cells of the dentate gyrus onto pyramidal cells of CA3, via the mossy fibers. The third synapse is made by axon collaterals of the CA3 pyramidal cells onto the pyramidal cells of the CA1 subfield, known as the Schaffer collateral (Atoji and Wild, 2006; Blackstad, 1956). The dentate gyrus cells project to CA3 field whereas the CA3 cells do not generally project back to the dentate granule cells. Similarly, CA1 pyramidal cells do not project back to CA3 (Atoji and Wild, 2006; Blackstad, 1956; Neves et al., 2008). All these major subfields in the trisynaptic circuit have an elegant laminar organization in which the cell bodies are tightly packed in an interlocking C-shaped arrangement, with afferent fibers terminating on selective regions of the dendritic tree (Neves et al., 2008).

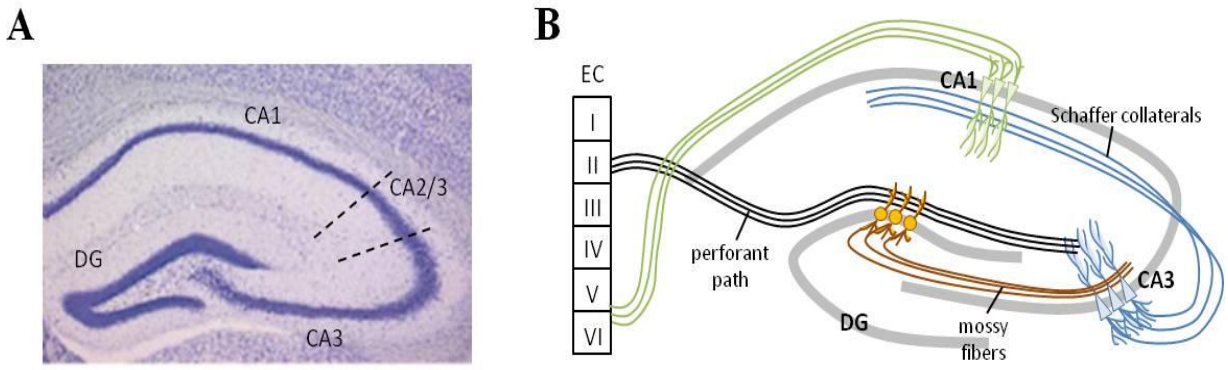

Figure 5. The neural circuitry in the hippocampus. (A) Identification of CA subfields and DG (dentate gyrus) (B) The traditional excitatory trisynaptic pathway (entorhinal cortex (EC)-DG-CA3-CA1-EC) is depicted.

2.2.Preparation of Hippocampal Slices

Hippocampal slices in my experiments were obtained from postnatal day (P) 28 to 35 Sprague-Dawley rats or C57B/6J mice. Where stated, experiments were carried out on slices of P42 to P49 CA1-NR1 KO mice (NR1 *fl/fl*; CaMKII-*Cre*) or littermate controls (NR1 *fl/fl*) (Tsien et al., 1996). Animals were anesthetized with 2-Bromo-2-chloro-1,1,1-trifluroethane (Halothane, Sigma) and then decapitated. All my experimental procedures were performed in accordance with the regulations of the guidelines of the Animal Experiment Committee of the RIKEN Brain Science Institute. The brain was then quickly removed and placed in chilled 'cutting' artificial cerebrospinal fluid (ACSF) consisting of (mM): 75 sucrose, 87 NaCl, 2.5 KCl, 0.5 $CaCl_2$, 7 $MgCl_2$, 1.25 NaH_2PO_4, 25 $NaHCO_3$, and 4.4 glucose, continuously bubbled with a mixture of 95% O_2 and 5% CO_2 to maintain pH at 7.4. The osmolarity was adjusted to 315-320 mOsm. Hippocampi were dissected from each hemisphere, embedded in agar, and then glued to the inclined stage (20°) of a slicing chamber filled with chilled cutting ACSF. Cutting in this

orientation maintains the integrity of the Schaffer collateral connection from pyramidal cells in CA3 to those in CA1. Transverse slices (350-400 μm) were cut from the middle third of each hippocampus with a vibratome (Microm HM650V, Thermo Fisher Scientific Inc., USA) (Fig. 6). After sectioning, slices were immediately placed in a submerged chamber containing warmed cutting ACSF at 34℃ for 20min and then moved to interface chamber with 'storage' ACSF solution containing (mM): 127 NaCl, 2.5 KCl, 1.25 NaH_2PO_4, 25 $NaHCO_3$, 1 $CaCl_2$, 1 $MgCl_2$, and 11 glucose, with osmolarity adjusted to 295-300 mOsm. The slices were then kept at room temperature for at least 1 hr before experiments.

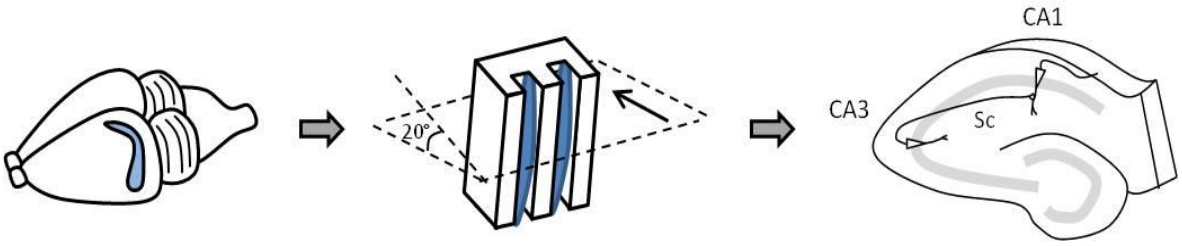

Figure 6. Schematic illustration of hippocampal slice preparation

Where specified, sulforhodamine 101 (SR101), a specific marker for astrocytes was used (Nimmerjahn et al., 2004). Spectrum and structure of SR101 are shown in Fig. 7. Following sectioning, slices were kept at 34℃ for 20 min in cutting ACSF containing 0.5-1 μM SR101, followed by 10 min incubation in normal ACSF at 34℃. Afterwards, slices were transferred to an interface chamber and kept at room temperature until they were used for experiments. During all these processes, slices were protected from light.

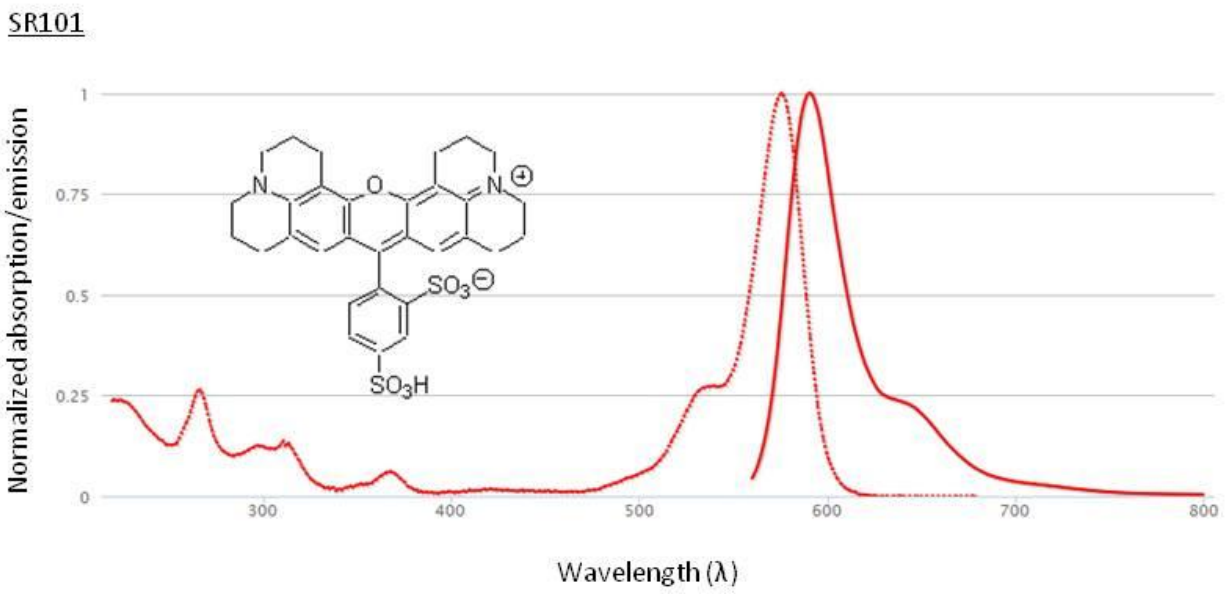

Figure 7. Molecular structure and spectra of SR101. The indicator was excited at 575 nm and emission was collected above 590 nm. Dotted line, excitation spectrum; solid line, emission spectrum; data from invitrogen.

3. Electrophysiology and Imaging Techniques

3.1.Extracellular Field Recordings

3.1.1. Principle

Extracellular field potentials are local current sinks or sources that are generated by the collective activity of many neurons. The response usually includes two components: the initial fast component results from the action potentials generated in the presynaptic fibers (fiber volley, FV) and the later synaptic component corresponding to the current sink into the postsynaptic neurons (field excitatory postsynaptic potential, fEPSP) (Fig. 8). When recording extracellular field potentials, one of the advantages is that the magnitude of the presynaptic fiber volley can be monitored, together with the fEPSP, as a measure of the number of activated axons during the

experiment. Another advantage, compared to the whole cell configuration, is that the cells that contribute to the response have their intracellular composition left intact. A disadvantage, on the other hand, is that we do not know exactly which cells contribute to this field response. Because of the orderly arrangement of the pyramidal neurons and their dendrites in hippocampus, the extracellular signals add up and can be easily detected with a field electrode. Extracellular field recordings are therefore especially suitable to detect population neuronal response in this brain area.

3.1.2. Field Potential Recording in Acute Hippocampal Slices

Slices were transferred to recording chamber and perfused with recording ACSF containing (mM): 127 NaCl, 2.5 KCl, 1.25 NaH_2PO_4, 1 $MgCl_2$, 2 $CaCl_2$, 25 $NaHCO_3$, and 11 D-glucose, equilibrated with 95% O_2/5% CO_2 and delivered via a gravity fed perfusion system (2-3 $mlmin^{-1}$). During experiments, a grid consisting of nylon threads glued to a U-shaped platinum wire was put on top of the slices in the recording chamber, in order to fix the slices in place. For extracellular field potential recordings, 100 μM picrotoxin was included in recording ACSF to block $GABA_A$ receptor mediated inhibitory synaptic responses. To prevent epileptiform discharges, a surgical cut was always made between CA1 and CA3. A glass pipette (3-5 MΩ) filled with 3M NaCl was positioned at *stratum radiatum* of CA1 to record field neuronal activity. A bipolar stainless steel electrode (FHC, Bowdoinham, ME, USA) was positioned a few hundred micrometers from the recording pipette and Schaffer collateral fibers were stimulated at 0.033 Hz. Only evoked response with the amplitude ratio of fEPSP/FV > 2 was included for further analysis. The magnitude of the fEPSP was measured as the slope of the first 0.8 ms of the initial slope for data analysis. For pairing experiment, a second stimulus electrode was placed in the

alveus to elicit backpropagating action potentials by antidromic stimulation. The electrical stimulus was 100 μs with an intensity of 50-320 μA, which was adjusted to 40-50 % of the maximal response. All signals were filtered at 2 kHz and digitized at 10 kHz.

3.1.3. Release Probability Monitored by Paired-Pulse Ratio (PPR)

Where indicated, two consequent stimuli were applied with an interval of 50 ms. The paired-pulse ratio (PPR) was defined as the ratio of slope 2 to slope 1 (Fig. 8). The second response of a paired-pulse stimulation is either enhanced (paire-pulse facilitation, PPF, PPR>1) or depressed (paired-pulse depression, PPD, PPR<1) (Brown and Reymann, 1995; Platt and Withington, 1997; Zucker and Regehr, 2002), depending on the initial release probability (Dobrunz and Stevens, 1997). In general, the smaller the release probability of the first pulse, the more facilitated is the response to the second pulse. This phenomenon is accounted for by the residual calcium hypothesis, according to which the small fraction of calcium entering the terminal during the first spike increases the probability of transmitter release to a second action potential (Zucker and Regehr, 2002).

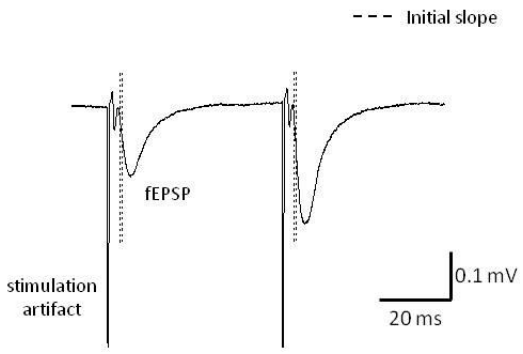

Figure 8. The field response to a paired-pulse stimulus

3.2.Patch-Clamp Recording

3.2.1. Principle

Compared to extracellular field potential recordings, the patch-clamp technique offers the possibility to measure membrane potential or membrane current of a single cell (in whole-cell recordings and perforated patches) or current across a patch of membrane (in cell-attached or inside-/outside-out configurations).

Two modes are frequently used in patch clamp recordings: voltage clamp and current clamp. In current-clamp, the amount of current injected into the cell is kept constant and changes in membrane potential are measured. In voltage-clamp, the membrane potential of the cell is kept constant and equal to the command potential, which allows measurement of electric current resulting from ion fluxes across the plasma membrane. Because the patch-clamp amplifier allows us to measure voltage and to inject current through the same pipette to maintain the cell at the command potential, an influx of positive ions into a cell in whole-cell mode results in a negative current and an outflow of positive ions a positive current.

3.2.2. Patch-Clamp Recording of Astrocytes

For patch-clamp recordings, slices were transferred to a recording chamber and visualized under an upright microscope (BX-61; Olympus, Japan) with differential interference contrast optics and a water immersion objective lens (60X, NA of 1.0, Olympus, Japan). Recording ACSF solution was saturated with 95% O_2 and 5% CO_2. 100 μM picrotoxin, 5 μM CGP52432, and 200 μM S-MCPG were routinely added to the solution to block $GABA_A$, $GABA_B$, and mGluR

receptors, respectively, unless stated otherwise. Somatic whole-cell patch-clamp recordings in visually identified astrocytes were carried out using borosilicate glass pipette (Harvard Apparatus, Edenbridge, Kent, UK) of 3 to 5 MΩ resistance, filled with internal solution containing (mM): 135 KCH_3SO_3, 10 HEPES, 10 Na_2-phosphocreatine, 4 $MgCl_2$, 4 Na_2ATP and 0.4 Na_2GTP (290 mOsm, pH 7.2). The cells were approached with a patch pipette using motorized manipulators (Luigs & Neumann, Germany). Hippocampal passive astrocytes were voltage-clamped at their resting membrane potential and currents were recorded with the patch-clamp amplifier (Multiclamp 700B; Axon Instruments Inc.; Union City, CA, USA). The series resistance of recorded cells was measured by injection of hyperpolarizing pulses (-3 mV, 100ms) and not compensated. Cells that showed a >20% change in series resistance were discarded. For analysis, 4-10 consecutive traces were averaged. The data were acquired using software WinWCP (supplied free of charge to academic users by Dr. John Dempster, University of Strathclyde, UK), digitized at 4-10 kHz and filtered at 2 kHz.

3.3.Puff Application

L-glutamate and NMDA dissolved in recording-ACSF containing 1μM tetrodotoxin (TTX) was pressure injected focally to the recorded astrocytes in slices using brief (5-50 ms) pulses of pressure (15-20 psi) applied to the back of a patch electrode using a Pneumatic Picopump (PV820, World Precisio Instruments, Sarasota, FL). The distance between puff and recording pipettes were kept at 50-100 μm.

3.4.Immunohistochemistry

In some experiments, 6.7 mM biocytin (Sigma, St. Louis, MO, USA) was included in the internal solution to fill the recorded astrocytes. Astrocytes were filled by passive diffusion of biocytin from the patch pipette for at least 15 min after electrophysiological recording. After it, pipettes were withdrawn and slices were fixed overnight in 4% paraformaldehyde in 0.1 M phosphate buffer (PB, pH 7.4) at 4℃. Slices were then rinsed with PB at least three times after fixation and pretreated for endogenous peroxidase by incubating for 10 min in 1 % H_2O_2 PB solution. After wash the slices with PB for additional 3 times, slices were subject to immunostaining procedures without further sectioning. Briefly, slices were rinsed in 0.03% Triton X-100 in phosphate-buffered saline (PBST), and incubated for 1h at room temperature in PBST containing 2% bovine serum albumin (BSA), 10% normal goat serum (NGS). The slices were then incubated overnight at 4℃ in PBST containing avidin biotinylated horseradish peroxidase macromolecular complex (ABC, 1:400, PK-6100, Vector Laboratories, CA, USA). After rinses in 0.1 M PB, the slices were visualized with a nickel-diaminobenzidine (Ni-DAB) reaction (Nacalai Tesque Inc, Japan) in darkness. Slices were thoroughly rinsed in PB, placed on gelatin coated slides, air dried, and mounted with permount.

3.5.Ca^{2+} Imaging of Presynaptic Terminals

Calcium dynamics within presynaptic boutons were assessed by multibouton Ca^{2+} imaging experiments with indicator Oregon Green-488-BAPTA-1-AM (OGB1-AM) and single bouton Ca^{2+} imaging experiments with indicator Fluo-5F.

3.5.1. Ca^{2+} Imaging Principle

The concentration of free Ca^{2+} ions is generally very low within cells. Whereas the extracellular Ca^{2+} concentration is around 2 mM, its intracellular concentration is a factor of more than 10^4 less and varies in hundred nanomolar range (Brenowitz and Regehr, 2007). Hence, the ideal tool for measuring $[Ca^{2+}]_i$ needs to be highly sensitive and specific for Ca^{2+}.

Ca^{2+} fluorescent indicator dyes are valuable tools for measuring such small concentration changes (Tsien et al., 1985; Grynkiewicz et al., 1985). Most Ca^{2+} indicators consist of an aromatic ring system, the double bonds of which are responsible for the characteristic fluorescence properties of the dye. The K_d of a Ca^{2+} indicator is a measure for its affinity to Ca^{2+}. In general, a specific indicator can be used when the expected signal is in the range of 0.1 to 10 times of K_d of the dye. Upon binding Ca^{2+}, the indicator undergoes a conformational change resulting in a change in fluorescence intensity. In this thesis, I chose two Ca^{2+} indicators: OGB1 with a K_d of 210 nM and Fluo-5F with a K_d of 1.3 μM; both are well suited for measuring $[Ca^{2+}]_i$ in the physiological range.

buffer	λ_{max} (excitation)	λ_{max} (emission)	K_d
OGB1	494 nm	523 nm	210 nM
Fluo-5F	494 nm	516 nm	1.3 μM

Table 1. Properties of used Ca^{2+} indicators

3.5.2. Bolus Loading of Ca^{2+} Indicator Dye and Multibouton Ca^{2+} Imaging

Multibouton Ca^{2+} imaging was performed with the AM form of OGB1 (OGB1-AM): here the carboxylates are masked as acetoxymethyl (AM) esters and the substance can pass cell membranes. Once intracellular, ubiquitous esterases cleave the AM esters, the indicator becomes ion-sensitive and membrane-impermeant (Tsien, 1981). These indicators diffuse within cells, and with time, indicator concentration equilibrates throughout each cell. As Schaffer collateral fiber tracts are well-segregated, nonmyelinated fiber tracts that contain a homogeneous population of presynaptic terminals, away from the small range of indicator fill site, the only structures labeled with the Ca^{2+} indicator are the axons and their associated terminals, making this approach suited to the study of multibouton Ca^{2+} imaging in the CA1 area.

Typically, OGB1-AM was dissolved in dimethyl sulphoxide (DMSO) plus 20% Pluronic F-127 to yield a concentration of 5 mM. This stock solution was diluted on the day of experiment with recording ACSF to a final concentration of 0.5 mM (Pelkey et al., 2006). Axons and presynaptic boutons of Schaffer collateral were stained by local pressure injection of this labeling solution into the extracellular space of the *stratum radiatum* where the axon bundle is located. Two hour after OGB1-AM injection, labeled terminals were identified approximately 300 μm from the site of injection with confocal microscopy. A water-immersion objective lens (16X, NA of 0.8 or 60X, NA of 1.0) was used. The OGB1 fluorescence was excited at 488 nm with a laser diode and detected through a long-pass emission filter (cut-off 505 nm). Ca^{2+} transients (average of 5-6 responses) evoked by electrical stimulation were typically measured by scanning a line along a number of boutons. For Ca^{2+} transient analysis, fluorescence background was subtracted from

fluorescence intensity averaged over the region of interest. Changes in fluorescence were calculated relative to baseline and expressed as $\%\Delta F/F = [(F-F_{rest})/F_{rest}] \times 100$.

3.5.3. Single Bouton Ca^{2+} Imaging Using Two-photon excitation (TPE) Microscopy

I used a two-scanner FV1000-MPE laser-scanning microscope (TPE-LSM, Olympus, Japan) with a 60X, water immersion objective with 1.0 numerical aperture (NA) (Olympus, Japan) and a mode-locked (<140 fs pulse width) tunable 720-930 nm laser (Chameleon XR, Coherent, USA). Whole-cell recordings in pyramidal neurons were performed with patch pipettes (5-7 MΩ) filled with an intracellular solution containing (mM): 130 KCH_3SO_3, 8 NaCl, 10 HEPES, 10 Na_2-Phosphocreatine, 0.4 Na_2GTP, 4 MgATP, 3 Na-Ascorbate (290 mOsm, pH 7.2). Where specified, the NMDA receptor antagonist, (5*R*,10*S*)-(+)-5-methyl-10,11-dihydro-5*H*-dibenzo [*a*,*d*] cyclo-hepten-5,10-imine (MK-801) was added to the intracellular solution. Data were collected at least 15 min after reaching the whole-cell configuration, the time required for MK-801 (5 mM) to diffuse into the cell. Effect of internal MK-801 (iMK-801) was calculated as the decrease percentage of EPSC amplitude before and 5 min after bath application of DL-2-amino-5-phosphonopentanoic acid (AP5, NMDA receptor antagonist, 50 μM).

The recording solution always contained the morphological tracer Alexa Fluor 594 (A594, 50 μM) and the Ca^{2+} indicator Fluo-5F. A single excitation wavelength of 810 nm was effective for simultaneous excitation of both fluorophores (Svoboda and Yasuda, 2006), and their fluorescence was chromatically separated and detected with two independent photomultiplier tubes (PMTs) (Fig. 9). In CA3 pyramidal cells with intact axons (see Fig. 25 & 26), 20-30 min were initially allowed for indicator diffusional equilibration before switching the system into fluorescence

mode to trace the axon. Image acquisition was controlled by Fluoview software, and synchronized with electrophysiological recordings. Fluorescence responses were recorded in line-scan mode (scan frequency around 500 Hz, intersweep interval, 1 min) and stored for off-line analysis. The fluorescent measurements of Ca^{2+} transient were represented as $\Delta G/R$: (G - $G_{baseline}$) / ($R_{baseline}$- $R_{dark\ noise}$) for the time dependent Ca^{2+} transients and $\Delta G_P/R$: (G_{peak} - $G_{baseline}$) / ($R_{baseline}$- $R_{dark\ noise}$) for the peak transient. Where G is the Fluo-5F fluorescence, and R is A594 fluorescence. $G_{baseline}$ and $R_{baseline}$ are averaged fluorescence 40 ms in baseline. G_{peak} is averaged fluorescence 40 ms at peak of the stimulation. $G_{dark\ noise}$ and $R_{dark\ noise}$ are the dark currents of the corresponding PMTs, collected when the laser shutter was closed in every recording. For illustration purposes, single traces were averaged from 5-6 traces, and then processed by 3 point average. Baseline Ca^{2+} mediated signals were represented by *baseline G/R*: (($G_{baseline}$ - $G_{dark\ noise}$) / ($R_{baseline}$- $R_{dark\ noise}$)). If this ratio changed during the experiment for more than 2 SE (standard error), the cell was discarded. Data were analyzed using Fluoview (Olympus, Japan) and ImageJ (NIH, USA). Statistical analysis was performed using Excel (Microsoft, US) and Origin 8 (OriginLab Corp.).

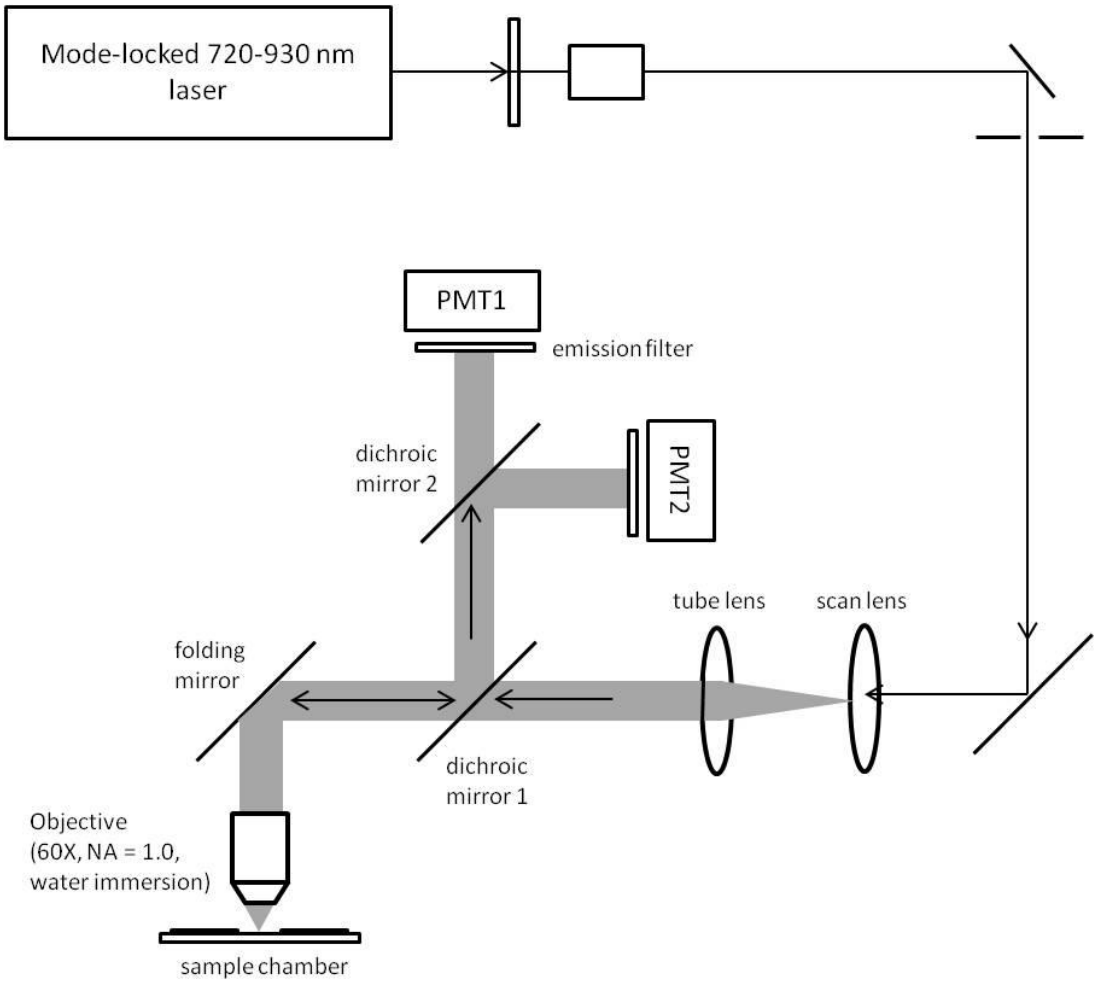

Figure 9. Schematic of the TPE-LSM

Specimen is excited with a tunable 720-930 nm laser. The combination of scan lens and tube lens expanded the excitation laser beam and back-filled the microscope objective. Two-photon absorption-induced fluorescence was collected in the epifluorescence path by the objective and redirected to two PMTs (red & green channel) using dichroic mirror 1 (RDM690, Olympus) and 2 (DM570, Olympus) followed by emission filters.

3.6.Flash Photolysis of Caged Glutamate

For flash photolysis experiments, MNI-caged-L-glutamate (200 μM) was perfused in the recording chamber and uncaged with 405 nm laser. I used the bright A594 emission to identify the processes of the astrocytes, and uncaging spot was positioned near the soma or along the cellular process as indicated. An uncaging point was selected in point scan mode. The laser power and duration were adjusted to produce glutamate transporter current 50% of the maximal response. Current responses due to the glutamate uncaging were recorded from the soma in whole-cell voltage clamp at resting membrane potential and were analyzed off-line with Clampfit 10.2 (Axon Instruments).

3.7.Analysis

3.7.1. Centroid

The centroid of a waveform is the midpoint of the spectral distribution of the waveform.

$$< t > = \frac{\int \mathrm{tf(t)dt}}{\int \mathrm{f(t)dt}} \quad (1)$$

where f(t) represents the waveform of the recorded current. The onset of the current was set to t = 0, and the centroid was calculated in a time window corresponding to 0.1 of the peak, before and after the peak of the current. Each point in this range was multiplied by its corresponding time and integrated. This integration result was then divided by the integral of the current alone. The centroid calculated in this manner can be regarded as a combined parameter of both rise and decay kinetics, and was used in estimating the kinetic change of currents in several studies (Diamond, 2005; Scimemi et al., 2009).

3.7.2. Nernst Equation

The Nernst fits represented in text were obtained from the Nernst equation:

$$E_K = -\frac{RT}{zF} \ln \frac{[K^+]_i}{[K^+]_o} \quad (2)$$

where R is the gas constant, T is the absolute temperature, F is the Faraday constant, z is the valence of the ion, in this case 1.

3.7.3. Statistics

Results are expressed as mean ± SE, and *n* refers to the number of cells. In some figures, box-and-whisker plots were used. These indicate the median value (line), the 25–75th percentiles (box) and the 10–90th percentiles (whiskers). Statistical significance for paired and independent samples was evaluated using paired or unpaired Student´s *t*-test. For some experiments, comparison among groups was made using one-way ANOVA; the Tukey post hoc test was used to identify intergroup differences, as appropriate. Differences were considered significant if $p < 0.05$.

Chapter 3: Characterizing Astrocytes and their Responses to Schaffer Collateral Stimulation

1. Identification of Hippocampal Astroctyes

I made whole-cell voltage-clamp recordings from astrocytes in hippocampal slices. The cell bodies of astrocytes in *stratum radiatum* of area CA1 were visualized using infrared DIC. These cells were distinguished from neurons by their small (< 10 μm) and oval shaped somata. The identification was confirmed by low input resistances (16.3 ± 1.4 MΩ, n = 16), high resting membrane potential (-84.0 ± 0.5 mV; n = 16) and a linear I-V relationship (Fig. 10B). When whole-cell recording of an astrocyte was performed with a biocytin-filled pipette, numerous spongiform ramifications of fine processes could be seen extending from the major branches (Fig. 10A, left). The overall morphology was approximately fusiform in shape, with their long axis oriented parallel to the descending apical dendrites of CA1 pyramidal neurons, as described previously (Wallraff et al., 2006). Multiple cell bodies often were labeled when a single astrocyte was filled with biocytin, consistent with strong gap junction coupling between adjacent astrocytes (Fig. 10A, right). These morphological and electrophysiological traits are characteristic of hippocampal astrocytes (Bergles and Jahr, 1997). Occasionally, members of complex glia were encountered (Jabs et al., 2005; Matthias et al., 2003; Zhou and Kimelberg, 2001), and were not studied further in this thesis.

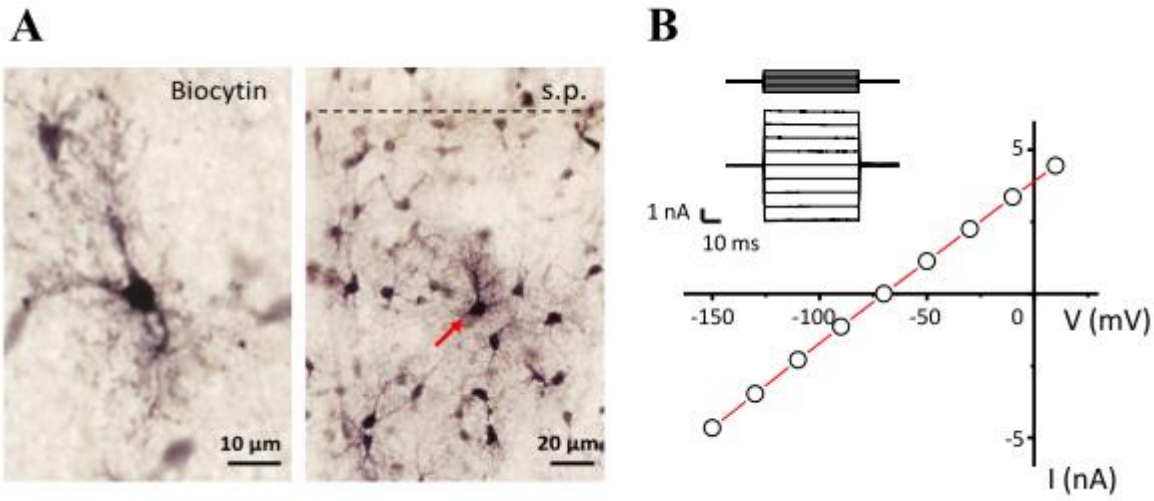

Figure 10. Astrocyte identification in hippocampal slices. (A) Left: morphology of a typical passive astrocyte with prominent primary processes and dense net of fine processes. Hippocampal astrocytes display a bipolar morphology with an orientation perpendicular to the stratum pyramidale. Right: functional coupling of passive astrocytes in stratum radiatum visualized by diffusion of biocytin via dialysing during whole-cell recording of one astrocyte (red arrow). Note the extensive coupling of neighboring astrocytes and the vessel walls encircled by astrocytic endfeet. (s.p., stratum pyramidale layer). (B) The hippocampal astrocyte shown in A had a linear current-voltage relationship, typical of passive astrocyte (50 ms steps, from -150 to +10 mV; V_{hold} = -70 mV).

2. Astrocyte Response to Schaffer Collateral Stimulation Consists of Two Components

Stimulation of the Schaffer collaterals (100 μs, 50-350 μA) elicited a complex current in astrocytes voltage clamped at their resting potential. Two distinct components of the inward current could be distinguished: a transient current followed by a slow one (Fig. 11A). Bath application of nonselective glutamate transporter inhibitor TBOA (50 μM) inhibited the transient current (Fig. 11B, left), thus identifying it as a synaptically activated glutamate transporter current (TC). The slow current remained in the presence of TBOA, and can be inhibited by 200 μM $BaCl_2$ (Fig. 11B, right). At this concentration, Ba^{2+} effectively blocks inward rectifier K^+ channels (IRKs) that are highly expressed in astrocytes (D'Ambrosio et al., 2002; Newman, 1993). Because K^+ accumulates in the *stratum radiatum* after Schaffer collateral stimulation (Poolos et al., 1987), the Ba^{2+} sensitive component is consistent with IRK-dependent current in response to extracellular K^+ accumulation, and is called I_K hereafter.

Surprisingly, Ba^{2+} also strongly potentiated TC (from -36.4 ± 19.9 pA to -129.8 ± 68.9 pA, n = 5) (Fig. 12A). A typical 3-5 min application of Ba^{2+} was enough to reach a steady-state level of the TC amplitude and the holding current ($I_{(hold)}$) change (Fig. 12A). Interestingly, the recovery of TC amplitude during washout of Ba^{2+} was always clearly slower than that for holding current (Fig. 12A). After washout for 10 min, the holding current recovered to 7.6 ± 62.2 pA, which was not significantly different from baseline holding current (6.4 ± 29.3 pA, n = 5, p = 0.97), while TC remained potentiated (baseline: -36.4 ± 19.9 pA, washout: -100.7 ± 34.3 pA, n = 5, p =0.003) (Fig. 12B). This suggests that the mechanisms of Ba^{2+}-induced depolarization and TC augmentation are likely different.

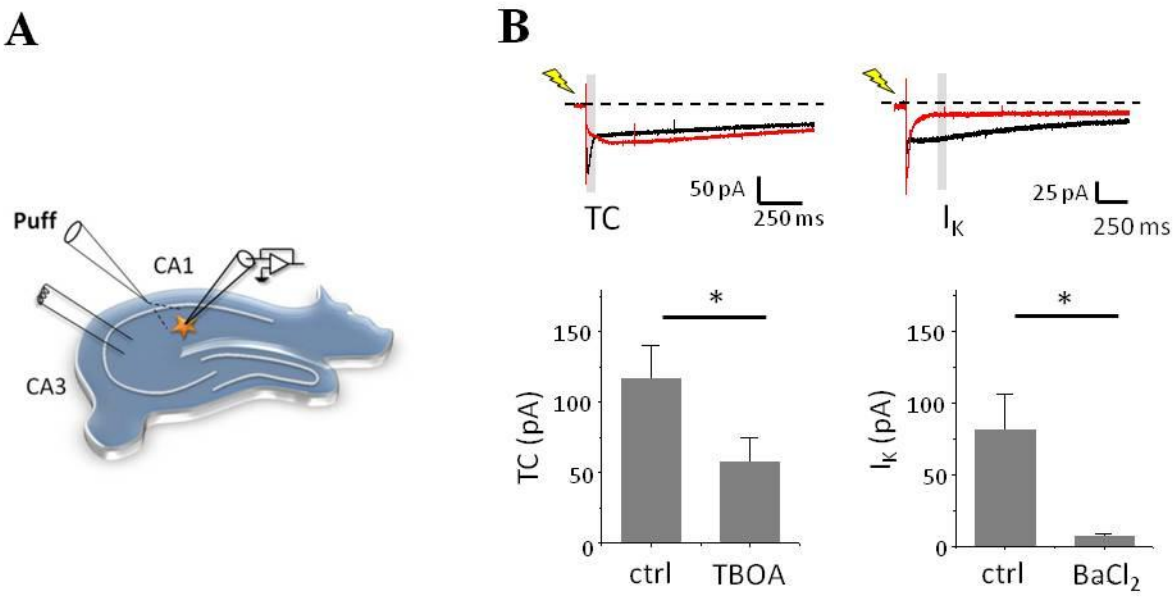

*Figure 11. The astrocyte response is composed of a glutamate transporter current (TC) and a potassium current (I_K). (A) Schematic drawing of the experimental arrangement showing the position of the stimulating electrode (or puff application) and recording electrodes in the hippocampal slice preparation. (B) A typical two-component current evoked in an astrocyte by stimulation the Schaffer collateral. Left: extracellular perfusion of the glutamate transporter blocker, TBOA (50 μM), depressed the transient component (light gray box). Black trace – control (ctrl), red trace – TBOA, yellow lightning – stimulation. Right: the slow component (light gray box, 250 ms away from stimulation) was blocked by the potassium channel blocker Ba^{2+} (200 μM). Black trace – ctrl, red trace – $BaCl_2$, yellow lightning – stimulation. Bottom is the graph summarized the results from five cells for each.*P < 0.05, paired t-test.*

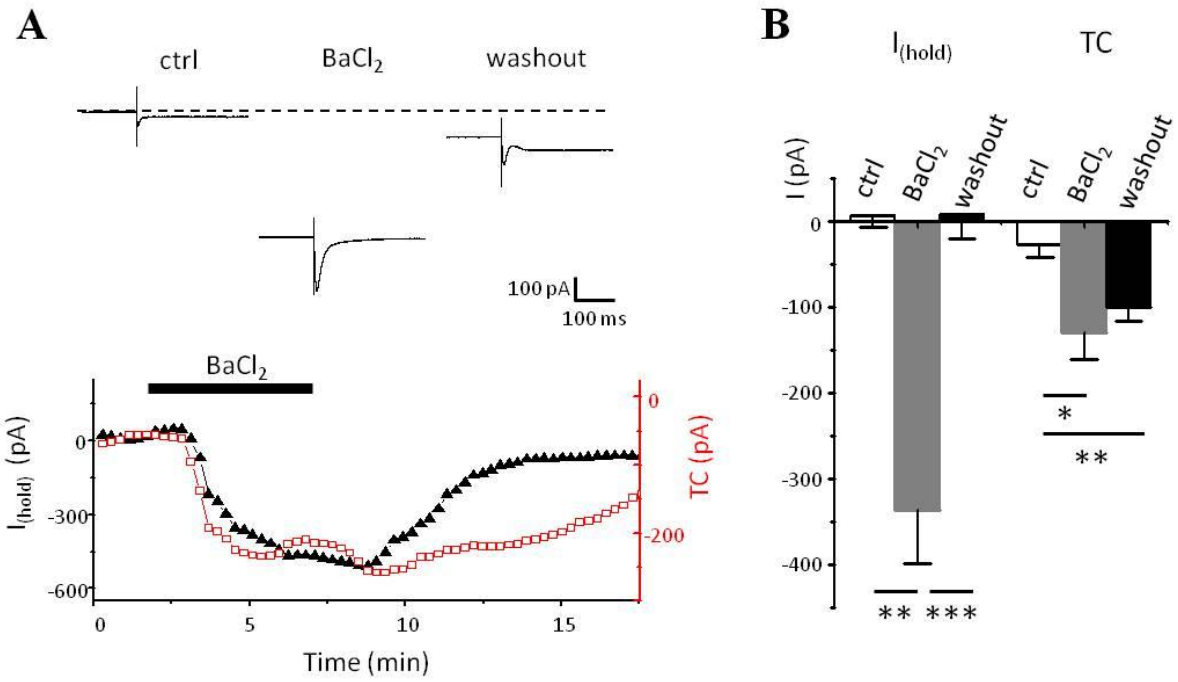

*Figure 12. Characterization of $BaCl_2$ effects on astrocytic response. (A) Current traces: astrocytic currents evoked by stimulation of Schaffer collateral at baseline (ctrl), 5 min after $BaCl_2$ application ($BaCl_2$) and 10 min after washout (washout). Bottom: time course of holding current ($I_{(hold)}$, black triangle) and glutamate transporter current (TC, red square) during 200 μM $BaCl_2$ application. Note the delayed recovery of TC compared to $I_{(hold)}$ while washout. (B) Summary of the $BaCl_2$ effect on $I_{(hold)}$ and TC. *P < 0.05, **P < 0.01, *** P < 0.001, paired t-test.*

Chapter 4: Mechanisms Underlying Astrocytic I_K

1. Postsynaptic NMDA Receptors Dominated I_K in Recorded Astrocyte

Measurements of $[K^+]_o$ with potassium ion-sensitive microelectrodes showed that activity-evoked increases in $[K^+]_o$ derive predominantly from postsynaptic neurons in *stratum radiatum* (Poolos et al., 1987). If this is the case, I_K should be inhibited by antagonists of postsynaptic glutamate receptors. Indeed, postsynaptic inhibition of AMPA and NMDA receptors with NBQX (25 μM) and AP5 (50 μM) did reduced most of the response (88.5 ± 5.9 % reduction, n = 5) (Fig 13A). The rest of the I_K could be blocked by TTX (1 μM) (Fig 13A). I then attempted to estimate the distinct contribution of AMPA and NMDA receptors on I_K by applying AP5 and NBQX sequentially. I found out AP5 has a much stronger blocking effect (62.3 ± 8.0 % reduction, n = 6) compared to subsequent applied NBQX (24.3 ± 7.3 % reduction, n = 5) (Fig. 13B), suggesting that under basal neuronal activity, slow I_K was mainly caused by $[K^+]_o$ accumulation associated with NMDA receptors.

In fact, AP5 can reduce excitability of presynaptic neurons and therefore recruitment of their axons by extracellular stimulation. To rule out this possibility, I puff applied glutamate (15-20 psi, 30-50 ms) 100 μm away from the recorded astrocyte in the presence of TTX (1 μM), NBQX (25 μM), MCPG (200 μM), and picrotoxin (100 μM) (Fig. 14A). I found that exogenous glutamate (400 μM) also produces a slow inward current sensitive to NMDA receptor antagonist, MK-801 (10 μM) (72.9 ± 6.1 % reduction, n = 4) (Fig. 14A). Moreover, by taking advantage of non-transportable property of NMDA, puff-applied 1 mM NMDA (Shah and Haylett, 2002) could induce I_K without TC (Fig. 14B). The puff-induced I_K was sensitive to both $BaCl_2$ and AP5 as well ($BaCl_2$: 95.9 ± 2.1 % reduction, n = 5; AP5: 93.8 ± 1.9 % reduction, n = 3) (Fig. 14B, bottom). I also confirmed that these puff-induced current was not due to mechanical stimulation,

because NMDA-free puff solution (ACSF) did not evoke such current on recorded astrocyte.

It has been reported that functional NMDA receptors are also present in astrocytes of some brain area, such as cortical cortex (Lalo et al., 2006). This opens the possibility that my recorded current actually resulted from astrocytic NMDA receptors. However, this is unlikely because I_K showed highly Mg^{2+}-sensitivity (Fig. 21), in contrast to the general agreement of astrocytic NMDA receptors in cortex (Lalo et al., 2006). In addition, previous immunocytochemical data indicated no expression of GluN1 subunit in hippocampal astrocytes which is indispensable for the formation of functional NMDA receptors under physiological condition (Cull-Candy et al., 2001; Dunah et al., 1999); this suggests functional astrocytic NMDA receptors may not exist in hippocampus.

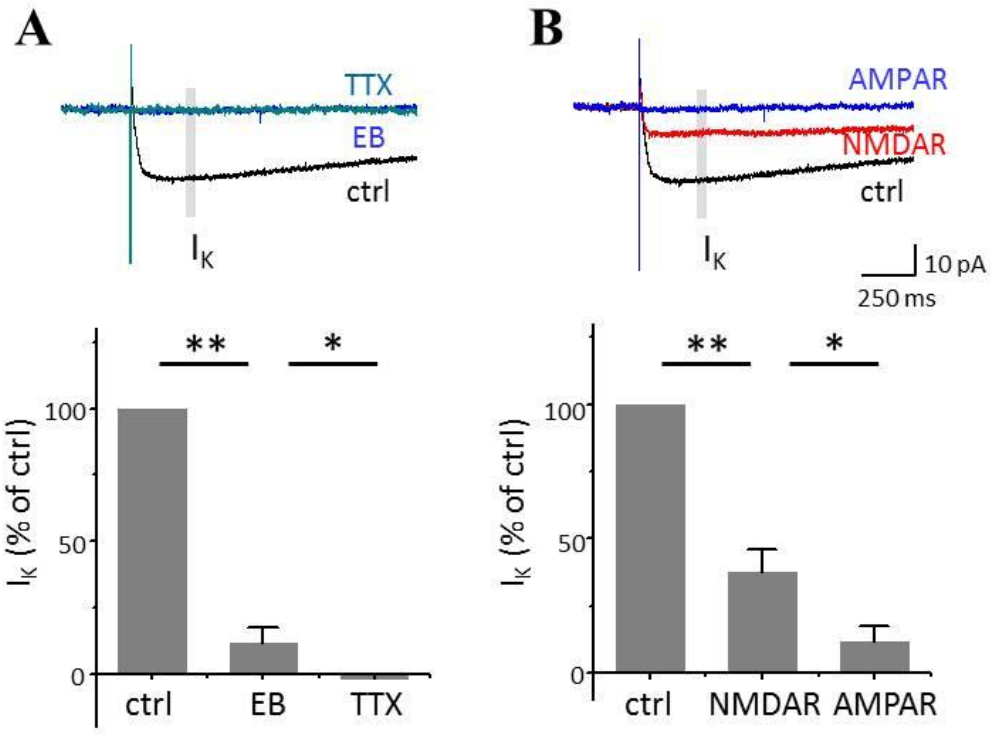

*Figure 13. NMDA receptors dominate I_K in recorded astrocytes. (A) top: example of electrical stimulation-induced I_Ks in a typical astrocyte and their inhibition by excitatory synaptic blocker (Excitatory blockers (EB) = NBQX and AP5, blue trace). Subsequent application of TTX abolished remaining I_K (green trace). (B) Similar recordings as shown in A, but AP5 (red trace) and NBQX (blue trace) were added sequentially. Note NMDAR contributes more to I_K than AMPAR. *P < 0.05, ** P <0.01, paired t-test.*

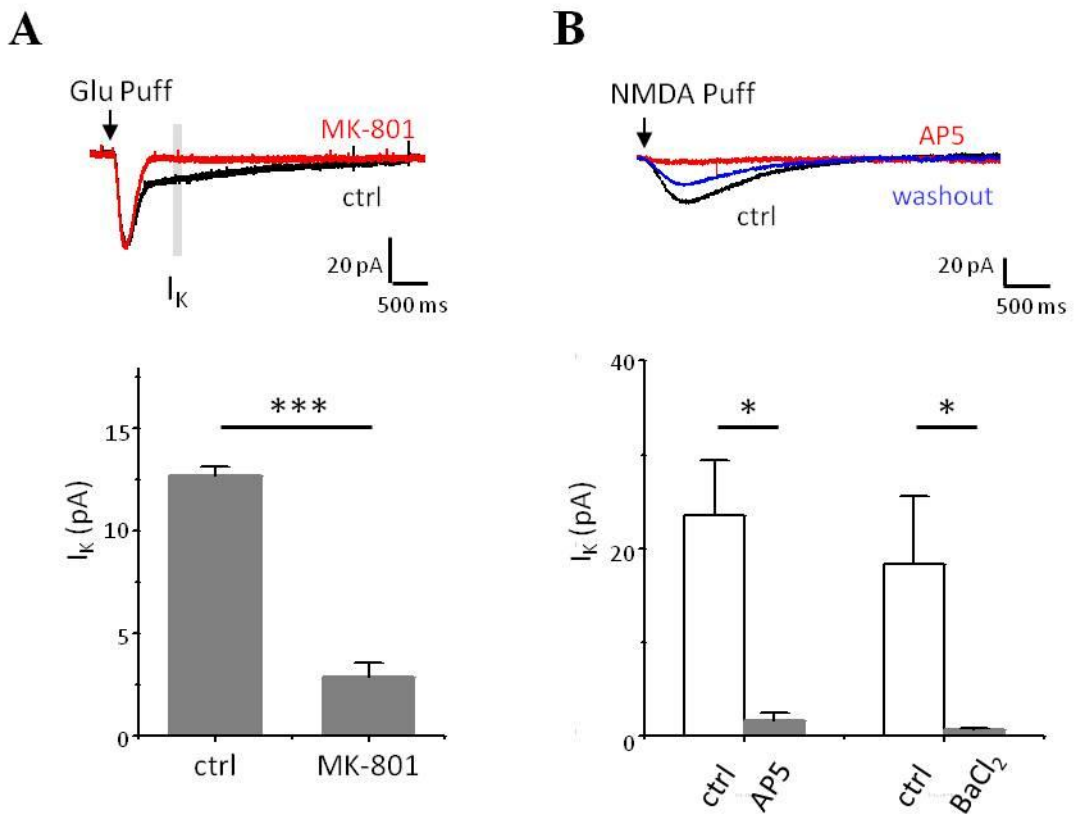

*Figure 14. Puff application of L-glutamate and NMDA evoked the slow K^+ current in hippocampal astrocytes. (A) Representative astrocyte responses to puffs of 400 μM L-glutamate in control solution (black trace) and with 10 μM MK-801 (red trace). MK801 significantly reduced the amplitude of the I_K. Arrow indicates when L-glutamate application was started (puff lasted for 50 ms). (B) Direct pressure application of 1mM NMDA in 1 μM TTX isolated the pure I_K responses without preceding glutamate transporter current in hippocampal astrocytes. Black trace – ctrl, red trace – AP5, blue trace – washout. Application of either AP5 or $BaCl_2$ blocked the puff-induced I_K. Bottom panel summarizes the reduction outcomes of AP5 and $BaCl_2$. *P < 0.05, *** P < 0.001, paired t- test.*

Because the pharmacological data suggest that NMDA receptors are the major source of I_K, I therefore sought to confirm whether these NMDA receptors are located at pre- or postsynaptic sites. The effect of NMDA receptor block on I_K was tested in CA1-NR1-knockout mice and their control littermates. In these CA1-NR1 KO mice strain, the GluN1 gene was postnatally knocked out specifically in postsynaptic CA1 pyramidal cells (McHugh et al., 1996; Nakazawa et al., 2004; Tsien et al., 1996). Previous *in situ* hybridization and immunohistochemistry studies showed that GluN1 mRNA level started to decrease in CA1 and subiculum from 1-month-old mutants, and disappeared almost entirely at 1.5 months of age (Fukaya et al., 2003). Because the identification of astrocytes with traditional IR-DIC microscopy in old animals (> 1.5 months) is difficult, I used astrocyte specific red fluorescence dye sulforhodamine 101 (SR101) (Nimmerjahn et al., 2004) to target astrocytes in this series of experiments (Fig. 15A). When exciting SR101 at 575 nm and collecting fluorescence emission above 590 nm, numerous SR101 labeled cells were observed throughout the *stratum radiatum* and hippocampus. Consistent with a previous report (Kafitz et al., 2008), SR101 positive cells had typical astrocyte morphology with several faintly labeled processes that emanated from a small cell body (Fig. 15A, right). I_K recorded in these stained cells revealed similar AP5-sensitivity in control slices. Conversely, I_K in CA1-NR1 KO slices was not significantly altered by AP5 (ctrl slice: 44.0 ± 2.7 % reduction; CA1-NR1 KO slice: 16.2 ± 6.6 % reduction, n = 6 for each, p = 0.002) (Fig. 15B), revealing that NMDA receptors located at postsynaptic sites are key players in the potassium flux during synaptic activity.

One might expect, therefore, that I_K induced in CA1-NR1 KO slices differs from that in control slices, either in amplitude or kinetic. Direct comparison of the I_K amplitude between control and

CA1-NR1 KO slice is difficult to interpret because of the varied distance between stimulus electrode and recorded astrocyte in each experiment. Normalization of I_K to TC is a reasonable resolution to this problem, but measuring the amplitude of TC proved to be difficult, as it was usually overlapped by following I_K. Therefore, I adjusted the stimulus amplitude to get similar amplitude of I_K in each experiment and compared the kinetic of I_K between control and CA1-NR1 KO mice by measuring the centroid (<t>, see Material and Methods, chapter 2.7.1). In astrocytes from control slices, the I_K centroids were significantly slower than those recorded in mutant slices ($<t>_{ctrl}$: 55.1 ± 3.4 ms, n = 9; $<t>_{mutant}$: 37.3 ± 3.6 ms, n = 6; p = 0.0077) (Fig. 15C). Notably, addition of AP5 in control slices shifted the centroid of I_K to smaller value as in mutant slices ($<t>_{AP5}$: 28.2 ± 3.7 ms, n = 6; p = 0.218), reflecting a faster mechanism, such as AMPA receptors or action potentials are responsible for the $[K^+]_o$ rise in KO mice. Indeed, blockade of AMPA receptors with NBQX resulted in a complete inhibition of I_K in the mutant slices (Fig. 15D). These results raise an intriguing possibility that AMPA receptors provide a virtual responsibility for the potassium release machinery in CA1-NR1 KO mice.

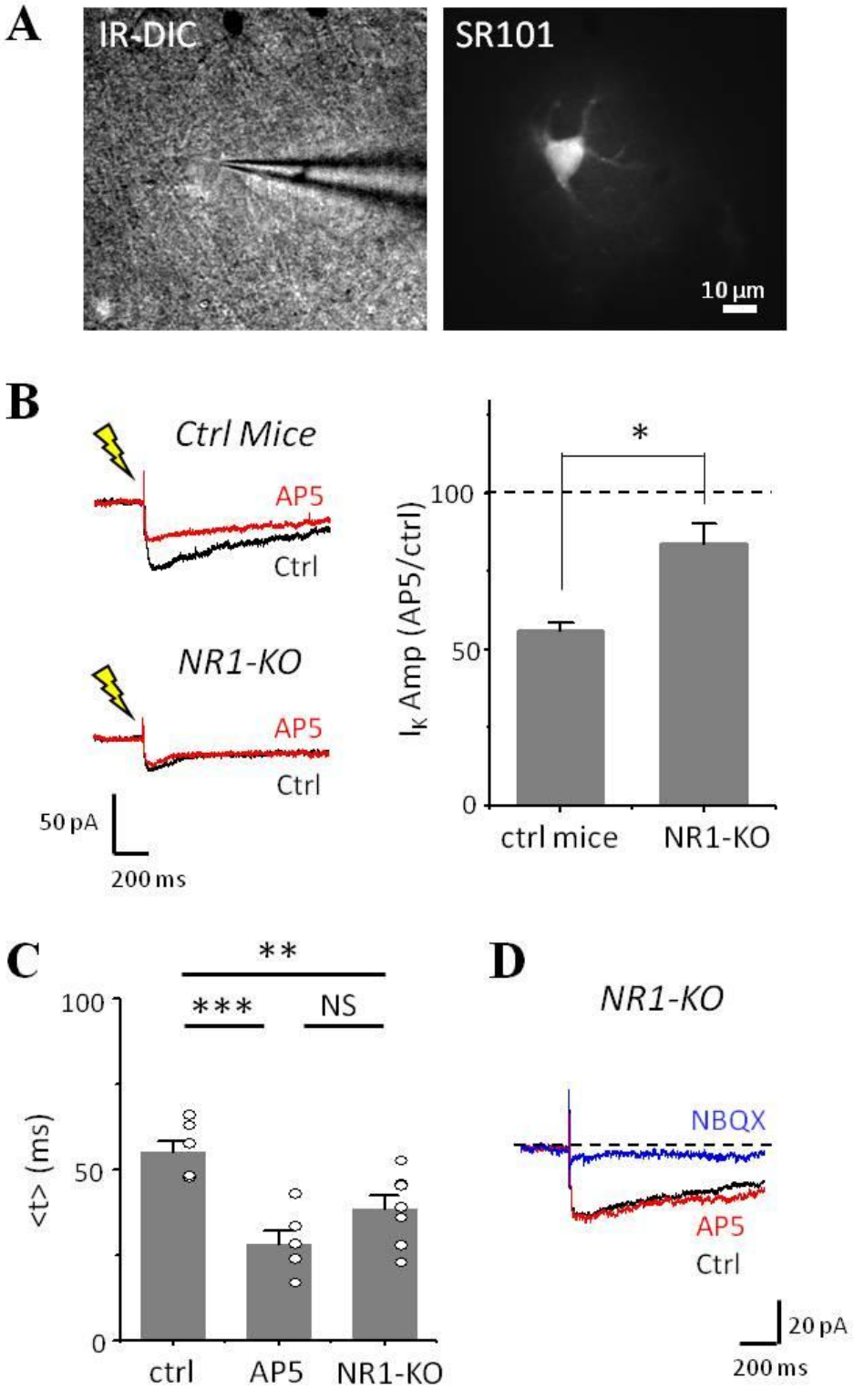
A
IR-DIC
SR101
10 µm
B
Ctrl Mice
AP5
Ctrl
NR1-KO
AP5
Ctrl
50 pA
200 ms
*
100
50
0
I_K Amp (AP5/ctrl)
ctrl mice
NR1-KO
C
**
***
NS
100
50
0
<t> (ms)
ctrl
AP5
NR1-KO
D
NR1-KO
NBQX
AP5
Ctrl
20 pA
200 ms

*Figure 15. The extracellular potassium rise depends on postsynaptic NMDA receptors. (A) Astrocytes of CA1-NR1 KO mice (> 1.5 months) were difficult to observe with standard IR-DIC illumination (left). Note the location of the patch electrode. Visulization with fluorescent illumination resulted in SR101 labeled cell with small cell bodies that were easily targeted for electrophysiology (right). (B) Left: representative traces of I_K recorded from ctrl (top trace) and NR1-KO (bottom trace) astrocyte. Black trace – ctrl, red trace – AP5. Right: Summary data for I_K perserved in AP5 in ctrl and NR1-KO animals. *P < 0.05, unpaired t-test. (C) Summary data showing that I_Ks recorded in NR1-KO astrocytes exhibited faster centroids than that in ctrl animal. Addition of AP5 shifted the current time course of I_K in ctrl animals to the same level as that in NR1-KO mice. (D) Bath application of NBQX completely inhibited I_K in NR1-KO astrocyte, indicating the origin of these currents is AMPA receptors. Black trace – ctrl, red trace – TBOA, blue trace – NBQX. *P < 0.05, ** P <0.01, ***P < 0.001, one-way ANOVA with post hoc Tukey test.*

2. NMDA Receptor-Mediated K^+ Release Does Not Require K_{Ca} and K_V Activation

The NMDA receptor is permeable to Na^+, Ca^{2+} and K^+, and its activation can cause local depolarization. Thus, extracellular K^+ elevation following activation of NMDA receptors can be mediated either by Ca^{2+}-dependent K^+ conductance (K_{Ca}) (Faber et al., 2005; Ngo-Anh et al., 2005) or voltage-gated potassium channels (K_V). To address the first possibility, I measured the potassium current induced by 1 mM NMDA puff in hippocampal astrocytes in control and in Ca^{2+}-free solution (Fig. 16A). I found that the amplitude of I_K remain unchanged even when extracellular Ca^{2+} was decreased (ctrl: 26.1 ± 3.4 pA; low Ca^{2+}: 31.7 ± 6.1 pA; n = 5 for each, p > 0.05) (Fig. 16B), pointing to its Ca^{2+}-independency.

K_V channels enriched in spines are another possibility (Alonso and Widmer, 1997; Kim et al., 2005). To study the regional voltage change during astrocyte recording, I simultaneously performed field recording with an extracellular electrode placed close to the recorded astrocytes. Stimulus-induced astrocytic I_Ks were lead by a negative shift in field potential in all experiments (Fig. 17A). When I compared the pharmacological sensitivity of I_K and field recording, I found that AP5 significantly attenuated I_K with only a minor effect on field potential (I_K: 37.7 ± 8.0 % of ctrl; fEPSP: 83.3 ± 4.6 % of ctrl, n = 6) (Fig. 17B). Subsequent NBQX application preferentially blocked the field potential (I_K: 11.5 ± 5.9 % of ctrl; fEPSP: 2.3 ± 4.9 % of ctrl, n = 5) (Fig. 17B). The results suggest that although stimulation leads to a synchronized AMPA-mediated depolarization in an adjacent group of pyramidal neurons, astrocytic potassium conductance did not depend on membrane potential change in nearby neurons.

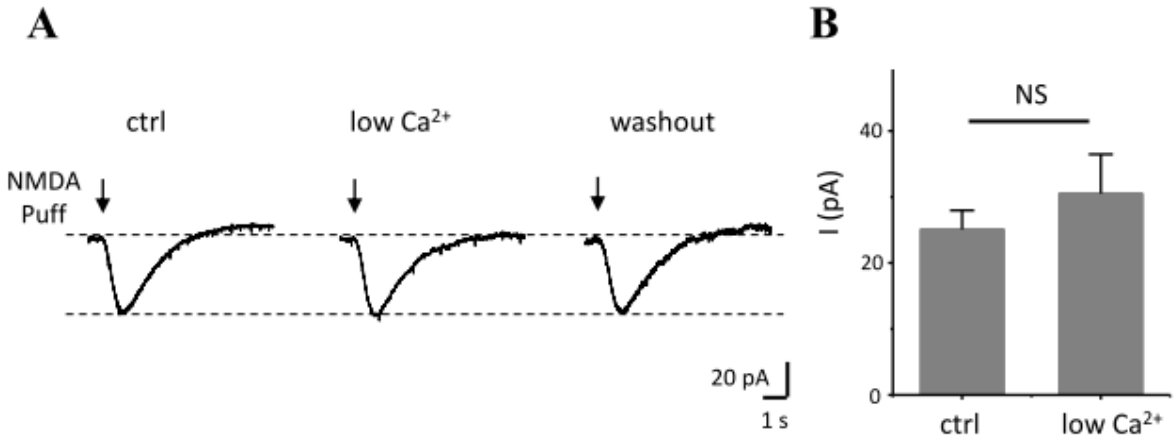

Figure 16. NMDA receptor-mediated K^+ release is independent on K_{Ca} (A) Example of the I_K present in baseline, during low Ca^{2+} buffer, and washout. (B) Comparison of the mean amplitude of I_K in control condition and present with low Ca^{2+} buffer. Graphs show means ± SE. There is no significant difference between these two conditions.

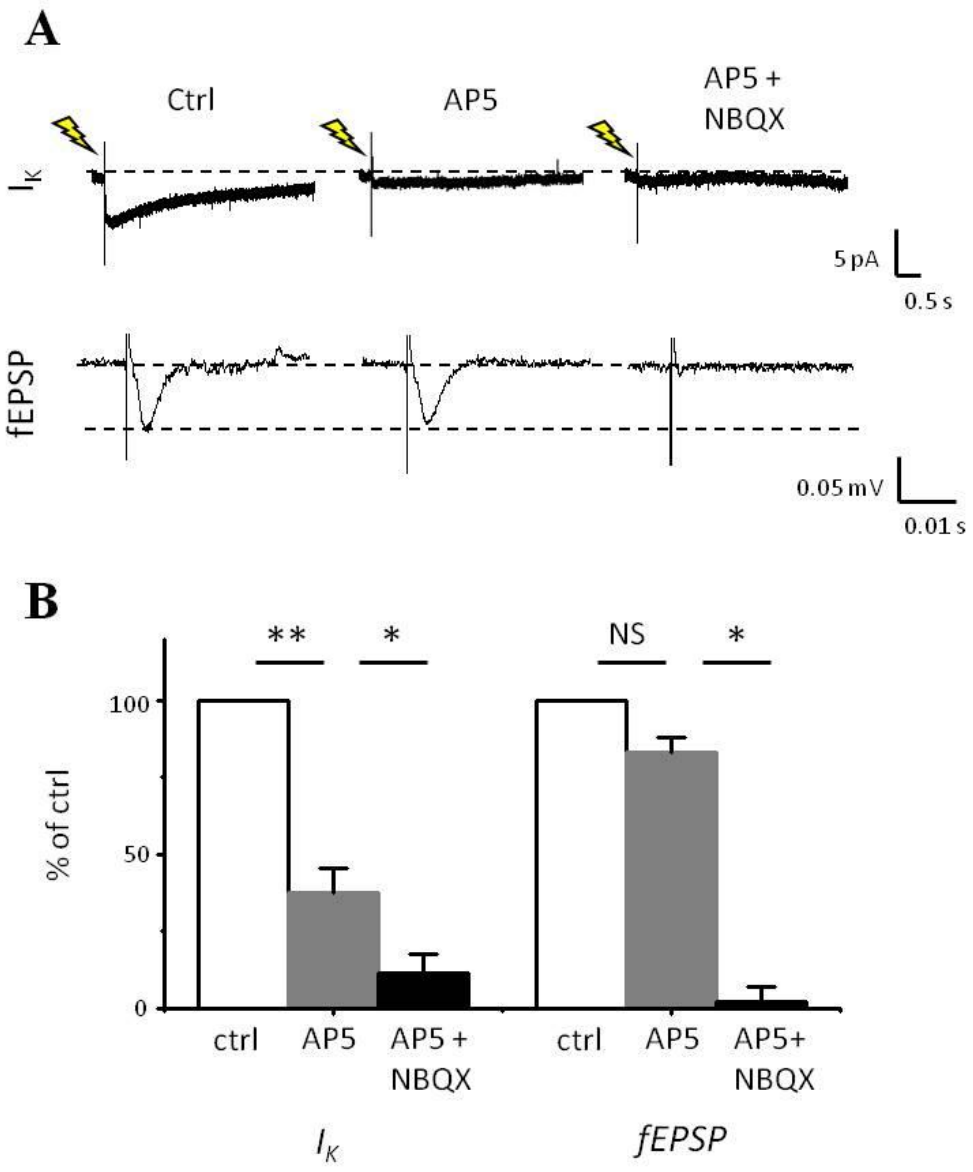

*Figure 17. Minor contribution of K_V on NMDAR-mediated K^+ release. (A) Upper: Example trace of astrocytic potassium current in control, application of AP5 and later NBQX. Bottom: Example trace of concomitant fEPSP recording. (B) Comparison of the mean amplitude of I_K and fEPSP under these three conditions, normalized to amplitude in control. AP5 siginificantly attenuated I_K with small effect on fEPSP; whereas subsequent NBQX has opposite effect. *P < 0.05, ** P <0.01, paired t-test.*

Chapter 5: NMDAR-Dependent K^+ Elevation Localized to Active Synapse

1. Simulated Potassium Concentration Time Course around the Synaptic Cleft

The experiments described thus far indicate that activation of NMDA receptors contributes a significant proportion of $[K^+]_o$ during synaptic transmission. Because in mature animals NMDA receptors concentrated synaptically (Hardingham and Bading, 2010; Rosenmund et al., 1995), I expect the associated $[K^+]_o$ elevation would be correspondingly larger within the synapse. Thus, a simple simulation was performed to obtain a quantitative estimate of NMDA receptor-mediated $[K^+]_o$ within the synapse, which cannot be measured by available techniques (Fig. 18). In my simulation, the synapse was represented as two flat cylinders, pre- and postsynapse, located opposite to each other at a cleft distance δ (20 nm). The radius of the circular surface defines the extent of the contact zone (R_s, 300 nm) (Barbour and Hausser, 1997) (Fig. 18A). The postsynaptic receptors were distributed within a smaller disk, with a radius, R_{az} (100 nm) < R_s. This configuration is consistent with electron microscopic images of central synapses (Triller and Korn, 1982), where the synaptic region may extend appreciably beyond the region delineated by the apposing postsynaptic density (PSD). The latter in turn is often associated with the receptor matrix, and generally does not encompass the full contact zone. The receptor disk is concentric with the contact zone, with its center apposed to the presynaptic release site. Exocytosis is approximated with the instantaneous placement of a predefined number of molecules (3000 glutamate) in a packet apposing the presynaptic "release site", which is centered in the contact zone. Diffusion spreads the quantal packet throughout the contact zone, and some molecules will reach the postsynaptic receptors. Diffusion is modeled as a random walk process (Kruk et al., 1997; Stibitz, 1969), with each transmitter molecule moving in the x and y dimensions independently of other molecules. After a large number of time steps, the probability of finding the molecule at any grid point in the cleft will approach a Gaussian distribution centered around

the point of departure. Interaction of molecules with borders was modelled as an elastic collision. The free diffusion with the coefficient D_{in} inside the cleft and D_{out} (> D_{in}) outside the cleft was simulated using the Monte Carlo algorithm.

The K^+ flowed from postsynaptic neurons through NMDA receptors in the cleft and changed the $[K^+]_o$ in the cleft. The modification of $[K^+]_o$ was calculated inside different sphere with maximum radius of 5 PSD radius (up to 500 nm). At any discrete time, the $[K^+]_o$ inside each *i-th* ring of radius r_i and width *dr* was calculated using the diffusion equations below for inside and outside of PSD, respectively.

$$\frac{\partial[P]}{\partial t} = D\frac{1}{r}\frac{\partial}{\partial r}(r\frac{\partial[P]}{\partial r}) + \frac{N\gamma[0](E_m - E_{NMDA})}{F\,V} \quad [P]_{out} = 2.5mM \qquad \text{for } r < R_{az}$$

$$\frac{\partial[P]}{\partial t} = D\frac{1}{r}\frac{\partial}{\partial r}(r\frac{\partial[P]}{\partial r}) \qquad \text{for } r > R_{az}$$

Where [P] is $[K^+]_o$, D is the diffusion coefficient of K^+, N is the total number of NMDA receptors, [0] is a proportion of open NMDA receptors, F is Faraday constant, $V = \pi\delta R_{AZ}^2$ is the cleft volume.

The $[K^+]_o$ in each sphere was used to calculate the reversal potential of regional NMDA receptors according to the formula ($V_{NMDAR} = \frac{RT}{F} Ln(\frac{P_{Na}[Na^+]_0 + P_{Ca}[Ca^+]_0 + P_K[K^+]_0}{P_{Na}[Na^+]_i + P_{Ca}[Ca^+]_i + P_K[K^+]_i})$). The total postsynaptic current was calculated as $I_{NMDAR}=N\gamma(V_m-V_{NMDAR})$, where N was the number of

NMDAR, γ was single receptor conductance, and V_m was the resting membrane potential.

Glutamate release in the simulated synapse triggered NMDA receptor currents (I_{NMDA}) that increased with the number of postsynaptic NMDARs (N) (Fig 18B). Electron microscopy data has suggested 0-35 NMDARs per hippocampal synapse (Racca et al., 2000). In my simulation, activation of 10 NMDARs produced a peak $[K^+]_o$ of 7 mM. Increasing the number of NMDARs to 30 produced more than 15 mM $[K^+]_o$ (Fig. 18C). Additionally, this model predicted the confined dispersion of elevated $[K^+]_o$ (Fig. 18D). $[K^+]_o$ approached a peak concentration at the center of the modelled synapse, but dropped substantially with distance. At the edge of the synapse (300 nm from the center), $[K^+]_o$ almost fell back to the basal value. Hence, activation of physiological number of NMDARs could produce high $[K^+]_o$ restrained mainly inside the synapse or vicinity of the synaptic cleft.

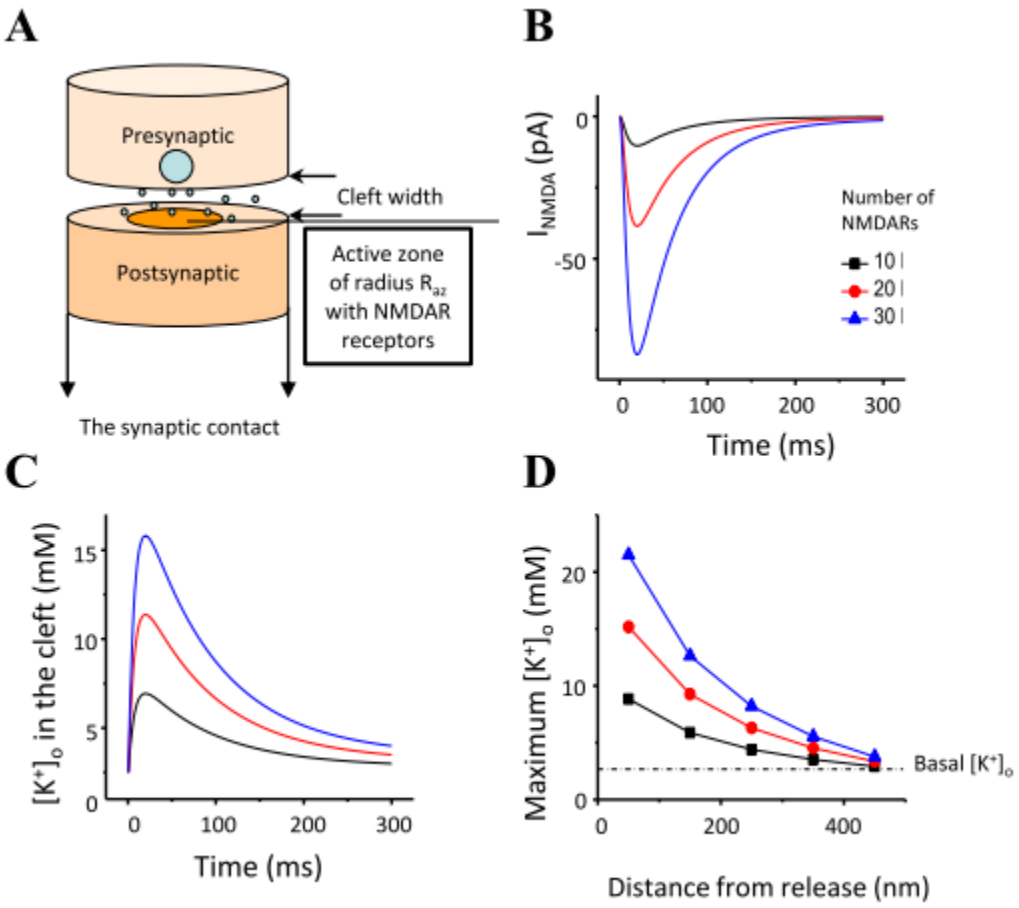

Figure 18. The effect of adjusting postsynaptic NMDA receptor numbers on $[K^+]_o$. (A) A schematic diagram of a model synapse. The width of a cleft is 15-25 nm, and the radius of active zone (R_{az}) is 60-160 nm. Both NMDA current (B) and extracellular potassium concentration (C) increased with the inserted NMDA receptor numbers. Note that insertion of 10 NMDA receptors is enough to induce $[K^+]_o$ more than 5 mM (D) Extracellular potassium concentration quickly declined with the distance from the release site for different inserted number of NMDA receptors. Black trace – 10 NMDAR, red trace – 20 NMDAR, blue trace – 30 NMDAR.

2. Extracellular Presynaptic Afferent Volleys in Response to NMDAR-Mediated $[K^+]_o$

This simplified model presented above allowed us to explore the possible concentration and spatial distribution of NMDAR-mediated $[K^+]_o$. My model, however, had certain limitations such as free diffusion of K^+ outside of the synaptic cleft and a lack of K^+ uptake. In fact, K^+ uptake by astrocytes should effectively clean K^+ outside the synaptic cleft, while tortuous extracellular space should slow down its diffusion. These mechanisms should not however affect the model prediction; if anything they could further reduce spill of synaptically released K^+ outside of the cleft. I further confirmed that NMDAR dependent K^+ efflux does significantly contribute to extrasynaptic K^+ concentration by estimating its effect on the presynaptic fiber volley (PrV) during prolonged activity. Properties of PrV are sensitive to extracellular potassium change (Meeks and Mennerick, 2004; Poolos et al., 1987). Bath perfusion of different $[K^+]_o$ induce biphasic change of the amplitude of PrV (Fig. 19); 5 mM $[K^+]_o$ increased the amplitude (104.5 ± 0.8 % of ctrl, p = 0.025), while 7.5 mM $[K^+]_o$ decreased it (87.3 ± 2.2 % of ctrl, p = 0.005) (Fig. 19B, left). $[K^+]_o$ also affected the rise time. Application of 7.5 mM $[K^+]_o$ prolonged the rise time of presynaptic volley to 111.3 ± 0.4 % of ctrl (Fig. 19B, right, p = 0.0008). I then tested if high frequency stimuli would produce an NMDAR-mediated $[K^+]_o$ buildup in the extracellular space (Fig. 20). A train of 10 stimuli was applied at 20, 50 and 100 Hz. I found the final presynaptic volleys (10^{th}) were significantly depressed and prolonged compared to the 1^{st} one at high frequency stimulation (100Hz) (amp: 81.0 ± 6.7% of 1^{st}, p = 0.036; rise time: 108.9 ± 1.6 % of 1^{st}, p = 0.0016, Fig. 20B). However, AP5 application showed no significant effects on both properties of the presynaptic volleys evoked by train of stimuli ($10^{th}/1^{st}$ amp: 97.5 ± 4.8 % of ctrl, p = 0.62, $10^{th}/1^{st}$ rise time: 98.7 ± 1.2 % of ctrl, p = 0.35, Fig. 20B). These results implied that NMDAR-mediated K^+ might work locally and rather minor axon conduction regulation can be

associated with NMDAR-dependent K^+.

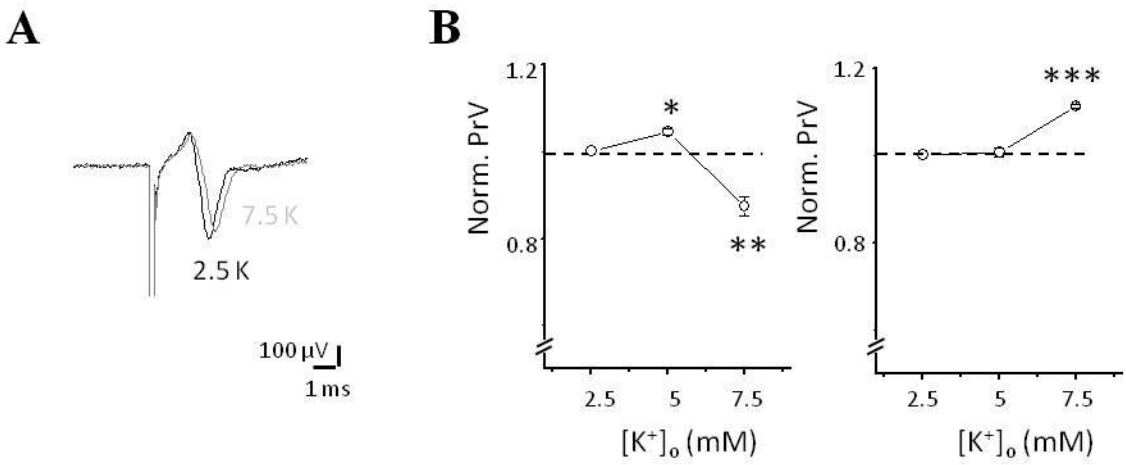

*Figure 19. Effects of extensive $[K^+]_o$ rise on afferent volleys. (A) Example trace of afferent volley waveforms; each trace represents the average of five trials. The control $[K^+]_o$ (2.5 mM, black trace) condition is plotted as the black trace and high $[K^+]_o$ (7.5 mM, gray trace) condition as gray trace. Synaptic field potentials are blocked in both conditions. (B) Summary of different $[K^+]_o$ effect on afferent volley amplitudes (left) and time to peak (right). Raising $[K^+]_o$ caused a biphasic modulation of amplitudes, while time to peak was increased at 7.5 mM $[K^+]_o$. *P < 0.05, ** P <0.01,*** P < 0.001, paired t-test.*

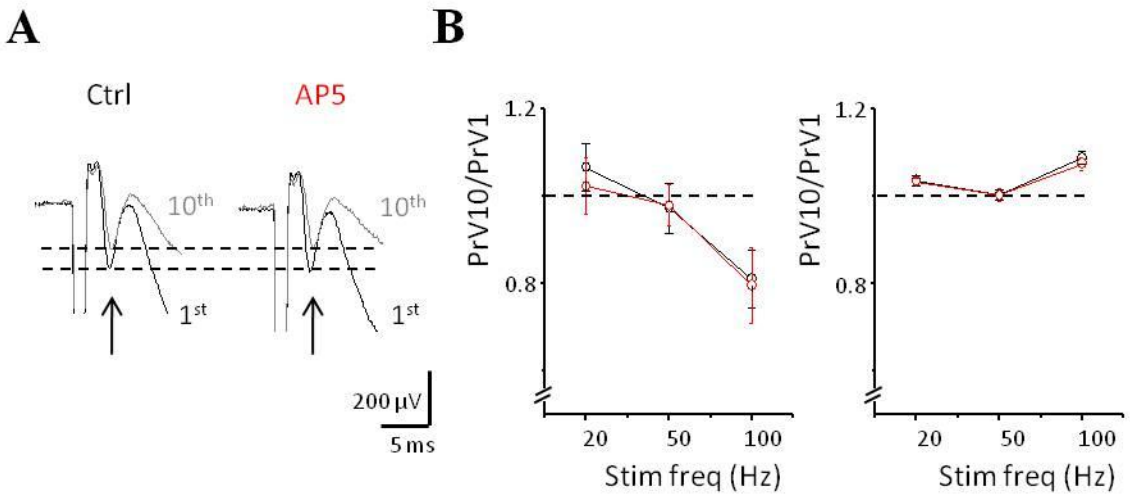

Figure 20. Effect of NMDA receptor antagonist on afferent volley trains. (A) Averaged traces showing the first conditioning (stimulus 1, black trace) and last (stimulus 10, gray trace) response from a 10 pulse train delivered at 50 Hz. Arrows indicate afferent volley peaks in the test condition. (B) Summary of the effect of AP5 on amplitude (left) and time to peak (right) of the afferent volley trains at different stimulation frequencies. Black circles, control; red circles, responses in AP5 No significant effect of AP5 was observed in the frequency-dependent depression of the fiber volley.

Chapter 6: Activity-Dependent Regulation of NMDA Receptor-Mediated K^+ Efflux

1. Mg^{2+}-dependence

NMDA receptors are blocked in a voltage-dependent manner by extracellular Mg^{2+} (Mayer et al., 1984; Nowak et al., 1984). I thus examined if I_K is regulated in the same manner as NMDA receptors. Indeed, removal of Mg^{2+} significantly enhanced synaptic-induced I_K from 52.5 ± 20.9 pA to 207.6 ± 58.9 pA (p = 0.029) (Fig. 21). Similar enhancement was observed with puff application of NMDA; the I_K increased from 36.0 ± 7.7 pA to 88.2 ± 17.6 pA (p = 0.007) (Fig. 21).

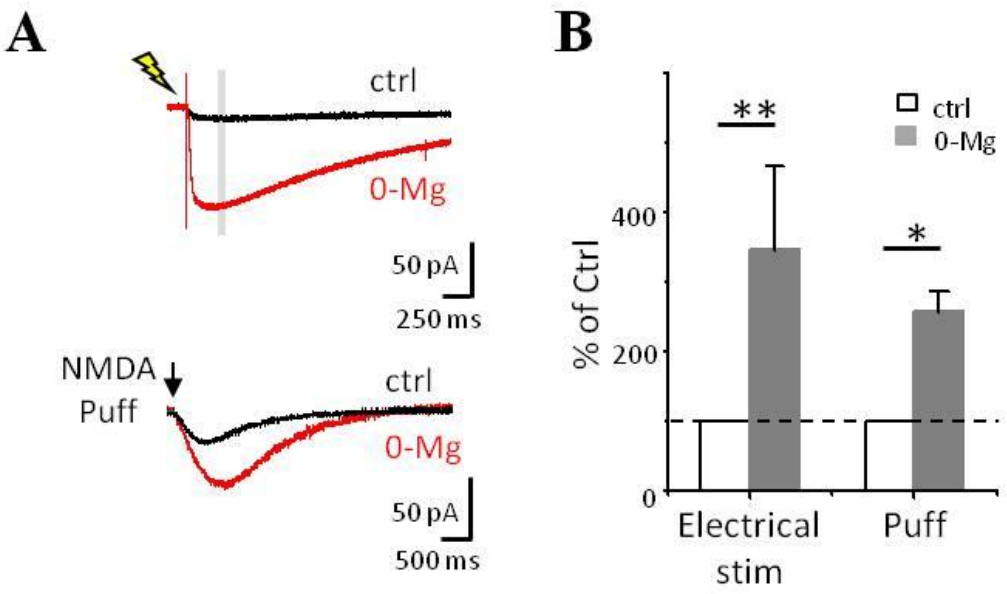

*Figure 21. Magnesium removal enhances the K^+ current. (A) In the absence of extracellular Mg^{2+}, the electrical stimulation (top trace) or puff application of NMDA (bottom trace) induced a significant increase in the amplitude of astrocytic K^+ current. Black trace – ctrl, red trace - Mg^{2+}-free solution (0-Mg). (B) Summary showing the significant effects of Mg^{2+}-free solution on conditioning K^+ current induced by either electrical stimulation or puff. *P < 0.05, ** P <0.01, paired t-test.*

2. Dependence of I_K on Number of Stimuli

Under physiological conditions, Mg^{2+}-block of NMDA receptors can be relieved through depolarization of the neuron, such as following synaptic activity via trains of stimuli. I next studied I_Ks elicited by single stimulus and burst stimuli with high frequency stimulation, which mimicked the natural spiking patterns in hippocampus (Dobrunz and Stevens, 1999; Suzuki and Smith, 1985). The dependence of I_K on the number of spikes in the short presynaptic bursts is demonstrated at Fig. 22. The amplitude of I_K induced by burst stimuli was always normalized to that of the single stimulus. The normalized amplitude of I_K was 5.4 ± 1.6 with 3 stimuli (n = 6) and 8.5 ± 2.2 with 5 stimuli (n = 6, p = 0.013) (Fig. 22B, left). Addition of AP5 decreased the I_K amplitude in each condition, and linearized the relationship between the synaptic stimulus number and I_K amplitude (3.2 ± 0.5 with 3 stimuli; 4.9 ± 0.8 with 5 stimuli) (Fig. 22B, right).

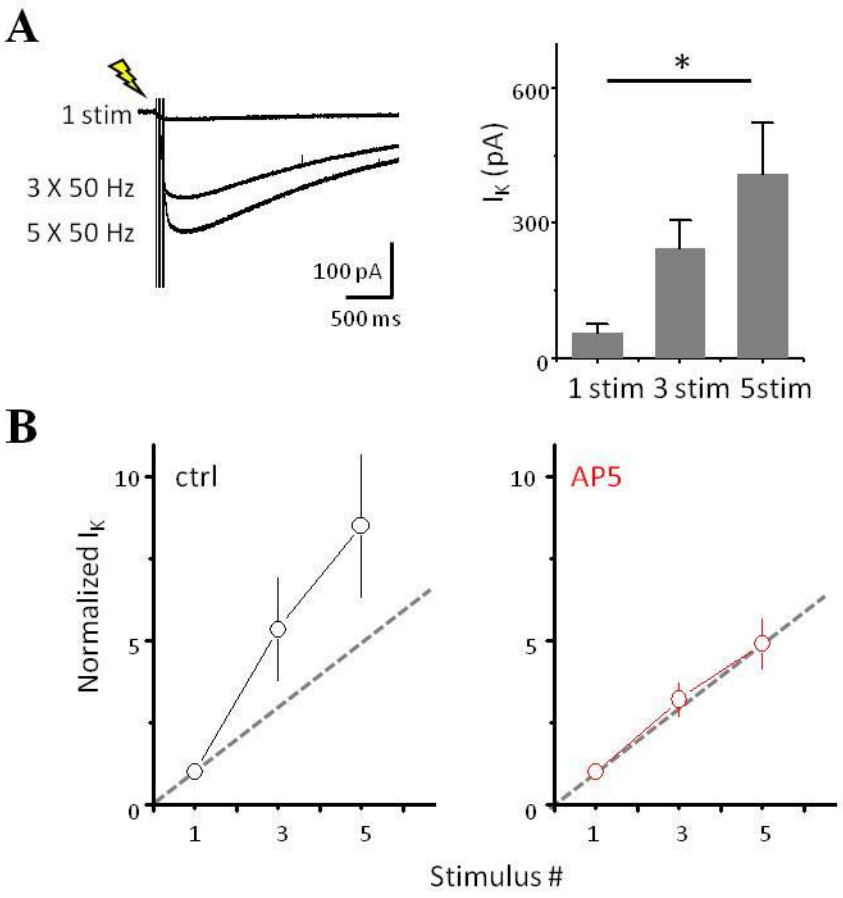

*Figure 22. Supralinear increase in I_K with number of stimuli. (A) Left: example trace of I_K induced by a single pulse (1 stim) and by 3 and 5 pulses at 50 Hz. Right: the averaged amplitude of I_K increased as a function of stimuli number. (B) The averaged I_K amplitude by a single pulse and the train stimulation recorded in control solution (black circle) and in the presence of AP5 (red circle). I_K induced by single pulse was taken as 100%. The dashed line indicates a linear response. *P < 0.05, one-way ANOVA followed by Tukey test.*

3. Pre/Post Pairing Results in Supralinear Rise of I_K

Mg^{2+} block of NMDA receptors can also be relieved by backpropagating action potentials (bAPs). I thus paired synaptic and antidromic stimulations by arranging recording and

stimulating electrodes as shown in Fig. 23A. The synaptic response (Fig. 23B, left trace) was elicited by a stimulating electrode placed in the *stratum radiatum* and sensitive to NBQX, while the antidromic response was elicited by the stimulating electrode placed in the outer border of the alveus and was insensitive to NBQX (Fig. 23B, right trace). As illustrated, synaptic stimulations (3 stimuli, 33-50 Hz) caused a prominent K^+ current preceded by transient glutamate transporter current in recorded astrocytes (Fig. 23C, left trace), whereas bAPs (3 stimuli, 33-50Hz) produced only K^+ current (Fig. 23C, middle trace). Combining bAPs with synaptic stimulation, however, resulted in a supralinear summation of astrocytic K^+ currents (Fig. 23C, right trace). The response to pairing of synaptic and antidromic stimulation induced K^+ currents that reached 129.3 ± 12.6 % of the computed sum of each response separately (n = 10 , Fig. 23D), and this supralinear summation was completely abolished by administration of AP5. The amplification ratio decreased back to 99.8 ± 4.5 % in AP5 (p = 0.001, n = 5, Fig. 23D). These findings provide direct evidence that K^+ efflux through NMDA receptors is closely related to activity-dependent Mg^{2+} unblock of NMDA receptors, and can be a potential feedback factor to regulate the strength of synaptic connection in activity dependent manner.

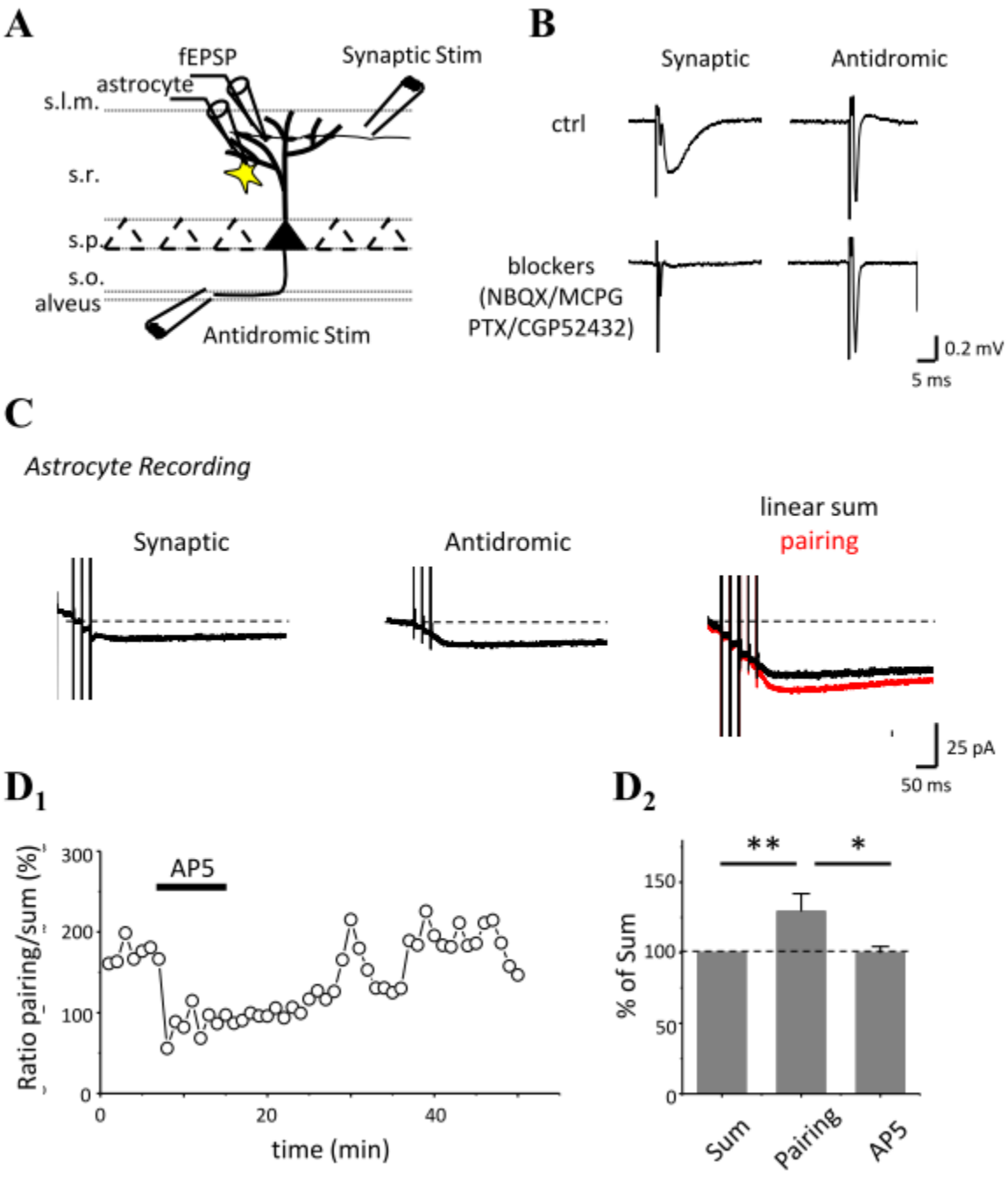
A
fEPSP
Synaptic Stim
astrocyte
s.l.m.
s.r.
s.p.
s.o.
alveus
Antidromic Stim
B
Synaptic
Antidromic
ctrl
blockers
(NBQX/MCPG
PTX/CGP52432)
0.2 mV
5 ms
C
Astrocyte Recording
Synaptic
Antidromic
linear sum
pairing
25 pA
50 ms
D1
Ratio pairing/sum (%)
AP5
300
200
100
0
0
20
40
time (min)
D2
% of Sum
150
100
50
0
**
*
Sum
Pairing
AP5

*Figure 23. Supralinear effect of pairing on I_K. (A) Schematic illustration showing the placement of two recording and two stimulating electrodes. Field potential (fEPSP) and astrocyte patch clamp recording (astrocyte) were obtained simultaneously. Stimulus electrodes were placed in s. radiatum and alveus to induce synaptic and antidromic responses, respectively. (B) Examples of fEPSPs evoked by either synaptic or antidromic stimulation in control and in the presence of blockers. Note that only the synaptic response was sensitive to blockers. (C) Representitive recording of astrocytic I_K evoked by synaptic stimulation (3 stimuli, 33-50 Hz), antidromic stimulation (3 stimuli, 50Hz), and positive pairing of two stimuli at 3 ms interval. The black line in pairing condition indicates the computed sum of I_K evoked by either synaptic or antidromic stimulation in isolation, and red line is the paring result. (D_1) Example plot showing the effect of AP5 on I_Ks evoked by pairing stimulation. (D_2) Normalized changes in I_K amplitude of linear sum, during pairing protocol, and pairing in the presence of AP5. *P < 0.05, ** P <0.01, paired t-test.*

Chapter 7: NMDA Receptor-Mediated K^+ Efflux Modulates Presynaptic Functions

1. NMDA Receptor-Mediated Changes in $[K^+]_o$ Modulate Ca^{2+} Transients in Single Boutons

An increase in $[K^+]_o$ can lead to presynaptic depolarization, and in turn modulate the efficacy of transmitter release (Barish et al., 1996; Hori and Takahashi, 2009). I therefore tested the effect of NMDAR-mediated $[K^+]_o$ on presynaptic Ca^{2+} concentration with two-photon Ca^{2+} imaging. Because spike-evoked axonal $[Ca^{2+}]_i$ is usually in hundred nanomolar range or even higher (Brenowitz and Regehr, 2007; Koester and Sakmann, 2000), I chose a calcium indicator, Fluo-5F, which has low Ca^{2+} affinity (K_d of 1.6 μM at 24 ℃) (Yasuda et al., 2004). To confirm the fluorescence response of Fluo-5F would not be saturated by the high frequency stimuli, I first loaded cells with 200 μM Fluo-5F and, after indicator diffusional equilibration, recorded Ca^{2+} mediated fluorescence in presynaptic boutons in response to 30 APs at 100 Hz (Fig. 24C). The resulting linear increase in fluorescence suggests that Fluo-5F did not reach saturation even under this strong stimulation.

I then performed whole-cell current-clamp recordings from CA3 pyramidal neurons with pipettes containing Fluo-5F (200-300 μM, green, G) and morphological tracer, A594 (50 μM, red, R) (Fig. 24A & 25A). At the light microscopy (LM) level, individual CA3 → CA1 branches are seen as thin unmyelinated axons with numerous putative presynaptic boutons (identified as ~1 μm swellings on axon collaterals occurring, on average, approximately every 3-5 μm) (Fig. 24A, inset) (Andersen et al., 1994; Shepherd and Harris, 1998; Sik et al., 1993). Line scans around 500 Hz were performed across individual boutons and the fluorescent signals of A594 and Fluo-5F were simultaneously acquired (Fig. $25B_1$). For each experiment, a set of 12 frames (line scan) were captured in an interval of 1 minute to quantify calcium dynamics: six frames for control and six frames after 5 minutes of solution exchange or drug application (Mg^{2+}-free ACSF or AP5).

The baseline fluorescence (G_0/R) was taken as the average fluorescent signal before action potential induction. A train of action potentials (50 Hz, 5 stimuli) was evoked by somatic current injection (indicated by the arrow in Fig. $25B_2$), and the resulting change in Ca^{2+} was monitored as the change in peak green fluorescence normalized to the average red fluorescence ($\Delta G_P/R$) (Fig. $25B_2$, bottom). In no case was a failure of Ca^{2+} response observed within repeated trials in each responsive bouton. Trials in which no current was injected are shown for comparison (Fig. 24B). Intriguingly, I found that CA3 boutons showed a large variation in the peak amplitude of the AP-evoked Ca^{2+} transient, even when they were located within a short segment of the same axon (Fig. 25C). For two boutons on the same axon segment, the percentage difference of $\Delta G_P/R$ can range from 0.2 % to 15.6 % (n = 20 axons). These experiments establish that I was able to reliably detect presynaptic Ca^{2+} transients in single bouton in response to action potential trains, and the signal-to-noise ratio of the fluorescence transients were sufficiently high to clearly distinguish action potential-evoked Ca^{2+} transients from control trials in which no action potential was evoked.

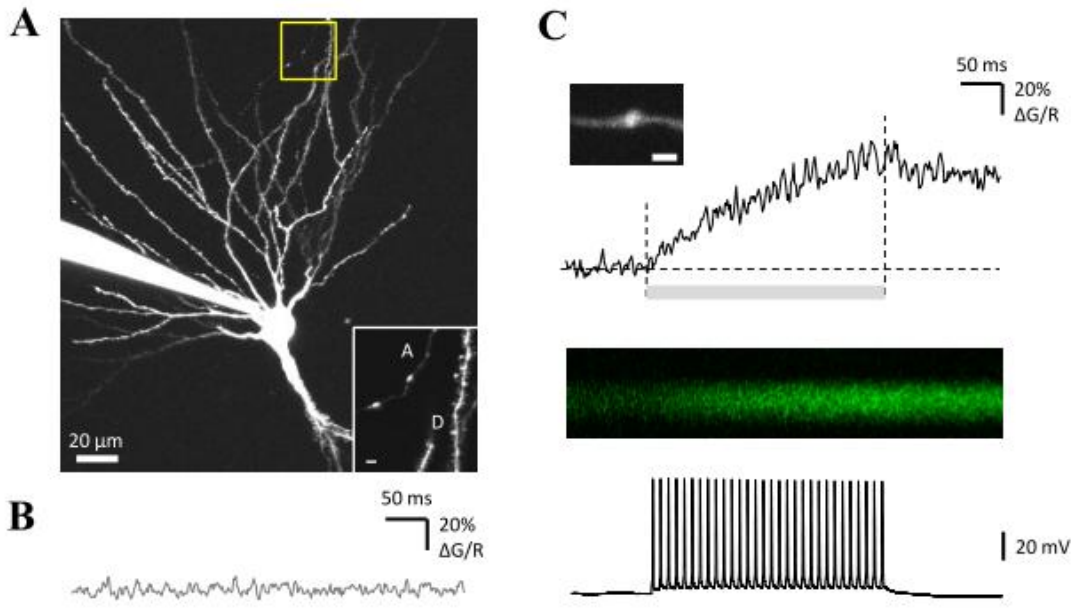

Figure 24. Measuring presynaptic calcium in single CA3 pyramidal cell bouton. (A) Two-photon image of a CA3 pyramidal cell loaded with a patch pipette with 200 µM Fluo-5F and 50 µM A594. Inset, field of the yellow box shown at higher zoom. Axon (A) and dendrites (D) can be easily distinguished by their distinct morphologies. Inset scale bars, 1 µm. (B) An example line-scan fluorescence time course in which no AP was induced. (C) The identified bouton (inset) and the corresponding line-scan ΔG/R signal (trace and middle panel; recorded at 500 Hz) in response to 30 APs at 100 Hz (bottom panel). Gray bar represents the interval of AP application. Note the fluorescent response is not saturated with this stimulation.

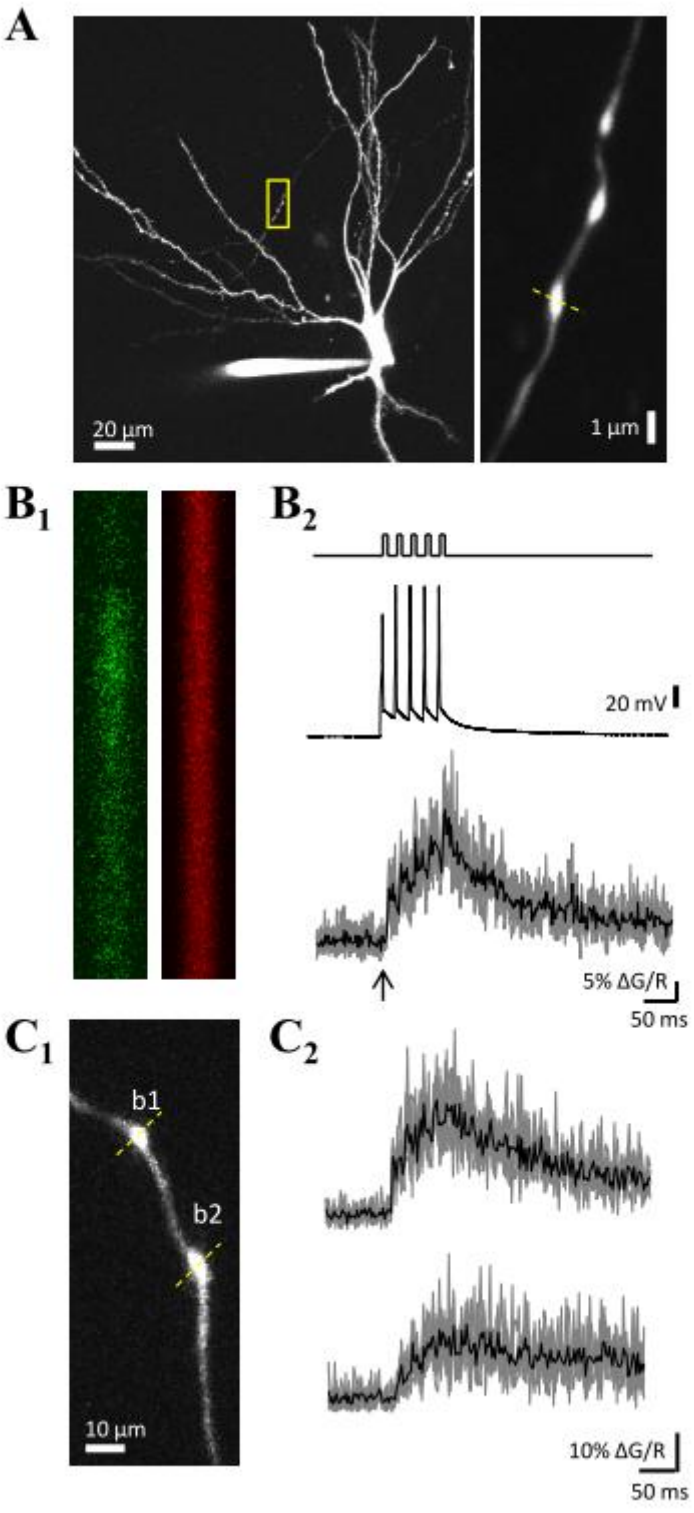
A
20 µm
1 µm
B1
B2
20 mV
5% ΔG/R
50 ms
C1
b1
b2
10 µm
C2
10% ΔG/R
50 ms

Figure 25. CA3 boutons show reliable but heterogeneous action potential train (train-AP)-evoked Ca^{2+} transients. (A) Left: two-photon stack image showing a dye-loaded CA3 pyramidal neuron. Right: Higher-magnification image of the axon in left panel (box). Individual boutons appear as bead-like varicosities along the axon. Fluorescence measurements were made by performing a line scan across a bouton (dotted line). (B_1) A representative line-scan image of both Fluo-5F (green) and A594 (red) evoked by a train-AP at the bouton in A. The corresponding Ca^{2+} transient trace is shown in B_2 (bottom). The train AP (B_2, middle trace) was evoked by five, 3 ms depolarizing pulse at the soma (B_2, top trace), with the amplitude adjusted just beyond the threshold. The train-AP evoked Ca^{2+} transients were plotted as $\Delta G/R$ over time. Six individual trials are shown in gray, and the average is superimposed in black. (C_1) Ca^{2+} imaging was performed sequentially on two neighboring boutons indicated by b1 and b2. (C_2) Train-AP evoked Ca^{2+} transients measured sequentially from b1 (top) and b2 (bottom) shown in C_1 illustrate the variation in amplitude. The traces from six trials of each bouton are shown in gray, and the averaged trace is shown as superimposed black line.

A control experiment was first performed to check the stability of the Ca^{2+} response over repeated trials. I found out a minor but significant decrease in AP-evoked Ca^{2+} transients over time. On average, the $\Delta G_P/R$ decreased from 12.2 ± 2.3 % (0 minute) to 10.2 ± 1.9 % (15 minute) ($p = 0.021$, $n = 6$) (Fig. 26B). A local or global increase in resting $[Ca^{2+}]_i$ caused by phototoxicity may reduce the measured $\Delta G_P/R$. Because increased resting $[Ca^{2+}]_i$ should be immediately evident as a change in the baseline fluorescence, I checked G_0/R at 0 minute and 15 minutes. I found no significant change of G_0/R between these two periods ($p = 0.067$, $n = 6$, Fig. 26C),

excluding the effect of poor cell condition caused by phototoxicity. One other possible factor is an increased Ca^{2+} buffer capacity during experiment progression. Ca^{2+} indicators act as buffers, thus increasing indicator concentration in the tiny bouton may lead to a smaller $\Delta G_P/R$ (Neher and Augustine, 1992). Indeed, monitoring the indicator loading level by R (A 594) showed a gradual elevation accompanied with a decrease of $\Delta G_P/R$ (Fig. 26A). Extending the indicator loading time up to 30 minutes before data collection did not prevent this minor decrease of $\Delta G_P/R$, suggesting that local indicator concentration in ascending boutons can only reach a sort of steady state within my experiment design. All the following Ca^{2+} imaging results were thus corrected offline to the decrease percentage of $\Delta G_P/R$ at corresponding time point in this control experiment.

I next examined the influence of AP5 on train-AP evoked Ca^{2+} transients. To my surprise, the addition of AP5 did not cause a significant change in $\Delta G_P/R$ (97.9 ± 6.2% of ctrl, n = 5, p = 0.41) (Fig. 27A, left trace). It is possible that depolarization of single axon may not relieve block of enough NMDA receptors to produce significant $[K^+]_o$. To test this possibility, I compared the train-AP evoked Ca^{2+} transients in control versus in Mg^{2+}-free ACSF (0-Mg). In 0-Mg, train-AP evoked Ca^{2+} transients were significantly enhanced (119.0 ± 5.1 % of ctrl, n = 7, p = 0.016) (Fig. 27A middle trace). The same experiment was repeated in AP5 containing 0-Mg. As shown in Fig. 27A (right trace), train-AP evoked Ca^{2+} responses in AP5 containing 0-Mg became statistically indistinguishable from that seen in control slices (103.9 ± 4.7 % of ctrl, n = 7, p = 0.30).

In the above experiments, it is unclear whether the NMDA receptors critical for $[K^+]_o$ modulation of presynaptic Ca^{2+} transients were located pre- or post-synaptically (Fig. 27). To test this, iMK-

801 (open NMDA channel blocker) was applied to presynaptic CA3 pyramidal neuron via the patch pipette (Berretta and Jones, 1996; Humeau et al., 2003; Samson and Pare, 2005). Excitatory postsynaptic currents were pharmacologically isolated with picrotoxin (100 μM) and CGP52432 (5 μM). Pyramidal neurons were firstly held in voltage-clamp mode at -70 mV. Synaptic stimulation paired with a depolarization step (70 mV, 1.5s) was applied every 15 s for at least 10 min before isolating NMDAR-mediated EPSCs with AP5. Under this condition, iMK-801 (5mM) reduced the NMDA current by 85% relative to control cells with normal internal (percentage of AP5-sensitive component for cells with iMK-801: 6.4 ± 3.5 %, n =6; control: 43.5 ± 6.4 %, n = 5) (Fig. 28A). Despite powerful block of NMDA currents, iMK-801 treated boutons showed similar enhancement of train-AP evoked Ca^{2+} in 0-Mg (120.8 ± 3.89 % of ctrl, n = 9) (Fig. 28B). The sensitivity of the train-AP evoked Ca^{2+} transients to 0-Mg with iMK-801 rules out the possible role of presynaptic NMDARs.

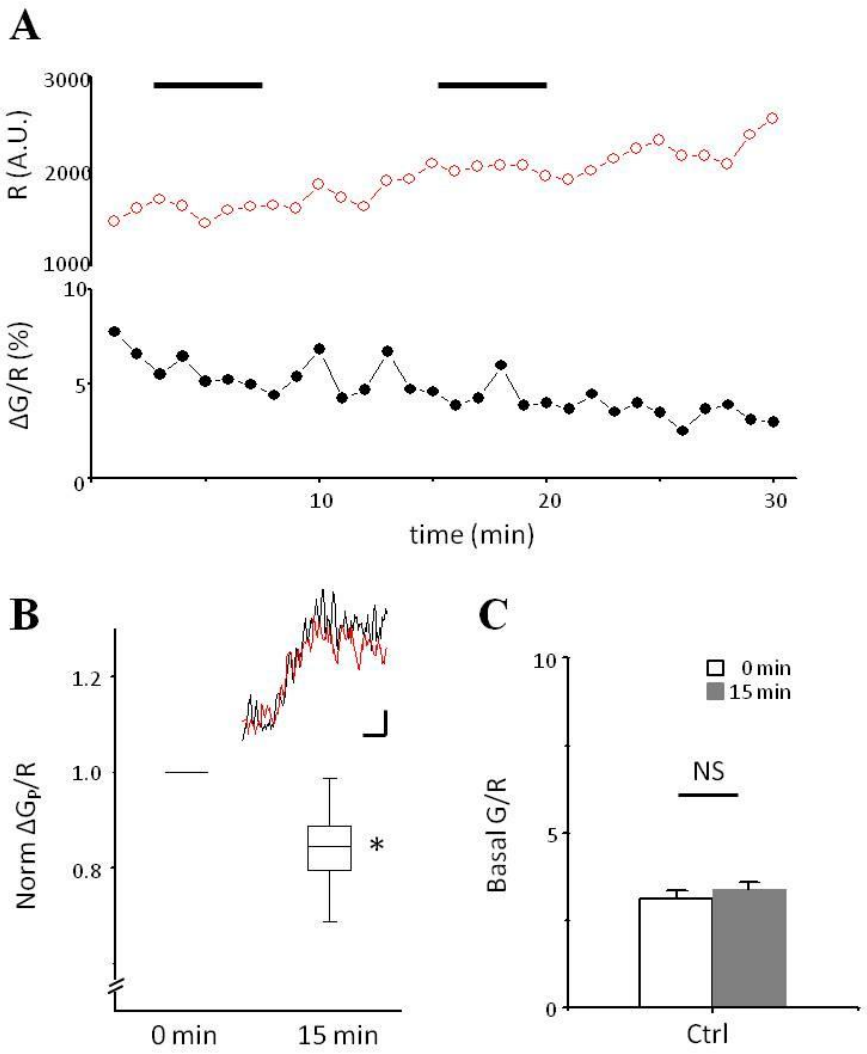

*Figure 26. Ca^{2+} transients reduce gradually during control experiment procedure. (A) Added buffer capacity and peak [Ca] in response to train-AP were monitored by Alexa Fluor 594 fluorescence (red circle) and ΔG/R (black circle) respectively. Each experiment was started at least 20 minutes after break-in. Ca^{2+} imaging was performed in line-scan mode as indicated, once per minute, lasting for 20 minutes. As the red fluorescence gradually enhanced, the evoked Ca^{2+} transient was decreased. (B) Box plot summary of relative changes in $\Delta G_P/R$ at the beginning (0 min) and 15 minute later. Inset: example trace of 0 min (black trace) and 15 min (red trace). Scale bar: 1% ΔG/R and 50 ms (C) Relative changes in baseline signal G/R collected at same time points as B. *P < 0.05, paired t-test.*

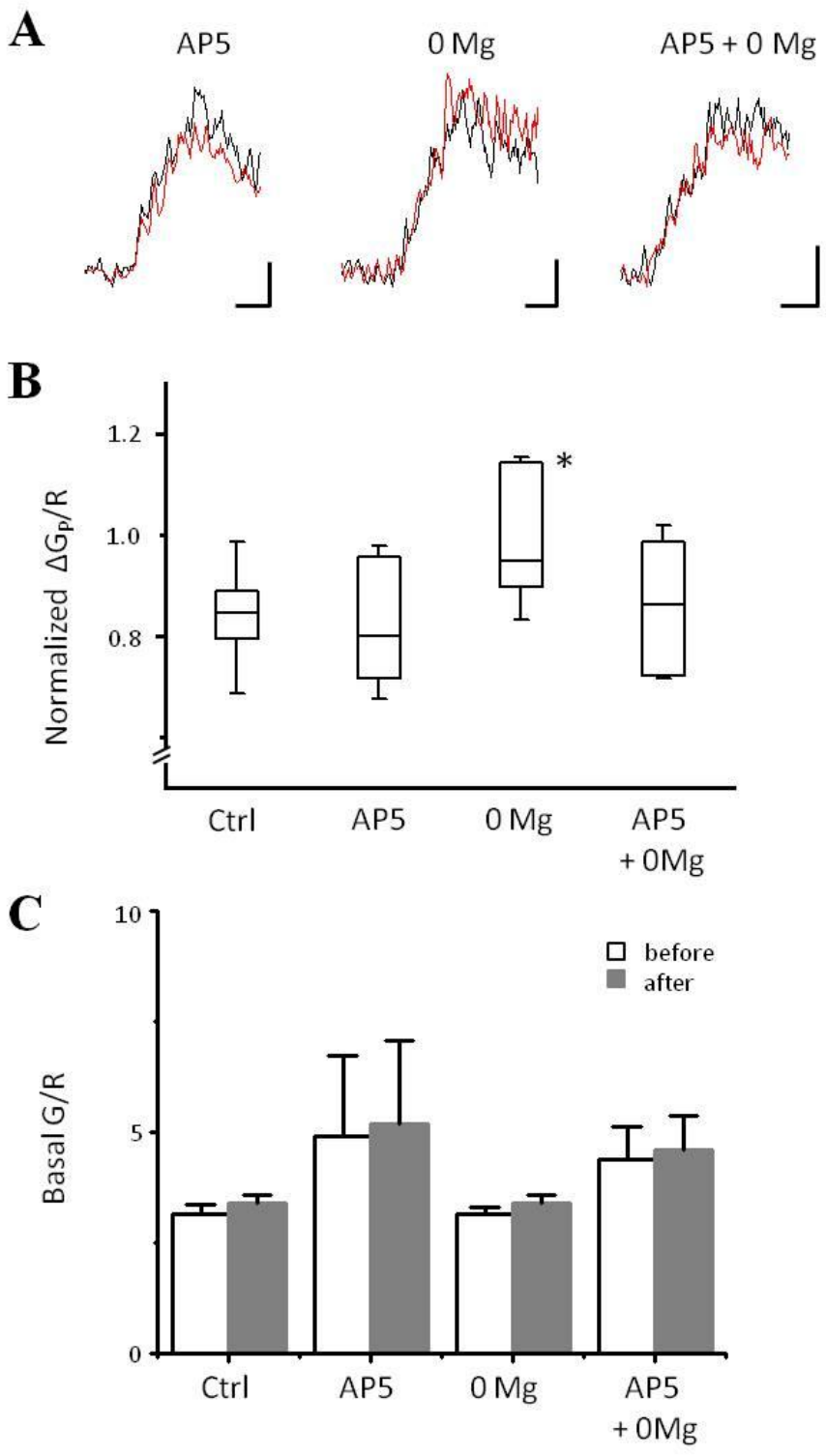
A
AP5
0 Mg
AP5 + 0 Mg
B
Normalized ΔGp/R
1.2
1.0
0.8
*
Ctrl
AP5
0 Mg
AP5
+ 0Mg
C
Basal G/R
10
5
0
before
after
Ctrl
AP5
0 Mg
AP5
+ 0Mg

*Figure 27. Relief of NMDA receptors from Mg^{2+} block by Mg^{2+}-free ACSF enhances train-AP evoked Ca^{2+} transients. (A) Top: sample traces of train-AP evoked Ca^{2+} transients at single CA3 boutons in ctrl (black trace), AP5 (left, red trace) Mg^{2+}-free ACSF (middle, red trace), and AP5 containing Mg^{2+}-free ACSF (right, red trace). Scale bar: 1% $\Delta G_P/R$ and 50 ms. (B) Box plot summary of the changes in train-AP evoked Ca^{2+} transients ($\Delta G_P/R$) before and after each treatment. (C) Summary bar graph showing that no significant change of baseline G/R before and after each treatment. *P < 0.05, paired t-test.*

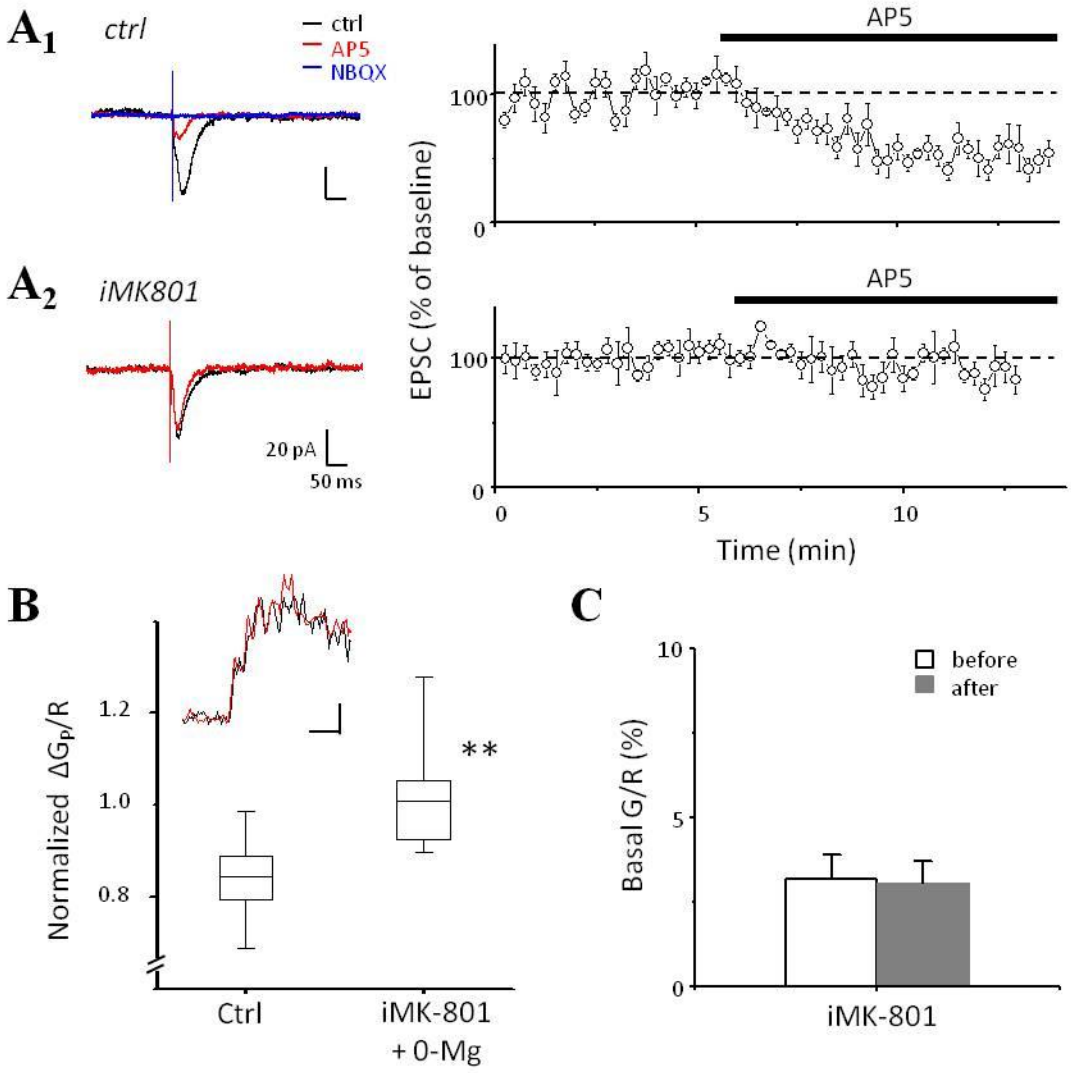
A1
ctrl
ctrl
AP5
NBQX
A2
iMK801
20 pA
50 ms
AP5
AP5
100
0
100
0
EPSC (% of baseline)
0
5
10
Time (min)
B
Normalized ΔGp/R
1.2
1.0
0.8
**
Ctrl
iMK-801
+ 0-Mg
C
10
5
0
Basal G/R (%)
before
after
iMK-801

*Figure 28. Blockade of presynaptic NMDA currents by internal MK-801 does not affect 0-Mg enhancement of Ca^{2+} response. (A) Left: sample EPSCs evoked by synaptic stimulation in the CA3 pyramidal neuron held at -40 mV. With ctrl intracellular solution, EPSP was reduced by AP5 (A_1). With intracellular solution containing MK-801 (iMK801, 5 mM), EPSC was not significantly affected by AP5 (A_2). Right: Graph plotting the amplitude of EPSCs (y-axis) as a function of time (x-axis) is shown. AP5 was applied at the time period indicated by the black bar. Data were normalized to baseline response amplitudes. Error bars represent SE. (B) Box plot summary of Ca^{2+} transient results. Train-AP evoked Ca^{2+} with presynaptic NMDA receptors blocked by iMK-801 was still enhanced in 0-Mg treatment. Inset: sample trace before (black) and after (red) 0-Mg treatment. (C) Summary bar graph showing no change of baseline G/R before and after 0-Mg treatment with iMK-801. ** P <0.01, paired t-test.*

2. Coincident Relief NMDA Receptors from Mg^{2+} Block is Necessary for Presynaptic Modulation by K^+

I have suggested that NMDAR-mediated elevation of $[K^+]_o$ induced by single axon activation may be insufficient to modulate presynaptic Ca^{2+} signaling in the above experiments. For further investigation, a bipolar stimulating electrode was placed in the *stratum radiatum* to activate bundles of Schaffer collateral axons at the same time. Corresponding changes in presynaptic Ca^{2+} were measured by wide-range, multibouton Ca^{2+} imaging (Kamiya et al., 2002). Following local injection of OGB1-AM into the *stratum radiatum* (Fig. 29A), a bright fluorescent band extended away from the injection site, in parallel with the pyramidal cell layer. The fluorescent band was considered to represent labeled Schaffer collaterals. To verify the presynaptic origin of

the observed Ca^{2+} transients, I examined the effects of the glutamate receptor antagonists NBQX and AP5. Transient increases in OGB1-AM fluorescence and fEPSPs evoked by electrical stimuli to Schaffer collaterals were recorded simultaneously. The representative Ca^{2+} transient and fEPSP are shown in Fig. 29B. The fEPSPs evoked by single stimulus were blocked completely by glutamate receptor antagonists, whereas Ca^{2+} transients under the same condition were not affected (Fig. 29B), suggesting that the Ca^{2+} transients arose exclusively from the presynaptic structures. I then gave a train of stimuli (50Hz, 5 stimuli); in contrast with the results of single axon activation in the single bouton Ca^{2+} imaging experiment, Ca^{2+} transients evoked by axon bundles were significantly suppressed by bath application of AP5, with its $\Delta F/F$ value from 13.9 ± 1.7% to 9.3 ± 0.7% ($n = 12$, $p = 0.03$) (Fig. 29C). This result supported my assumption of the necessity of massive activation of NMDA receptors in K^+-mediated presynaptic regulation.

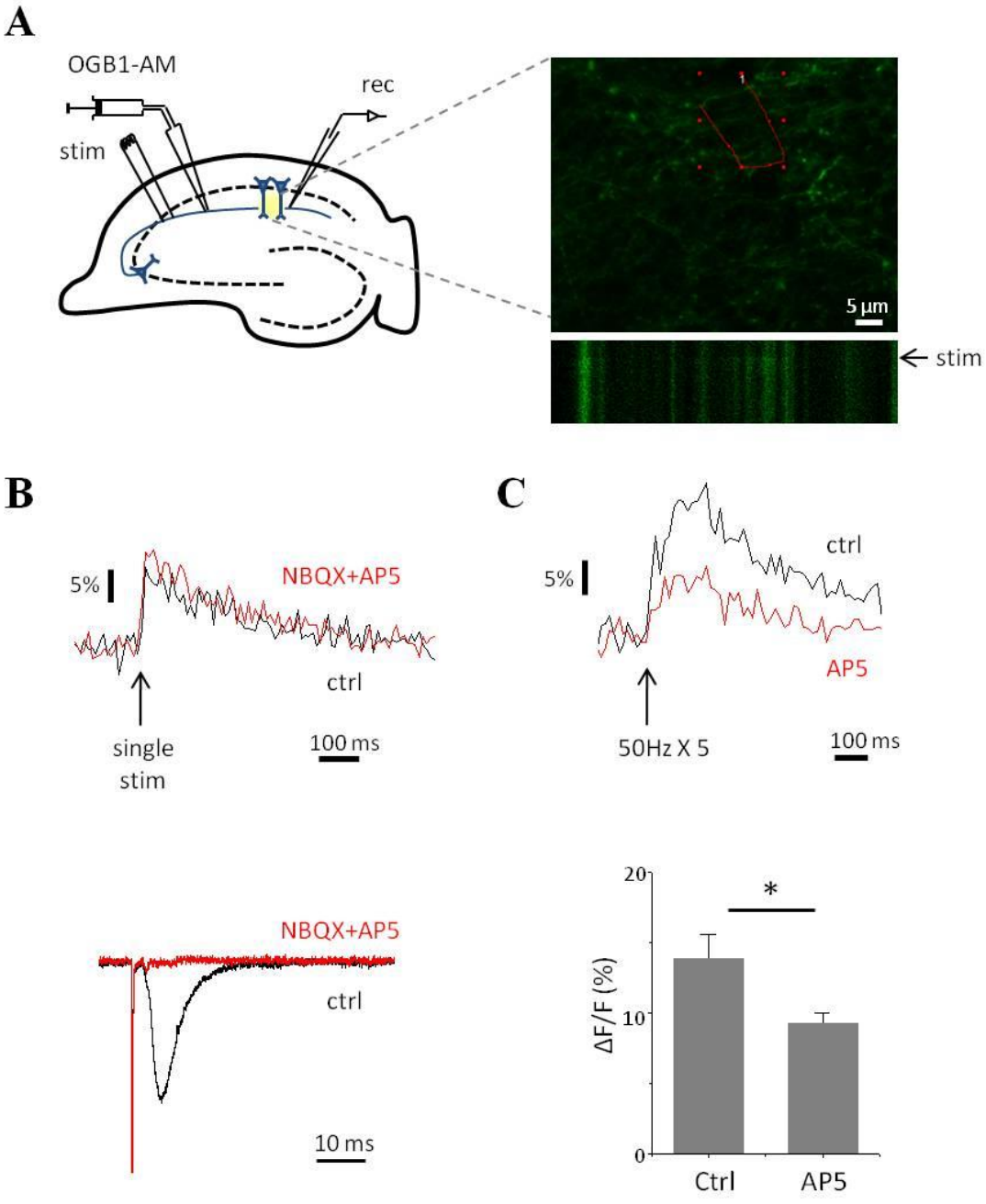
A
OGB1-AM
rec
stim
5 µm
stim
B
5%
NBQX+AP5
ctrl
single
stim
100 ms
NBQX+AP5
ctrl
10 ms
C
5%
ctrl
AP5
50Hz X 5
100 ms
20
10
0
ΔF/F (%)
*
Ctrl
AP5

*Figure 29. Ca^{2+} transient in response to activation of axon bundles showed AP5-sensitivity. (A) Left: schematic diagram showing the experimental arrangement. Bundles of Schaffer collaterals were stimulated with a bipolar electrode. OGB1-AM was pressure-ejected into the stratum radiatum, resulting in selective loading of the presynaptic terminals through the Schaffer collateral pathway. Fluorescence was measured from the yellow region 300 μm away from the injection site. Right: confocal image of the yellow region from a sample experiment. Line scan (red line) was placed to monitor presynaptic Ca^{2+} signals. (B) Effects of a mixture of AMPA and NMDA receptor antagonists (NBQX and AP5) on the Ca^{2+} transient (top trace) and simultaneously recorded fEPSP (bottom trace). Ca^{2+} signals were measured as relative fluorescence changes (ΔF/F), where F is the resting fluorescence level and ΔF is the peak amplitude of fluorescence change caused by the stimulus. Black trace – ctrl, red trace – NBQX and AP5. (C) Top: representative records of presynaptic Ca^{2+} transient evoked by 5 stimuli (50 Hz) before (black trace) and during application of AP5 (red trace). Bottom: group data illustrating the depressed presynaptic Ca^{2+} signals by AP5. *P < 0.05, paired t-test.*

3. NMDA Receptor-Mediated K^+ Modulate Neurotransmitter Release Probability

It is well known that Ca^{2+} triggers neurotransmitter release in a marked nonlinear fashion, with a high cooperativity of 3-4 when varying the extracellular or the intracellular Ca^{2+} concentration (Bollmann et al., 2000; Schneggenburger and Neher, 2000). Assuming that the fluorescence responses to the train of action potentials (Fig. 29C) are approximately proportional to the underlying increases in intracellular Ca^{2+} (Maravall et al., 2000), this change in presynaptic Ca^{2+} signaling observed would be expected to induce apparent alteration in paired-pulse ratio, a monitor of changes in release probability (Dobrunz and Stevens, 1997; Katz and Miledi, 1968; Manabe et al., 1993). Again, Schaffer collateral axons were stimulated with a bipolar electrode placed in the *stratum radiatum*. In response to paired-pulse stimulation with an interstimulus interval of 50 ms, fEPSPs showed strong paired-pulse facilitation, and AP5 was applied after obtaining a stable baseline of fEPSPs. In five of six slices tested, the paired-pulse ratio reduced in AP5. Without this outlier, the paired-pulse ratio decreased from 1.54 in control to 1.36 in AP5 ($n = 5$; $p = 0.02$) (Fig. 30A) with no effect on the slope of the first fEPSP (102.1 ± 9.0 % of baseline, $n = 5$, $p = 0.67$) (Fig. 30B). This finding showing an increase in use-dependent, but not the baseline, probability of glutamate release in CA3-CA1 synapses is consistent with the enhancement of presynaptic Ca^{2+} transients by postsynaptic NMDA receptors during synaptic discharges.

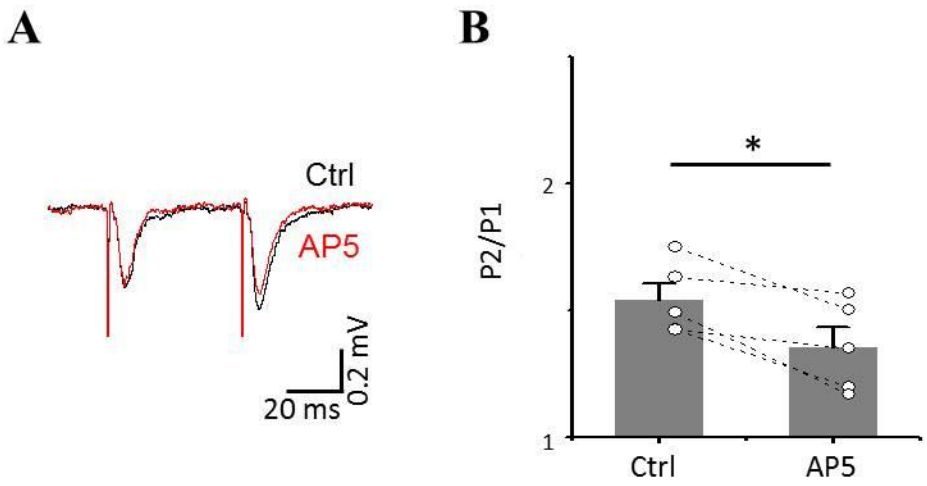

*Figure 30. AP5 reduced facilitation of second fEPSP in response to paired stimulation (A) Example traces of fEPSP in response to stimulus pairs at interval of 50 ms. Bath application of AP5 decreased the slope of the second fEPSP.Black trace – ctrl, red trace – AP5. (B) Statistical effect of AP5 on paired-pulse ratio.*P < 0.05, paired t-test.*

Chapter 8: K^+ Modulation of Astrocytic Glutamate Transporter Efficiency

Glutamate transporters expressed in perisynaptic astrocytic processes are critical for clearing synaptic glutamate (Bergles and Jahr, 1997; Oliet et al., 2001). Because the uptake of glutamate by astrocytic transporters is voltage-dependent (Levy et al., 1998), the transporter may also be affected by depolarization induced by K^+ release through activating NMDA receptors. I thus examined the transporter current under various conditions of $[K^+]_o$ and holding potential (Fig. 31). Based on the high resting conductance of astrocyte membranes, responses to uncaged glutamate was a very sensitive function of uncaging position with a decay constant of 14.2 ± 1.4 μm (n = 5) (Fig. 31B). To obtain a highly reproducible response, MNI-caged-L-glutamate (Matsuzaki et al., 2001) was set to uncage immediately next to the recorded astrocyte. Uncaging glutamate onto hippocampal astrocytes produced a pronounced fast rising inward current of 25.6 ± 3.4 pA in the presence of standard basal $[K^+]_o$ (n = 9) (Fig. 31C, inset). Increasing $[K^+]_o$ from 2.5 to 7.5 mM produced a 25.1 ± 3.6 % reduction of this current (n = 8). A further increase of $[K^+]_o$ to 20 mM induced a stronger depression (48.7 ± 7.8 % depression, n = 4) (Fig. 31C).

Interestingly, transporter depression can be rescued when cells are kept clamped at their resting potential (n = 12) (Fig. 31D), indicating K^+ affects glutamate transporter current primarily via depolarizing the cell membrane. If this is the case, this depression effect might be unmasked by holding the cells at the membrane potential corresponding to depolarization produced by different $[K^+]_o$. Firstly, I examined the membrane potential changes in astrocytes induced by perfusion of extracellular solutions with different $[K^+]_o$. I found that changing $[K^+]_o$ from 2.5 mM ($[K^+]_{rest}$) to 5, 7.5 and 20 mM induced an averaged depolarization of 9.8 ± 1.0 (n = 12), 18.6 ± 1.5 (n = 10), and 43.8 ± 1.3 mV (n = 4), estimated from resting membrane potential of each test (Fig. 31E), close to the prediction by Nernst equation (see Materials and Methods, chapter

2.7.2).

Glutamate transporter current was then evoked by point uncaging on cells depolarized to corresponding testing potentials (-85, -65 and -40 mV) (Fig. 31F, red circle) and compared to the depression effect caused by real $[K^+]_o$ elevation (Fig. 31F, black circle). Direct depolarization mimicked the depression effect caused by raising extracellular K^+ concentration (n = 9, 9, 7 for -85, -65 and -40mV, respectively. $p > 0.05$). Thus glutamate transporters appear to be modulated by K^+ via K^+-induced depolarization, indicating activity-dependent raise of $[K^+]_o$ may be an efficient modulator of glutamate uptake.

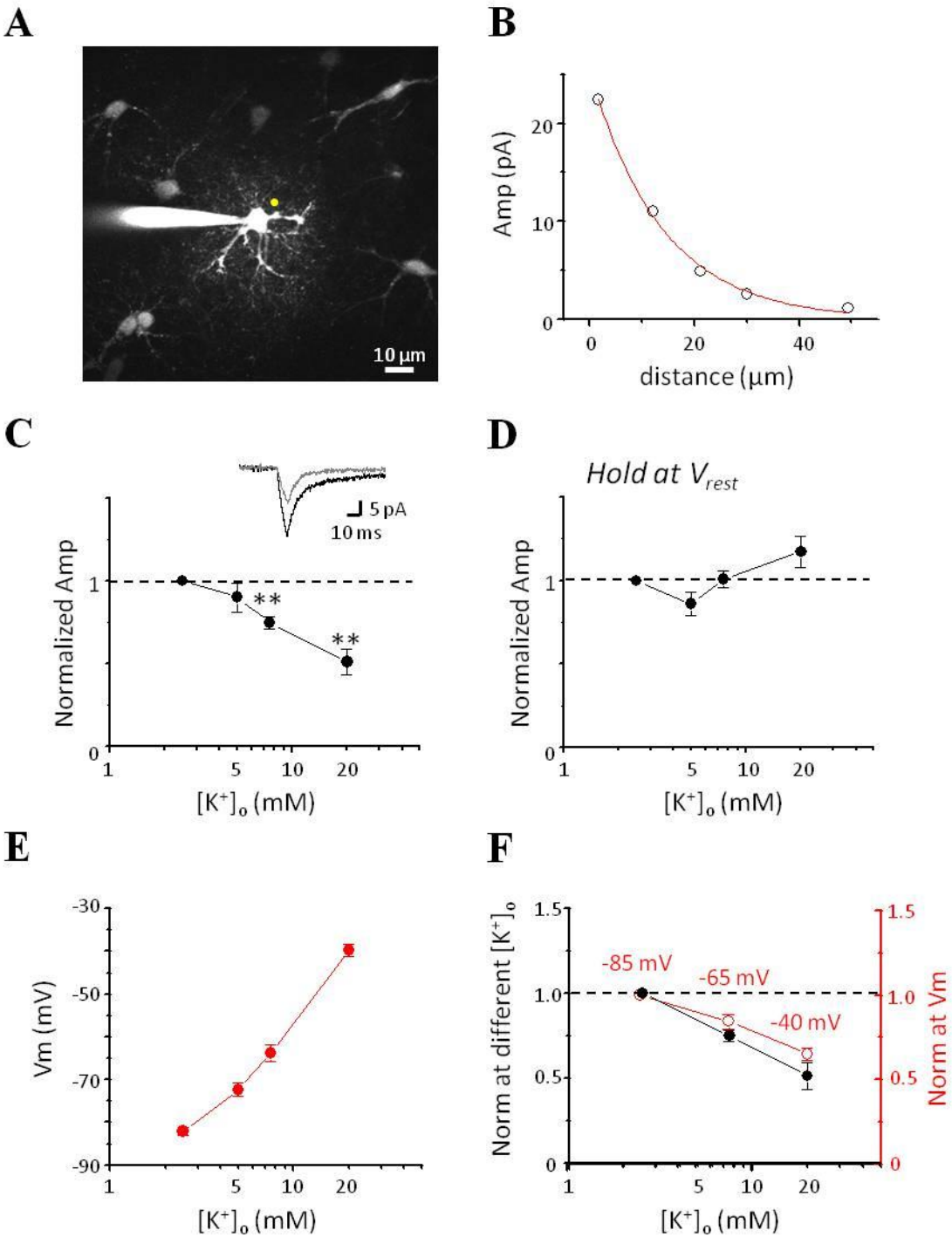
A
10 µm
B
Amp (pA)
distance (µm)
C
5 pA
10 ms
Normalized Amp
**
**
[K+]o (mM)
D
Hold at Vrest
Normalized Amp
[K+]o (mM)
E
Vm (mV)
[K+]o (mM)
F
Norm at different [K+]o
-85 mV
-65 mV
-40 mV
Norm at Vm
[K+]o (mM)

*Figure 31. Depression of TC by high $[K^+]_o$. (A) TPE fluorescence image of a hippocampal astrocyte filled with A594, which was dissolved in the patch solution. Yellow circle indicates the position of the UV light spot used for glutamate uncaging. (B) Dependence of TC evoked by glutamate uncaging on distance from the soma. Red line shows the single exponential fit. (C) Summary of the effect of $[K^+]_o$ at concentrations of 2.5, 5, 7.5 and 20 mM on the photolysis responses. Inset: sample trace of TC in 2.5 mM (black) and 20 mM (gray) $[K^+]_o$.**P < 0.01, paired t-test. (D) Increase of $[K^+]_o$ has no effect on TC when the recorded astrocytes were kept clamped at their resting potential (V_{rest}). (E) $[K^+]_o$ was increased from 2.5 to 20 mM, and measurements of astrocyte membrane potential (V_m) were made at each $[K^+]_o$. Results depict the V_m from astrocytes with V_{rest} more negative than -80 mV in 2.5 mM $[K^+]_o$. (F) Photolysis responses of 2.5, 7.5, and 20 mM $[K^+]_o$ (black circle) were compared to those from astrocytes held at corresponding Vm, -85, -65, and -40 mV (red circle) respectively.*

Chapter 9: Discussion

My results characterize three basic properties of $[K^+]_o$ based on astrocytic I_K recordings. First, ~ 60% of I_K is attributed to postsynaptic NMDA receptor activation. Addition of a NMDA receptor antagonist dramatically decreased I_K, and this effect disappeared in CA1-NR1 KO mice where postsynaptic NMDA receptors were specifically knocked out. Second, I_K is weakly linked to K_{Ca} and K_V, such that changes in the level of $[Ca^{2+}]_o$ and voltage leave I_K largely unchanged. Third, the $[K^+]_o$ rise produced during synaptic activity is well-restrained within the synapse. Outside the activated synapse, fiber volley conductance was not influenced by NMDAR-mediated $[K^+]_o$. In line with the dominant role of postsynaptic NMDA receptors in synaptic $[K^+]_o$ variation, I_K is tightly governed by Mg^{2+} unblock mechanisms and displayed activity-dependent features. Moreover, I revealed that NMDAR-mediated $[K^+]_o$ could be a potential signal in adjusting presynaptic transmitter release machinery and astrocyte glutamate transporters according to synaptic activity. Thus, my study places synaptic $[K^+]_o$ in a new position, not just as a byproduct passively produced by postsynaptic activation, but actively involved in communication in the tripartite synapse.

1. <u>Ba^{2+} Modulation on I_K and TC</u>

Treatment of Ba^{2+} at micromolar concentrations blocks K^+ uptake ability of astrocytes through IRK channels and has been extensively used as an pharmacological tool in investigations of $[K^+]_o$ functions (D'Ambrosio et al., 2002; Ransom and Sontheimer, 1995). Here, I also used 200 μM Ba^{2+} to confirm astrocytic I_K has a K^+ origin. At the same time, a downward shift in the holding current can be observed from hippocampal astrocyte recordings, consistent with a depolarizing effect caused by the loss of IRK conductance (Djukic et al., 2007; Tang et al., 2009). In principal, both disturbances of K^+ gradients and membrane depolarization by Ba^{2+} in poorly

voltage-clamped astrocytic processes should reduce the efficiency of electrogenic glutamate transporters (Bordey and Sontheimer, 2003; D'Ambrosio, 2004; Mennerick et al., 1999; Otis and Kavanaugh, 2000). To the contrary, I detected a significant increase in TC with Ba^{2+}. Several explanations for this result are possible. One potential interpretation is the decrease of current shunting resulting from increased membrane resistance arising by IRK channel blockade. If it is the case, TC should recover in similar rate as the holding current in the process of Ba^{2+} washout. However, potentiation of TC persisted while Ba^{2+} effect on holding current has already been washed out. Another possible reason is increased release of glutamate secondary to $[K^+]_o$-induced depolarization of presynaptic terminals. When astrocytic IRK channels are blocked by Ba^{2+}, $[K^+]_o$ easily accumulates around active neurons. The accompanying depolarization would increase the release probability, resulting in a larger TC. However, additional findings provided by Dr. Khiroug (our collaborator) did not support this hypothesis: 1) a similar potentiation of glutamate uncaging-mediated TC suggested that this phenomenon is independent of any effects of Ba^{2+} on presynaptic terminals; 2) the potentiation of TC amplitude was accompanied by a decrease in the centroid of uncaging-induced TC, which is consistent with an increased efficiency of uptake; 3) a significant effect on TC was observed at low micromolar Ba^{2+} concentration which did not produce any measurable effect on holding current. This opens a possibility that Ba^{2+} could act as a direct enhancer of glutamate uptake. In this case, Ba^{2+} may execute two concurrent effects: depolarization leads to TC decrease and direct modulation leads to TC augmentation. Further studies would be required to verify this hypotheses and underlying balance between these two effects. Finding such mechanisms may help to explain some of the notorious variability in the outcome using Ba^{2+}/Cs^+ to investigate $[K^+]_o$ functions (Skov et al., 2011).

2. NMDA Receptors, but not AMPA Receptors, Dominate I_K

Stimulus-induced I_K in astrocytes largely reflects the increase in $[K^+]_o$ caused by neuronal activity (Fig. 11). My finding that AP5 has a stronger blocking effect on I_K than NBQX (Fig. 13) further shows that the $[K^+]_o$ elevation responsible for astrocytic I_K with Schaffer collateral stimulation was mainly caused by activation of NMDA receptors. To our knowledge, such a clarification of the contributions of glutamate receptor types on $[K^+]_o$ has not been tested previously. Two studies in hippocampus (Bergles and Jahr, 1997; Ge and Duan, 2007) and one in olfactory bulb (De Saint Jan and Westbrook, 2005) showed that I_K is sensitive to a cocktail of glutamate receptor antagonists pointing out its postsynaptic origin, but did not demonstrate a difference with separate antagonist using the same protocol. My results thus provide an overview of distinct contributions AMPA and NMDA receptors on I_K and highlighted the NMDA receptors as the major contributor.

Specifically, I found that this NMDA receptor-mediated I_K is much less sensitive to Ca^{2+} and voltage change, suggesting minor involvement of K_{Ca} and K_V, two most well-known potassium channels downstream of NMDA receptor activation (Chen and Johnston, 2004; Faber et al., 2005; Ngo-Anh et al., 2005). What could be other candidate channels resulting in I_K? One appealing possibility is NMDA receptor itself. Although K^+ efflux directly via NMDA receptors (NMDA-K) has received little scrutiny, composite NMDA receptor currents normally have a reversal potential around 0 mV (Mayer and Westbrook, 1987), in accordance with simultaneous K^+ efflux and Na^+/Ca^{2+} influx when NMDA receptors are in the open state. K^+ is highly permeable and passes through the NMDA receptor ion permeation pathway rapidly. In symmetric, 100 mM divalent cation-free solutions, the NMDA receptor conductance is ~70 pS for K^+, which means

that at -60 mV, K^+ interacts with the channel for only < 0.04 μs (Zhu and Auerbach, 2001). The marked MK-801 and Mg^{2+}-sensitivity of my recorded I_K (Fig 14 & 21) is compatible with previous studies of this NMDA-K current in cortical neurons (Ichinose et al., 2003). Moreover, this NMDA-K is uniquely regulated in an activity-dependent manner, by which a depolarizing pre-pulse of a few seconds or a burst of brief depolarizing pulses selectively augments the subsequent NMDA-K current, but not the NMDA inward current (Ichinose et al., 2003).

K^+ has three binding sites in NMDA receptors: two that are external and one that is internal to the site of Mg^{2+} block. Any one of these three sites occupied by K^+ effectively prevents the association of Mg^{2+}. Occupancy of only the internal site can prevent Mg^{2+} permeation and increase the Mg^{2+} dissociation rate constant by approximately sevenfold. Under physiological intracellular ionic conditions and at -60 mV, K^+ occupancy of the external and internal sites would decrease the affinity of the channel for extracellular Mg^{2+} apparently and enhance the voltage dependence of Mg^{2+} block (Antonov and Johnson, 1999; Qian et al., 2002; Zhu and Auerbach, 2001). In addition, the flux of K^+ may also play an essential role in the modulation of Mg^{2+} block by 'pushing' Mg^{2+} leaving its block site (Yang et al., 2010). Because these concomitant flux-coupling effects of K^+, the Mg^{2+} block of the NMDA receptor would be weaker with a stronger tendency of NMDA-K, showing in essence use-dependency of great physiological and pathological concern. Although I cannot rule out additional types of K^+ channels that could contribute to I_K, these similar properties shared among NMDA-K and I_K highlight the possibility that the K^+ efflux via NMDA receptors might be subject to I_K of my study.

My pharmacological manipulations are consistent with postsynaptic NMDA receptors having a role in producing extracellular K^+ signal during synaptic activity, however, I am mindful that the other glutamate activated receptor, AMPA receptor, is also permeable to K^+ ions. In essence, this raises an interesting question: what could be the benefits for NMDA receptor to dominate synaptic $[K^+]_o$ level rather than AMPA receptor? The reason can be explained by different binding kinetics of NMDA and AMPA receptors. NMDA receptors are less sensitive to glutamate when it is present for only a very short time ($< 10^{-3}$ s) than when it is present for a longer time (10^{-3} - 10^{-2} s). Thus, a prolonged pulse of glutamate is necessary for NMDA receptor opening, whereas a briefer pulse of glutamate is already enough for activation of AMPA receptors (Attwell and Gibb, 2005; Kullmann, 1999). Aside from glutamate binding, adequate membrane depolarization is also necessary to activate NMDA receptors. Both prerequisites regulate NMDA receptor activation in parallel, which ensures the following K^+ efflux is finely tuned. Because $[K^+]_o$ level significantly alters neuronal excitability (Chamberlin et al., 1990; Meeks and Mennerick, 2004), the nature of NMDA receptor activation benefits the K^+ efflux through them under a stricter control than through AMPA receptors. On the other hand, NMDA receptors have a relatively large single channel conductance compared to AMPA receptors (Spruston et al., 1995), and the ratio of area NMDA to AMPA receptor-mediated current, on average, was about five in the Schaffer collateral pathway (Otmakhova et al., 2002). These properties enable NMDA receptors to act as a more efficient producer of K^+ once they open. Finally, slow deactivation of NMDA receptors may advantage accompanied K^+ efflux as a potential signal promoting associative signals. AMPA receptors deactivate rapidly on a millisecond timescale, whilst for NMDA receptors the duration can be up to hundreds of milliseconds (Attwell and Gibb, 2005). As a result, K^+ efflux through them would occur on a different timescale. I showed that I_K can be

supralinearly amplified during paired pre- and postsynaptic activation (Fig. 23), demonstrating K^+ has the ability to code two approximately coincident inputs. On the other hand, my data also showed that K^+ can modulate both presynaptic Ca^{2+} signaling and paired-pulse ratio (Fig 29 & 30). If K^+ flows primarily via AMPA receptors, activating for only a few milliseconds, the chances for K^+ to actively modulate the second input overlapping in time would be small. Hence, K^+ can function as a retrograde signal in temporal information integration only when it lasts for a sufficiently long time for there to be a reasonable chance of the other input occurring, which in turn would dictate the choice of utilizing NMDA receptors.

3. Possible Synaptic $[K^+]_o$ Estimated from Simulation and Experimental Results

How large could the NMDAR-dependent K^+ concentration be within the synaptic cleft? Although this cannot be directly determined with my current data, our simulation provided a rough idea of the relation between postsynaptic NMDA receptor numbers and the synaptic $[K^+]_o$ they could produce. Ten NMDA receptors inserted into the postsynaptic site is enough to generate ~7 mM synaptic $[K^+]_o$ increase in the proposed model. My experimental results from examination of the presynaptic Ca^{2+} signal and paired-pulse ratio also gave us some hints as to the possible extent of synaptic $[K^+]_o$ elevation. Nerve terminals can be moderately depolarized for a sustained period by extracellular K^+ accumulation resulting from neuronal activity (Malenka et al., 1981; Singer and Lux, 1973), and consequently, there can be changes of the presynaptic Ca^{2+} current and postsynaptic response (Awatramani et al., 2005; Hori and Takahashi, 2009; Matyushkin et al., 1995). Simultaneous pre- and postsynaptic voltage-clamp recordings at the calyx of Held synapse confirmed that this is a K^+ concentration-dependent modulation: with increased $[K^+]_o$, presynaptic terminals depolarized gradually with an accompanied biphasic

modulation on postsynaptic EPSC (Hori and Takahashi, 2009). Similar results were reported in neuromuscular junctions and hippocampus as well (Matyushkin et al., 1995; Nicholls and Wallace, 1978; Somjen, 2001). Clearly, both presynaptic Ca^{2+} facilitation and the direction of change in the postsynaptic response can be used to estimate the $[K^+]_o$ variation in the synapse. Because AP5 had a significant effect on the presynaptic Ca^{2+} transient evoked by a train of APs (Fig. 29), and it can also decrease the paired-pulse ratio (Fig. 30), the NMDA receptor activation under our stimulation protocol most likely induced elevation of $[K^+]_o$ to a range of ~4-10 mM (Hori and Takahashi, 2009). Notice all the presynaptic Ca^{2+} experiments were performed in GABA and mGlu receptor blockers, excluding the complexity of results explanation that could be caused by accompanied synaptic modulation via gliotransmitter release (such as D-serine) (Andersson et al., 2007; Henneberger et al., 2010). The predicted range of local $[K^+]_o$ change could be further explored with detailed modeling or advanced K^+ imaging. It is also of interest that in my results NMDAR-mediated $[K^+]_o$ varies in an activity-dependent manner, suggesting a chance of reversed inhibitory influence on presynaptic terminals if excessive NMDAR-mediated $[K^+]_o$ was produced by overexcited postsynaptic neurons. Taken together, because intraterminal Ca^{2+} and transmitter release can be potentially facilitated and depressed depending on $[K^+]_o$-induced presynaptic depolarization, the magnitude of NMDAR-mediated changes in $[K^+]_o$ could be an important determinant of the direction of presynaptic modulation.

4. <u>NMDAR-Mediated $[K^+]_o$ is Localized</u>

In order to estimate the spatial distribution of NMDAR-mediated $[K^+]_o$, I analyzed the afferent volley depression evoked by repetitive stimulus trains (Meeks and Mennerick, 2004). With this method, which is highly sensitive to $[K^+]_o$ elevation outside of synapses (Fig. 19), I found that

NMDAR-mediated $[K^+]_o$ had no significant influence on the afferent volley depression, reflecting its local nature. These observations are in agreement with the findings of Meeks and Mennerick (2007), who reported a small increase (~0.2 mM) of bulk $[K^+]_o$ with 10 stimuli at 50 Hz, measured directly by K^+ microelectrode. The synaptic depression by the end of a 10 pulse train thus must be attributed to a mechanism unrelated to potassium, such as the depletion of readily releasable transmitter stores (Zucker and Regehr, 2002).

5. Associative Potentiation of NMDAR-Mediated $[K^+]_p$

In this study, I used two different Ca^{2+} imaging techniques, single bouton imaging and bolus loading, and paired-pulse ratio measurement to explore the functional application of NMDAR-mediated $[K^+]_o$ on modulating synaptic transmission. Whereas Mg^{2+}-free ACSF caused an expected significant increase in Ca^{2+} transients measured with single-bouton imaging, application of the NMDA receptor antagonist, AP5, had no significant effect. Intriguingly, AP5 displayed significant depression of Ca^{2+} transients when observed with bolus loading techniques and paired-pulse ratio. One possible explanation for the observation of distinct Ca^{2+} transient modulation by AP5 is the nature of the stimulus. Given that the train of action potentials was induced by somatic current injection in single-bouton imaging experiments, only the postsynaptic spines contacting with this single axon could be activated. The fact that, most Schaffer collateral fibers (76%) make only a single apposition on single CA1 pyramidal neurons, and only additional 4% of the axons wound back and forth across individual dendrites forming multiple synapses closely spaced along the dendrites (Sorra and Harris, 1993), indicates that a large proportion of spines on single dendrite actually is not targeted by the same axon. Rather, it supports the view that action potential propagating along a single axon preferred to activate

spines dispersed at disparate dendritic branches, even at different CA1 pyramidal neurons. Thus, the postsynaptic depolarization resulting from single axon stimulation can hardly summate either spatially or temporally and might be insufficient to relieve the Mg^{2+} block of all the postsynaptic NMDA receptors in a way that leads to NMDA-K mediated presynaptic modulation. In addition, a recent study has described how the relief of Mg^{2+} block at NMDA receptors is not instantaneous (Kampa et al., 2004). Thus, the need for additional depolarization to induce enough K^+ efflux via NMDA receptors may arise from the need for a longer depolarization in order to effectively relieve Mg^{2+} block of NMDA receptors and thereby adequately activate the K^+ signal to affect transmission. Indeed, my results showed that either stimulating multiple axon fibers simultaneously with a bipolar stimulus electrode or removal of Mg^{2+} directly by Mg^{2+}-free ACSF could adequately induce the NMDA-K mediated presynaptic modulation, in line with the necessity of greater NMDA receptor activation in this modulation process.

6. Activation of NMDA Receptors Controlled by Input Pattern

How can this critical depolarization be met in physiological conditions? The depolarization of dendrites can usually be provided by synaptic potentials, back-propagating action potentials, or dendritic spikes. Thus, there are several scenarios that can be considered.

6.1 Summation of EPSPs

The simplest scenario is that temporal and/or spatial integration makes the EPSP itself large enough to activate more NMDA channels. Direct current injection via a recording electrode in the dendrites can eliminate the requirement for activation of many synapses (Gustafsson et al.,

1987), suggesting that the basis of 'cooperativity' is the requirement for sufficient postsynaptic depolarization. The traditional view is that a strong synaptic input can depolarize the local dendritic branch sufficiently to enable the activation of NMDA receptors at weak inputs on neighboring synapses (Bliss and Collingridge, 1993). Experiments using two-photon uncaging of glutamate or synaptic activation of dendrites from hippocampal pyramidal cells demonstrated that the majority of coincident afferent permutations can summate linearly (Araya et al., 2006; Cash and Yuste, 1999; Tamas et al., 2002). Specifically, a recent study points out that activating excitatory inputs on dendritic spines in a centripetal or centrifugal direction can lead to different level of postsynaptic depolarization and NMDA receptor activation (Branco et al., 2010), suggesting an intriguing notion of regulating NMDA receptor activation level by the order of given inputs.

6.2 Enhancement of bAP Propagation

In a second scenario, appropriately timed synaptic input can enhance the backpropagation of action potentials, resulting in a boost of postsynaptic NMDA receptor activation restricted to the site of synaptic input (Magee and Johnston, 1997). A backpropagating action potential serves as a global dendritic signal, inducing depolarization at a large fraction of synapses located on a single neuron. However, in CA1 pyramidal neurons, backpropagating action potentials strongly decline in amplitude with distance from the cell body due to increased density of A-type K^+ channels at distal dendrites (Hoffman et al., 1997). When a number of synaptic inputs timed to occur simultaneously with or just before action potential backpropagation, the A-type K^+ channels can be inactivated and bAP can be locally amplified three- to four-fold on the active branch (Sjostrom and Hausser, 2006; Sjostrom and Nelson, 2002; Stuart and Hausser, 2001), providing a

synaptically controlled, associative signal to the distal dendrites for modification of synaptic strength.

6.3 Local Dendritic Spikes

In a third scenario, clustered synaptic inputs, whenever they are sufficiently concentrated in space, and prolonged in time, can together trigger a local dendritic spike. The most prominent one is the NMDA spike, causing the regenerative activation of NMDA receptors as a result of the voltage-dependent relief of Mg^{2+} block for a 10-20 μm stretch of dendritic sub-branch (Major et al., 2008; Rhodes, 2006). NMDA spikes result in a nonlinear response near the strong synaptic inputs with an increase in dendritic depolarization, causing plateau potentials lasting from twenty to hundreds of milliseconds. Therefore, dendritic spikes provide an important source of the necessary postsynaptic depolarization, because their amplitudes are much larger and more spatially specific than back-propagating action potentials, especially in distal dendrites (Golding et al., 1999; Larkum et al., 2007). In addition, because the appearance of dendritic spikes shifts the manner of synaptic integration from linear to nonlinear, this is believed to help increase the neuronal computational power (Polsky et al., 2009; Tamas et al., 2002).

Further experiments will be needed to distinguish among these scenarios. In any case, dendritic integration exhibits a cooperative nature, which means that multiple synapses must be synchronously activated and/or spatially clustered in order for greater dendritic depolarization to occur. Once the local depolarization is potentiated, it would be expected to complement and enhance the ion flux through the relief of Mg^{2+} block of local NMDA receptors. The feature of the extent of NMDA receptor activation deriving from the different integration modes appear to

be reminiscent of those found in my results. I therefore propose a possible scheme linking input integration and the NMDAR-mediated K^+ signal, as summarized in Fig. 32.

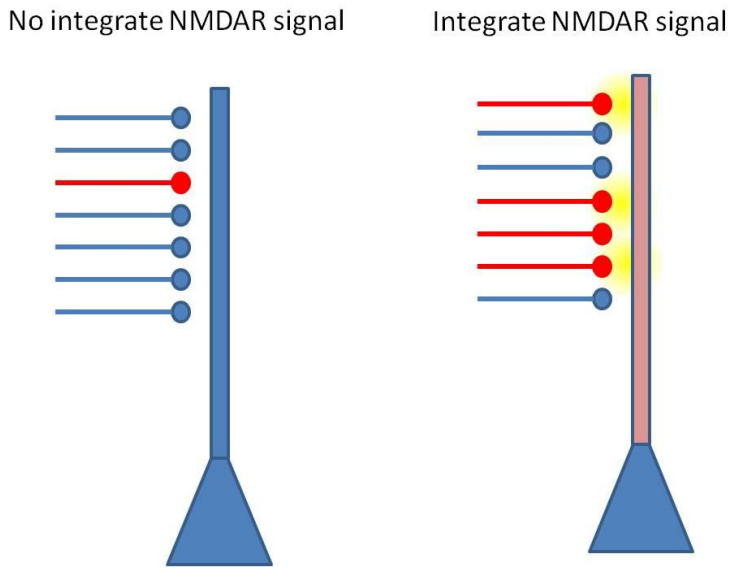

Figure 32. Single Input and Cooperative Inputs. The experiments conducted resulted in the following model of NMDA-K mediated presynaptic modulation. (A) Single input onto the dendrite is relatively weak with faint postsynaptic depolarization. In this case, no NMDA-K mediated presynaptic manipulation can be observed. (B) Integrated inputs are prone to induce large depolarization across the activated dendritic branch. With sufficient NMDA receptors engaged, spines tend to bring the feedback P_r regulation into operation via K^+ signals through NMDA receptors.
Red: activated; blue: not activated; yellow: retrograde K^+ signal

7. Physiological Implications of NMDA-K Mediated Presynaptic Modulation

What might be the physiological role of my findings in NMDA-K mediated presynaptic

modulation? In light of my data, because the NMDAR-mediated K^+ signal functions in a local mode, it could potentially separate the CA1 arbor into a large number of independent nonlinear computational units, each regulating its own synaptic strength. Theoretical predictions (Rabinowitch and Segev, 2006) and recent experimental evidence also point to a local control of synaptic strength (Ju et al., 2004; Liu, 2004; Sutton et al., 2006). Importantly, my results propose that NMDAR-mediated K^+ signals execute presynaptic manipulation only when enough postsynaptic NMDA receptors are relieved from Mg^{2+} blockade. This implies that some form of coincident presynaptic input and strong postsynaptic depolarization is needed, such as synaptic input paired with global backpropagating action potentials or dendritic spikes, for example. This form of regulation would allow neurons to respond not so much to the quantity of input but instead to the specific spatiotemporal input pattern. Furthermore, the K^+ influence on presynaptic transmitter release is biphasic, distinct from other retrograde messengers, and this could be implemented by known depolarization-based homeostatic regulation of release probability, such as the one described by Branco and colleages (2008). They suggest a feedback triggering of P_r homeostatis with increased dendritic depolarization and the resulting branch-specific distribution of release probability. Since transient synaptic potentials spread very efficiently through short dendritic branches but decay considerably with branching, this kind of P_r regulation would be expected to mainly affect activated synapses in the same branch of the dendrite. They propose this feedback P_r regulation acts within a very short integration window, quickly adapting release probability to the dendritic environment. Collectively, my results indicate that individual synapses can monitor activity of their neighbors and continually adjust their release probability through retrograde NMDAR-mediated K^+ signals. One important issue that remains to be fully characterized is the extent of the spatial spread of this feedback regulation, which will depend on

the underlying mechanism generating sufficient postsynaptic depolarization. Aside from preventing synaptic saturation, such a mechanism could function to match the strength of synaptic input to the degree of excitability of each dendritic compartment (Polsky et al., 2004).

8. Postsynaptic NMDARs, but not Presynaptic NMDARs, Contribute to Presynaptic Regulation

In accordance with the findings of single bouton Ca^{2+} imaging, I found that removal of Mg^{2+} block by Mg^{2+}-free ACSF had a discriminatory enhancement effect on the Ca^{2+} transients induced by trains of stimuli. Intriguingly, Mg^{2+}-free ACSF still facilitated presynaptic Ca^{2+} transients even when iMK-801 was specifically applied to presynaptic CA3 neurons. Since iMK-801 proved to work in my system (Fig. 28A), this finding indicates that this presynaptic modulation was primarily produced by postsynaptic NMDA receptors. This contradicts recent data (McGuinness et al., 2010) suggesting that presynaptic NMDA receptor activation is critical in producing facilitation of transmission in hippocampus. Here, a bimodally distribution of trial-by-trial amplitude of the evoked presynaptic Ca^{2+} transients in hippocampal boutons was observed and the activation of presynaptic NMDA receptors postulated to underlie larger Ca^{2+} transients. However, I did not detect such clear discrepancy of two Ca^{2+} transient groups within trial-by-trial AP stimulation (Fig. 25, gray traces). The contradictory results might be explained by the expression level of presynaptic NMDA receptors in mice at different ages. Even though accumulating evidence suggests the existence of presynaptic NMDA receptors in several brain regions (Bardoni et al., 2004; Brasier and Feldman, 2008; Corlew et al., 2007; Glitsch and Marty, 1999; Huang and Bordey, 2004; Paquet and Smith, 2000; Yang et al., 2006), including the hippocampus (Charton et al., 1999; Thompson et al., 2002) (Jourdain et al., 2007), functional

presynaptic NMDA receptors show a rapid developmental loss (Mameli et al., 2005; Mathew and Hablitz, 2011; Yang et al., 2006). Presynaptic NMDA receptors enhance neurotransmitter release at synapses onto visual cortex pyramidal cells in young mice (before P20), but they have no apparent effect after the onset of a critical period (> P23) (Corlew et al., 2007). Consistent with this proposition, freeze fracture data from our collaborator showed no expression of GluN1 subunit in the presynaptic region with animals at P26, around the age range (P28-P49) I used for all my experiments. By contrast, McGuiness et al (2010) used animals aged around P14 in their study. This may be the reason why they could identify GluN1 labeling at presynaptic loci at the electron microscope level. Therefore, my findings agree with a growing body of literature that the properties of presynaptic modulation by NMDA receptors must be considered within a developmental context.

9. Adjustment of Astrocytic Glutamate Transporter by NMDAR-Mediated $[K^+]_o$

As a result of the abundant expression of K^+ channels on astrocytes, my result confirmed that the membrane potential of astrocytes faithfully reflects the K^+ equilibrium potential and is very sensitive to a change in $[K^+]_o$ (Fig. 31C and also (Meeks and Mennerick, 2007; Orkand et al., 1966). In this case, NMDAR-mediated K^+ would be expected to disturb the activity of ion gradient-dependent transporters, such as glutamate transporter (Levy et al., 1998), because of its influence on ion gradients and accompanied membrane depolarization. Indeed, my experiments demonstrated > 25% reduction of glutamate uptake by 7.5 mM $[K^+]_o$, and depolarizing the recorded astrocyte to the expected membrane potential could duplicate the impact of corresponding $[K^+]_o$. These results suggested that $[K^+]_o$ modulates astrocytic glutamate uptake efficiency mainly via depolarization. Furthermore, by participating in the manipulation of the

membrane potential of the recorded astrocyte can restore normal operation of astrocyte glutamate transporters even with high $[K^+]_o$. In support of my findings, Swanson and Duan (1999) have demonstrated that the reduced efficiency of glial glutamate transporter after LTP induction reflecting the increased K^+ accumulation and membrane depolarization. Inhibition of astrocyte glutamate uptake has been shown to influence neuronal excitability and the efficacy of synaptic transmission in several different systems (Barbour et al., 1994; Tong and Jahr, 1994; Turecek and Trussell, 2000), as well as animal behavior (Rothstein et al., 1996; Tanaka et al., 1997; Watase et al., 1998). Given that processes of hippocampal passive astrocytes express high level glutamate transporters, reduction of astrocytic glutamate uptake by NMDAR-mediated $[K^+]_o$ would therefore be one appealing mechanism in modification of neuron-astrocyte communication.

10. Future work

In this thesis, I have shown several lines of evidence that K^+ ions can be a potential retrograde signal to modulate presynaptic function and perisynaptic astrocytic glutamate transporters. Although several attempts have been made to estimate synaptic K^+ concentration (simulation and Ca^{2+} imaging, etc.), the real spatial distribution and time scale of NMDAR-mediated $[K^+]_o$ near the synaptic neuropil remained to be elucidated. This question could be investigated by employing a membrane-impermeable K^+ sensor newly devised by Dr. Takuya Terai with improved sensitivity to physiological concentration of potassium (0-20 mM). Ideally, I would like to perform K^+ imaging close to the A594-labelled spines to map the stimulus evoked $[K^+]_o$ rise around the synapse.

Of additional interest would be to link the $[K^+]_o$ produced by various patterns of neuronal

activity to underlying bidirectional presynaptic modulation. Depolarizing the presynaptic terminal to -57 mV by raising extracellular K^+ concentration would facilitate transmitter release, but further depolarization produces depression (Hori and Takahashi, 2009). The required frequency and number of stimuli to produce NMDAR-mediated $[K^+]_o$ at these two ranges is unclear, and dissecting these conditions by combining simulation and electrophysiological experiments will certainly add interesting information to the understanding of the brain's computational capacity.

References

Abbott, L.F., and Nelson, S.B. (2000). Synaptic plasticity: taming the beast. Nat Neurosci *3 Suppl*, 1178-1183.

Adelman, W.J., Jr., and Fitzhugh, R. (1975). Solutions of the Hodgkin-Huxley equations modified for potassium accumulation in a periaxonal space. Fed Proc *34*, 1322-1329.

Alger, B.E. (2002). Retrograde signaling in the regulation of synaptic transmission: focus on endocannabinoids. Prog Neurobiol *68*, 247-286.

Alonso, G., and Widmer, H. (1997). Clustering of KV4.2 potassium channels in postsynaptic membrane of rat supraoptic neurons: an ultrastructural study. Neuroscience *77*, 617-621.

Amedee, T., Robert, A., and Coles, J.A. (1997). Potassium homeostasis and glial energy metabolism. Glia *21*, 46-55.

Andersen, P., Trommald, M., and Jensen, V. (1994). Low synaptic convergence of CA3 collaterals on CA1 pyramidal cells suggests few release sites. Adv Second Messenger Phosphoprotein Res *29*, 340-351.

Andersson, M., Blomstrand, F., and Hanse, E. (2007). Astrocytes play a critical role in transient heterosynaptic depression in the rat hippocampal CA1 region. J Physiol *585*, 843-852.

Angulo, M.C., Kozlov, A.S., Charpak, S., and Audinat, E. (2004). Glutamate released from glial cells synchronizes neuronal activity in the hippocampus. J Neurosci *24*, 6920-6927.

Antonov, S.M., and Johnson, J.W. (1999). Permeant ion regulation of N-methyl-D-aspartate receptor channel block by Mg(2+). Proc Natl Acad Sci U S A *96*, 14571-14576.

Araque, A., Parpura, V., Sanzgiri, R.P., and Haydon, P.G. (1998a). Glutamate-dependent astrocyte modulation of synaptic transmission between cultured hippocampal neurons. Eur J Neurosci *10*, 2129-2142.

Araque, A., Sanzgiri, R.P., Parpura, V., and Haydon, P.G. (1998b). Calcium elevation in astrocytes causes an NMDA receptor-dependent increase in the frequency of miniature synaptic currents in cultured hippocampal neurons. J Neurosci *18*, 6822-6829.

Araque, A., Sanzgiri, R.P., Parpura, V., and Haydon, P.G. (1999). Astrocyte-induced modulation of synaptic transmission. Can J Physiol Pharmacol *77*, 699-706.

Araya, R., Eisenthal, K.B., and Yuste, R. (2006). Dendritic spines linearize the summation of excitatory potentials. Proc Natl Acad Sci U S A *103*, 18799-18804.

Ascher, P., and Nowak, L. (1988). The role of divalent cations in the N-methyl-D-aspartate responses of mouse central neurones in culture. J Physiol *399*, 247-266.

Asztely, F., Erdemli, G., and Kullmann, D.M. (1997). Extrasynaptic glutamate spillover in the hippocampus: dependence on temperature and the role of active glutamate uptake. Neuron *18*,

281-293.

Atoji, Y., and Wild, J.M. (2006). Anatomy of the avian hippocampal formation. Rev Neurosci *17*, 3-15.

Attwell, D., and Gibb, A. (2005). Neuroenergetics and the kinetic design of excitatory synapses. Nat Rev Neurosci *6*, 841-849.

Awatramani, G.B., Price, G.D., and Trussell, L.O. (2005). Modulation of transmitter release by presynaptic resting potential and background calcium levels. Neuron *48*, 109-121.

Balestrino, M., Aitken, P.G., and Somjen, G.G. (1986). The effects of moderate changes of extracellular K+ and Ca2+ on synaptic and neural function in the CA1 region of the hippocampal slice. Brain Res *377*, 229-239.

Ballanyi, K., Grafe, P., and ten Bruggencate, G. (1987). Ion activities and potassium uptake mechanisms of glial cells in guinea-pig olfactory cortex slices. J Physiol *382*, 159-174.

Ballyk, B.A., and Goh, J.W. (1992). Elevation of extracellular potassium facilitates the induction of hippocampal long-term potentiation. J Neurosci Res *33*, 598-604.

Barbour, B., Brew, H., and Attwell, D. (1988). Electrogenic glutamate uptake in glial cells is activated by intracellular potassium. Nature *335*, 433-435.

Barbour, B., and Hausser, M. (1997). Intersynaptic diffusion of neurotransmitter. Trends Neurosci *20*, 377-384.

Barbour, B., Keller, B.U., Llano, I., and Marty, A. (1994). Prolonged presence of glutamate during excitatory synaptic transmission to cerebellar Purkinje cells. Neuron *12*, 1331-1343.

Bardoni, R., Torsney, C., Tong, C.K., Prandini, M., and MacDermott, A.B. (2004). Presynaptic NMDA receptors modulate glutamate release from primary sensory neurons in rat spinal cord dorsal horn. J Neurosci *24*, 2774-2781.

Barish, M.E., Ichikawa, M., Tominaga, T., Matsumoto, G., and Iijima, T. (1996). Enhanced fast synaptic transmission and a delayed depolarization induced by transient potassium current blockade in rat hippocampal slice as studied by optical recording. J Neurosci *16*, 5672-5687.

Bergles, D.E., and Jahr, C.E. (1997). Synaptic activation of glutamate transporters in hippocampal astrocytes. Neuron *19*, 1297-1308.

Bergles, D.E., Roberts, J.D., Somogyi, P., and Jahr, C.E. (2000). Glutamatergic synapses on oligodendrocyte precursor cells in the hippocampus. Nature *405*, 187-191.

Berretta, N., and Jones, R.S. (1996). Tonic facilitation of glutamate release by presynaptic N-methyl-D-aspartate autoreceptors in the entorhinal cortex. Neuroscience *75*, 339-344.

Bezzi, P., Carmignoto, G., Pasti, L., Vesce, S., Rossi, D., Rizzini, B.L., Pozzan, T., and Volterra, A. (1998). Prostaglandins stimulate calcium-dependent glutamate release in astrocytes. Nature *391*, 281-285.

Bi, G.Q., and Poo, M.M. (1998). Synaptic modifications in cultured hippocampal neurons: dependence on spike timing, synaptic strength, and postsynaptic cell type. J Neurosci *18*, 10464-10472.

Bielefeldt, K., and Jackson, M.B. (1993). A calcium-activated potassium channel causes frequency-dependent action-potential failures in a mammalian nerve terminal. J Neurophysiol *70*, 284-298.

Bittner, C.X., Valdebenito, R., Ruminot, I., Loaiza, A., Larenas, V., Sotelo-Hitschfeld, T., Moldenhauer, H., San Martin, A., Gutierrez, R., Zambrano, M., *et al.* (2011). Fast and reversible stimulation of astrocytic glycolysis by K+ and a delayed and persistent effect of glutamate. J Neurosci *31*, 4709-4713.

Blackstad, T.W. (1956). Commissural connections of the hippocampal region in the rat, with special reference to their mode of termination. J Comp Neurol *105*, 417-537.

Blank, T., Nijholt, I., Kye, M.J., Radulovic, J., and Spiess, J. (2003). Small-conductance, Ca2+-activated K+ channel SK3 generates age-related memory and LTP deficits. Nat Neurosci *6*, 911-912.

Bliss, T.V., and Collingridge, G.L. (1993). A synaptic model of memory: long-term potentiation in the hippocampus. Nature *361*, 31-39.

Bliss, T.V., and Lomo, T. (1973). Long-lasting potentiation of synaptic transmission in the dentate area of the anaesthetized rabbit following stimulation of the perforant path. J Physiol *232*, 331-356.

Bollmann, J.H., Sakmann, B., and Borst, J.G. (2000). Calcium sensitivity of glutamate release in a calyx-type terminal. Science *289*, 953-957.

Bordey, A., and Sontheimer, H. (2003). Modulation of glutamatergic transmission by bergmann glial cells in rat cerebellum in situ. J Neurophysiol *89*, 979-988.

Branco, T., Clark, B.A., and Hausser, M. (2010). Dendritic discrimination of temporal input sequences in cortical neurons. Science *329*, 1671-1675.

Branco, T., Staras, K., Darcy, K.J., and Goda, Y. (2008). Local dendritic activity sets release probability at hippocampal synapses. Neuron *59*, 475-485.

Brasier, D.J., and Feldman, D.E. (2008). Synapse-specific expression of functional presynaptic NMDA receptors in rat somatosensory cortex. J Neurosci *28*, 2199-2211.

Brenowitz, S.D., and Regehr, W.G. (2007). Reliability and heterogeneity of calcium signaling at

single presynaptic boutons of cerebellar granule cells. J Neurosci *27*, 7888-7898.

Brew, H.M., and Forsythe, I.D. (1995). Two voltage-dependent K+ conductances with complementary functions in postsynaptic integration at a central auditory synapse. J Neurosci *15*, 8011-8022.

Brookes, N., and Yarowsky, P.J. (1985). Determinants of deoxyglucose uptake in cultured astrocytes: the role of the sodium pump. J Neurochem *44*, 473-479.

Brown, R.E., and Reymann, K.G. (1995). Metabotropic glutamate receptor agonists reduce paired-pulse depression in the dentate gyrus of the rat in vitro. Neurosci Lett *196*, 17-20.

Buono, R.J., Lohoff, F.W., Sander, T., Sperling, M.R., O'Connor, M.J., Dlugos, D.J., Ryan, S.G., Golden, G.T., Zhao, H., Scattergood, T.M., *et al.* (2004). Association between variation in the human KCNJ10 potassium ion channel gene and seizure susceptibility. Epilepsy Res *58*, 175-183.

Burnashev, N., Zhou, Z., Neher, E., and Sakmann, B. (1995). Fractional calcium currents through recombinant GluR channels of the NMDA, AMPA and kainate receptor subtypes. J Physiol *485 (Pt 2)*, 403-418.

Bushong, E.A., Martone, M.E., and Ellisman, M.H. (2004). Maturation of astrocyte morphology and the establishment of astrocyte domains during postnatal hippocampal development. Int J Dev Neurosci *22*, 73-86.

Bushong, E.A., Martone, M.E., Jones, Y.Z., and Ellisman, M.H. (2002). Protoplasmic astrocytes in CA1 stratum radiatum occupy separate anatomical domains. J Neurosci *22*, 183-192.

Caesar, K., Hashemi, P., Douhou, A., Bonvento, G., Boutelle, M.G., Walls, A.B., and Lauritzen, M. (2008). Glutamate receptor-dependent increments in lactate, glucose and oxygen metabolism evoked in rat cerebellum in vivo. J Physiol *586*, 1337-1349.

Cai, X., Liang, C.W., Muralidharan, S., Kao, J.P., Tang, C.M., and Thompson, S.M. (2004). Unique roles of SK and Kv4.2 potassium channels in dendritic integration. Neuron *44*, 351-364.

Cash, S., and Yuste, R. (1999). Linear summation of excitatory inputs by CA1 pyramidal neurons. Neuron *22*, 383-394.

Casullo, J., and Krnjevic, K. (1987). Glial potentials in hippocampus. Can J Physiol Pharmacol *65*, 847-855.

Chamberlin, N.L., Traub, R.D., and Dingledine, R. (1990). Role of EPSPs in initiation of spontaneous synchronized burst firing in rat hippocampal neurons bathed in high potassium. J Neurophysiol *64*, 1000-1008.

Charton, J.P., Herkert, M., Becker, C.M., and Schroder, H. (1999). Cellular and subcellular localization of the 2B-subunit of the NMDA receptor in the adult rat telencephalon. Brain Res *816*, 609-617.

Chatterton, J.E., Awobuluyi, M., Premkumar, L.S., Takahashi, H., Talantova, M., Shin, Y., Cui, J., Tu, S., Sevarino, K.A., Nakanishi, N., *et al.* (2002). Excitatory glycine receptors containing the NR3 family of NMDA receptor subunits. Nature *415*, 793-798.

Chaudhry, F.A., Lehre, K.P., van Lookeren Campagne, M., Ottersen, O.P., Danbolt, N.C., and Storm-Mathisen, J. (1995). Glutamate transporters in glial plasma membranes: highly differentiated localizations revealed by quantitative ultrastructural immunocytochemistry. Neuron *15*, 711-720.

Chen, X., and Johnston, D. (2004). Properties of single voltage-dependent K+ channels in dendrites of CA1 pyramidal neurones of rat hippocampus. J Physiol *559*, 187-203.

Ciabarra, A.M., Sullivan, J.M., Gahn, L.G., Pecht, G., Heinemann, S., and Sevarino, K.A. (1995). Cloning and characterization of chi-1: a developmentally regulated member of a novel class of the ionotropic glutamate receptor family. J Neurosci *15*, 6498-6508.

Clark, B.A., and Barbour, B. (1997). Currents evoked in Bergmann glial cells by parallel fibre stimulation in rat cerebellar slices. J Physiol *502 (Pt 2)*, 335-350.

Coles, J.A., and Poulain, D.A. (1991). Extracellular K+ in the supraoptic nucleus of the rat during reflex bursting activity by oxytocin neurones. J Physiol *439*, 383-409.

Cooper, E.C., Milroy, A., Jan, Y.N., Jan, L.Y., and Lowenstein, D.H. (1998). Presynaptic localization of Kv1.4-containing A-type potassium channels near excitatory synapses in the hippocampus. J Neurosci *18*, 965-974.

Corlew, R., Wang, Y., Ghermazien, H., Erisir, A., and Philpot, B.D. (2007). Developmental switch in the contribution of presynaptic and postsynaptic NMDA receptors to long-term depression. J Neurosci *27*, 9835-9845.

Cottrell, J.R., Dube, G.R., Egles, C., and Liu, G. (2000). Distribution, density, and clustering of functional glutamate receptors before and after synaptogenesis in hippocampal neurons. J Neurophysiol *84*, 1573-1587.

Cowan, A.I., and Martin, R.L. (1992). Ionic basis of membrane potential changes induced by anoxia in rat dorsal vagal motoneurones. J Physiol *455*, 89-109.

Cull-Candy, S., Brickley, S., and Farrant, M. (2001). NMDA receptor subunits: diversity, development and disease. Curr Opin Neurobiol *11*, 327-335.

Cull-Candy, S.G., and Leszkiewicz, D.N. (2004). Role of distinct NMDA receptor subtypes at central synapses. Sci STKE *2004*, re16.

D'Ambrosio, R. (2004). The role of glial membrane ion channels in seizures and epileptogenesis. Pharmacol Ther *103*, 95-108.

D'Ambrosio, R., Gordon, D.S., and Winn, H.R. (2002). Differential role of KIR channel and

Na(+)/K(+)-pump in the regulation of extracellular K(+) in rat hippocampus. J Neurophysiol *87*, 87-102.

D'Ambrosio, R., Wenzel, J., Schwartzkroin, P.A., McKhann, G.M., 2nd, and Janigro, D. (1998). Functional specialization and topographic segregation of hippocampal astrocytes. J Neurosci *18*, 4425-4438.

Dan, Y., and Poo, M.M. (2004). Spike timing-dependent plasticity of neural circuits. Neuron *44*, 23-30.

Danbolt, N.C. (2001). Glutamate uptake. Prog Neurobiol *65*, 1-105.

De Saint Jan, D., and Westbrook, G.L. (2005). Detecting activity in olfactory bulb glomeruli with astrocyte recording. J Neurosci *25*, 2917-2924.

Debanne, D., Gahwiler, B.H., and Thompson, S.M. (1998). Long-term synaptic plasticity between pairs of individual CA3 pyramidal cells in rat hippocampal slice cultures. J Physiol *507 (Pt 1)*, 237-247.

Derouiche, A., and Frotscher, M. (2001). Peripheral astrocyte processes: monitoring by selective immunostaining for the actin-binding ERM proteins. Glia *36*, 330-341.

Devaux, J., Alcaraz, G., Grinspan, J., Bennett, V., Joho, R., Crest, M., and Scherer, S.S. (2003). Kv3.1b is a novel component of CNS nodes. J Neurosci *23*, 4509-4518.

Diamond, J.S. (2005). Deriving the glutamate clearance time course from transporter currents in CA1 hippocampal astrocytes: transmitter uptake gets faster during development. J Neurosci *25*, 2906-2916.

Diamond, J.S., Bergles, D.E., and Jahr, C.E. (1998). Glutamate release monitored with astrocyte transporter currents during LTP. Neuron *21*, 425-433.

Dingledine, R., Borges, K., Bowie, D., and Traynelis, S.F. (1999). The glutamate receptor ion channels. Pharmacol Rev *51*, 7-61.

Djukic, B., Casper, K.B., Philpot, B.D., Chin, L.S., and McCarthy, K.D. (2007). Conditional knock-out of Kir4.1 leads to glial membrane depolarization, inhibition of potassium and glutamate uptake, and enhanced short-term synaptic potentiation. J Neurosci *27*, 11354-11365.

Dobrunz, L.E., and Stevens, C.F. (1997). Heterogeneity of release probability, facilitation, and depletion at central synapses. Neuron *18*, 995-1008.

Dobrunz, L.E., and Stevens, C.F. (1999). Response of hippocampal synapses to natural stimulation patterns. Neuron *22*, 157-166.

Dodson, P.D., Billups, B., Rusznak, Z., Szucs, G., Barker, M.C., and Forsythe, I.D. (2003). Presynaptic rat Kv1.2 channels suppress synaptic terminal hyperexcitability following action

potential invasion. J Physiol *550*, 27-33.

Duan, S., Anderson, C.M., Stein, B.A., and Swanson, R.A. (1999). Glutamate induces rapid upregulation of astrocyte glutamate transport and cell-surface expression of GLAST. J Neurosci *19*, 10193-10200.

Dunah, A.W., Yasuda, R.P., Luo, J., Wang, Y., Prybylowski, K.L., and Wolfe, B.B. (1999). Biochemical studies of the structure and function of the N-methyl-D-aspartate subtype of glutamate receptors. Mol Neurobiol *19*, 151-179.

Ehinger, B., Zucker, C.L., Bruun, A., and Adolph, A. (1994). In vivo staining of oligodendroglia in the rabbit retina. Glia *10*, 40-48.

Enkvist, M.O., and McCarthy, K.D. (1994). Astroglial gap junction communication is increased by treatment with either glutamate or high K+ concentration. J Neurochem *62*, 489-495.

Faber, E.S., Delaney, A.J., and Sah, P. (2005). SK channels regulate excitatory synaptic transmission and plasticity in the lateral amygdala. Nat Neurosci *8*, 635-641.

Fellin, T., and Carmignoto, G. (2004). Neurone-to-astrocyte signalling in the brain represents a distinct multifunctional unit. J Physiol *559*, 3-15.

Fellin, T., Pascual, O., Gobbo, S., Pozzan, T., Haydon, P.G., and Carmignoto, G. (2004). Neuronal synchrony mediated by astrocytic glutamate through activation of extrasynaptic NMDA receptors. Neuron *43*, 729-743.

Ferraro, T.N., Golden, G.T., Smith, G.G., Martin, J.F., Lohoff, F.W., Gieringer, T.A., Zamboni, D., Schwebel, C.L., Press, D.M., Kratzer, S.O., *et al.* (2004). Fine mapping of a seizure susceptibility locus on mouse Chromosome 1: nomination of Kcnj10 as a causative gene. Mamm Genome *15*, 239-251.

Fertziger, A.P., and Ranck, J.B., Jr. (1970). Potassium accumulation in interstitial space during epileptiform seizures. Exp Neurol *26*, 571-585.

Fiacco, T.A., and McCarthy, K.D. (2004). Intracellular astrocyte calcium waves in situ increase the frequency of spontaneous AMPA receptor currents in CA1 pyramidal neurons. J Neurosci *24*, 722-732.

Fukaya, M., Kato, A., Lovett, C., Tonegawa, S., and Watanabe, M. (2003). Retention of NMDA receptor NR2 subunits in the lumen of endoplasmic reticulum in targeted NR1 knockout mice. Proc Natl Acad Sci U S A *100*, 4855-4860.

Gardner-Medwin, A.R., and Nicholson, C. (1983). Changes of extracellular potassium activity induced by electric current through brain tissue in the rat. J Physiol *335*, 375-392.

Ge, W.P., and Duan, S. (2007). Persistent enhancement of neuron-glia signaling mediated by increased extracellular K+ accompanying long-term synaptic potentiation. J Neurophysiol *97*,

2564-2569.

Giaume, C., and McCarthy, K.D. (1996). Control of gap-junctional communication in astrocytic networks. Trends Neurosci *19*, 319-325.

Glitsch, M., and Marty, A. (1999). Presynaptic effects of NMDA in cerebellar Purkinje cells and interneurons. J Neurosci *19*, 511-519.

Godwin, A.J., Green, L.M., Walsh, M.P., McDonald, J.R., Walsh, D.A., and Fletcher, W.H. (1993). In situ regulation of cell-cell communication by the cAMP-dependent protein kinase and protein kinase C. Mol Cell Biochem *127-128*, 293-307.

Golding, N.L., Jung, H.Y., Mickus, T., and Spruston, N. (1999). Dendritic calcium spike initiation and repolarization are controlled by distinct potassium channel subtypes in CA1 pyramidal neurons. J Neurosci *19*, 8789-8798.

Golomb, D., Yue, C., and Yaari, Y. (2006). Contribution of persistent Na+ current and M-type K+ current to somatic bursting in CA1 pyramidal cells: combined experimental and modeling study. J Neurophysiol *96*, 1912-1926.

Gordon, G.R., Choi, H.B., Rungta, R.L., Ellis-Davies, G.C., and MacVicar, B.A. (2008). Brain metabolism dictates the polarity of astrocyte control over arterioles. Nature *456*, 745-749.

Grosche, J., Kettenmann, H., and Reichenbach, A. (2002). Bergmann glial cells form distinct morphological structures to interact with cerebellar neurons. J Neurosci Res *68*, 138-149.

Grosche, J., Matyash, V., Moller, T., Verkhratsky, A., Reichenbach, A., and Kettenmann, H. (1999). Microdomains for neuron-glia interaction: parallel fiber signaling to Bergmann glial cells. Nat Neurosci *2*, 139-143.

Gu, N., Vervaeke, K., Hu, H., and Storm, J.F. (2005). Kv7/KCNQ/M and HCN/h, but not KCa2/SK channels, contribute to the somatic medium after-hyperpolarization and excitability control in CA1 hippocampal pyramidal cells. J Physiol *566*, 689-715.

Gustafsson, B., Wigstrom, H., Abraham, W.C., and Huang, Y.Y. (1987). Long-term potentiation in the hippocampus using depolarizing current pulses as the conditioning stimulus to single volley synaptic potentials. J Neurosci *7*, 774-780.

Halassa, M.M., Fellin, T., Takano, H., Dong, J.H., and Haydon, P.G. (2007). Synaptic islands defined by the territory of a single astrocyte. J Neurosci *27*, 6473-6477.

Hammond, R.S., Bond, C.T., Strassmaier, T., Ngo-Anh, T.J., Adelman, J.P., Maylie, J., and Stackman, R.W. (2006). Small-conductance Ca2+-activated K+ channel type 2 (SK2) modulates hippocampal learning, memory, and synaptic plasticity. J Neurosci *26*, 1844-1853.

Hansen, A.J. (1985). Effect of anoxia on ion distribution in the brain. Physiol Rev *65*, 101-148.

Hansen, A.J., Hounsgaard, J., and Jahnsen, H. (1982). Anoxia increases potassium conductance in hippocampal nerve cells. Acta Physiol Scand *115*, 301-310.

Hardingham, G.E., and Bading, H. (2010). Synaptic versus extrasynaptic NMDA receptor signalling: implications for neurodegenerative disorders. Nat Rev Neurosci *11*, 682-696.

Haydon, P.G. (2001). GLIA: listening and talking to the synapse. Nat Rev Neurosci *2*, 185-193.

He, Y., Janssen, W.G., and Morrison, J.H. (1998). Synaptic coexistence of AMPA and NMDA receptors in the rat hippocampus: a postembedding immunogold study. J Neurosci Res *54*, 444-449.

Hebb, D.O. (1949). The organization of behavior; a neuropsychological theory (New York,, Wiley).

Heinemann, U., and Lux, H.D. (1977). Ceiling of stimulus induced rises in extracellular potassium concentration in the cerebral cortex of cat. Brain Res *120*, 231-249.

Heinemann, U., Schaible, H.G., and Schmidt, R.F. (1990). Changes in extracellular potassium concentration in cat spinal cord in response to innocuous and noxious stimulation of legs with healthy and inflamed knee joints. Exp Brain Res *79*, 283-292.

Henneberger, C., Papouin, T., Oliet, S.H., and Rusakov, D.A. (2010). Long-term potentiation depends on release of D-serine from astrocytes. Nature *463*, 232-236.

Herreras, O., Largo, C., Ibarz, J.M., Somjen, G.G., and Martin del Rio, R. (1994). Role of neuronal synchronizing mechanisms in the propagation of spreading depression in the in vivo hippocampus. J Neurosci *14*, 7087-7098.

Higashi, K., Fujita, A., Inanobe, A., Tanemoto, M., Doi, K., Kubo, T., and Kurachi, Y. (2001). An inwardly rectifying K(+) channel, Kir4.1, expressed in astrocytes surrounds synapses and blood vessels in brain. Am J Physiol Cell Physiol *281*, C922-931.

Hirrlinger, P.G., Scheller, A., Braun, C., Hirrlinger, J., and Kirchhoff, F. (2006). Temporal control of gene recombination in astrocytes by transgenic expression of the tamoxifen-inducible DNA recombinase variant CreERT2. Glia *54*, 11-20.

Hoffman, D.A., Magee, J.C., Colbert, C.M., and Johnston, D. (1997). K+ channel regulation of signal propagation in dendrites of hippocampal pyramidal neurons. Nature *387*, 869-875.

Holthoff, K., and Witte, O.W. (2000). Directed spatial potassium redistribution in rat neocortex. Glia *29*, 288-292.

Hori, T., and Takahashi, T. (2009). Mechanisms underlying short-term modulation of transmitter release by presynaptic depolarization. J Physiol *587*, 2987-3000.

Hu, H., Shao, L.R., Chavoshy, S., Gu, N., Trieb, M., Behrens, R., Laake, P., Pongs, O., Knaus,

H.G., Ottersen, O.P., *et al.* (2001). Presynaptic Ca2+-activated K+ channels in glutamatergic hippocampal terminals and their role in spike repolarization and regulation of transmitter release. J Neurosci *21*, 9585-9597.

Hu, Y., and Wilson, G.S. (1997). A temporary local energy pool coupled to neuronal activity: fluctuations of extracellular lactate levels in rat brain monitored with rapid-response enzyme-based sensor. J Neurochem *69*, 1484-1490.

Huang, H., and Bordey, A. (2004). Glial glutamate transporters limit spillover activation of presynaptic NMDA receptors and influence synaptic inhibition of Purkinje neurons. J Neurosci *24*, 5659-5669.

Huang, Y.H., and Bergles, D.E. (2004). Glutamate transporters bring competition to the synapse. Curr Opin Neurobiol *14*, 346-352.

Humeau, Y., Shaban, H., Bissiere, S., and Luthi, A. (2003). Presynaptic induction of heterosynaptic associative plasticity in the mammalian brain. Nature *426*, 841-845.

Ichinose, T., Yu, S., Wang, X.Q., and Yu, S.P. (2003). Ca2+-independent, but voltage- and activity-dependent regulation of the NMDA receptor outward K+ current in mouse cortical neurons. J Physiol *551*, 403-417.

Ishikawa, T., Nakamura, Y., Saitoh, N., Li, W.B., Iwasaki, S., and Takahashi, T. (2003). Distinct roles of Kv1 and Kv3 potassium channels at the calyx of Held presynaptic terminal. J Neurosci *23*, 10445-10453.

Ivanov, A., Pellegrino, C., Rama, S., Dumalska, I., Salyha, Y., Ben-Ari, Y., and Medina, I. (2006). Opposing role of synaptic and extrasynaptic NMDA receptors in regulation of the extracellular signal-regulated kinases (ERK) activity in cultured rat hippocampal neurons. J Physiol *572*, 789-798.

Jabs, R., Pivneva, T., Huttmann, K., Wyczynski, A., Nolte, C., Kettenmann, H., and Steinhauser, C. (2005). Synaptic transmission onto hippocampal glial cells with hGFAP promoter activity. J Cell Sci *118*, 3791-3803.

Janigro, D., Gasparini, S., D'Ambrosio, R., McKhann, G., 2nd, and DiFrancesco, D. (1997). Reduction of K+ uptake in glia prevents long-term depression maintenance and causes epileptiform activity. J Neurosci *17*, 2813-2824.

Jensen, M.S., and Yaari, Y. (1988). The relationship between interictal and ictal paroxysms in an in vitro model of focal hippocampal epilepsy. Ann Neurol *24*, 591-598.

Johnson, J.W., and Ascher, P. (1987). Glycine potentiates the NMDA response in cultured mouse brain neurons. Nature *325*, 529-531.

Johnston, D., Hoffman, D.A., Magee, J.C., Poolos, N.P., Watanabe, S., Colbert, C.M., and Migliore, M. (2000). Dendritic potassium channels in hippocampal pyramidal neurons. J Physiol

525 Pt 1, 75-81.

Jonas, P., Koh, D.S., Kampe, K., Hermsteiner, M., and Vogel, W. (1991). ATP-sensitive and Ca-activated K channels in vertebrate axons: novel links between metabolism and excitability. Pflugers Arch *418*, 68-73.

Jourdain, P., Bergersen, L.H., Bhaukaurally, K., Bezzi, P., Santello, M., Domercq, M., Matute, C., Tonello, F., Gundersen, V., and Volterra, A. (2007). Glutamate exocytosis from astrocytes controls synaptic strength. Nat Neurosci *10*, 331-339.

Ju, W., Morishita, W., Tsui, J., Gaietta, G., Deerinck, T.J., Adams, S.R., Garner, C.C., Tsien, R.Y., Ellisman, M.H., and Malenka, R.C. (2004). Activity-dependent regulation of dendritic synthesis and trafficking of AMPA receptors. Nat Neurosci *7*, 244-253.

Kafitz, K.W., Meier, S.D., Stephan, J., and Rose, C.R. (2008). Developmental profile and properties of sulforhodamine 101--Labeled glial cells in acute brain slices of rat hippocampus. J Neurosci Methods *169*, 84-92.

Kaila, K., Lamsa, K., Smirnov, S., Taira, T., and Voipio, J. (1997). Long-lasting GABA-mediated depolarization evoked by high-frequency stimulation in pyramidal neurons of rat hippocampal slice is attributable to a network-driven, bicarbonate-dependent K+ transient. J Neurosci *17*, 7662-7672.

Kamiya, H., Ozawa, S., and Manabe, T. (2002). Kainate receptor-dependent short-term plasticity of presynaptic Ca2+ influx at the hippocampal mossy fiber synapses. J Neurosci *22*, 9237-9243.

Kampa, B.M., Clements, J., Jonas, P., and Stuart, G.J. (2004). Kinetics of Mg2+ unblock of NMDA receptors: implications for spike-timing dependent synaptic plasticity. J Physiol *556*, 337-345.

Kampa, B.M., Letzkus, J.J., and Stuart, G.J. (2006). Requirement of dendritic calcium spikes for induction of spike-timing-dependent synaptic plasticity. J Physiol *574*, 283-290.

Kang, J., Jiang, L., Goldman, S.A., and Nedergaard, M. (1998). Astrocyte-mediated potentiation of inhibitory synaptic transmission. Nat Neurosci *1*, 683-692.

Karavanova, I., Vasudevan, K., Cheng, J., and Buonanno, A. (2007). Novel regional and developmental NMDA receptor expression patterns uncovered in NR2C subunit-beta-galactosidase knock-in mice. Mol Cell Neurosci *34*, 468-480.

Karwoski, C.J., Lu, H.K., and Newman, E.A. (1989). Spatial buffering of light-evoked potassium increases by retinal Muller (glial) cells. Science *244*, 578-580.

Katz, B., and Miledi, R. (1968). The role of calcium in neuromuscular facilitation. J Physiol *195*, 481-492.

Kim, J., and Hoffman, D.A. (2008). Potassium channels: newly found players in synaptic

plasticity. Neuroscientist *14*, 276-286.

Kim, J., Jung, S.C., Clemens, A.M., Petralia, R.S., and Hoffman, D.A. (2007). Regulation of dendritic excitability by activity-dependent trafficking of the A-type K+ channel subunit Kv4.2 in hippocampal neurons. Neuron *54*, 933-947.

Kim, J., Wei, D.S., and Hoffman, D.A. (2005). Kv4 potassium channel subunits control action potential repolarization and frequency-dependent broadening in rat hippocampal CA1 pyramidal neurones. J Physiol *569*, 41-57.

Kimelberg, H.K. (2004). The problem of astrocyte identity. Neurochem Int *45*, 191-202.

Kirischuk, S., Tuschick, S., Verkhratsky, A., and Kettenmann, H. (1996). Calcium signalling in mouse Bergmann glial cells mediated by alpha1-adrenoreceptors and H1 histamine receptors. Eur J Neurosci *8*, 1198-1208.

Kjaerulff, O., Barajon, I., and Kiehn, O. (1994). Sulphorhodamine-labelled cells in the neonatal rat spinal cord following chemically induced locomotor activity in vitro. J Physiol *478 (Pt 2)*, 265-273.

Koester, H.J., and Sakmann, B. (1998). Calcium dynamics in single spines during coincident pre- and postsynaptic activity depend on relative timing of back-propagating action potentials and subthreshold excitatory postsynaptic potentials. Proc Natl Acad Sci U S A *95*, 9596-9601.

Koester, H.J., and Sakmann, B. (2000). Calcium dynamics associated with action potentials in single nerve terminals of pyramidal cells in layer 2/3 of the young rat neocortex. J Physiol *529 Pt 3*, 625-646.

Kofuji, P., Ceelen, P., Zahs, K.R., Surbeck, L.W., Lester, H.A., and Newman, E.A. (2000). Genetic inactivation of an inwardly rectifying potassium channel (Kir4.1 subunit) in mice: phenotypic impact in retina. J Neurosci *20*, 5733-5740.

Kofuji, P., and Newman, E.A. (2004). Potassium buffering in the central nervous system. Neuroscience *129*, 1045-1056.

Kohler, M., Hirschberg, B., Bond, C.T., Kinzie, J.M., Marrion, N.V., Maylie, J., and Adelman, J.P. (1996). Small-conductance, calcium-activated potassium channels from mammalian brain. Science *273*, 1709-1714.

Kohr, G. (2006). NMDA receptor function: subunit composition versus spatial distribution. Cell Tissue Res *326*, 439-446.

Konnerth, A., Heinemann, U., and Yaari, Y. (1984). Slow transmission of neural activity in hippocampal area CA1 in absence of active chemical synapses. Nature *307*, 69-71.

Korn, S.J., Giacchino, J.L., Chamberlin, N.L., and Dingledine, R. (1987). Epileptiform burst activity induced by potassium in the hippocampus and its regulation by GABA-mediated

inhibition. J Neurophysiol *57*, 325-340.

Kornau, H.C., Schenker, L.T., Kennedy, M.B., and Seeburg, P.H. (1995). Domain interaction between NMDA receptor subunits and the postsynaptic density protein PSD-95. Science *269*, 1737-1740.

Kozlov, A.S., Angulo, M.C., Audinat, E., and Charpak, S. (2006). Target cell-specific modulation of neuronal activity by astrocytes. Proc Natl Acad Sci U S A *103*, 10058-10063.

Krause, J.D., Foster, C.D., and Reinhart, P.H. (1996). Xenopus laevis oocytes contain endogenous large conductance Ca2(+)-activated K+ channels. Neuropharmacology *35*, 1017-1022.

Kreitzer, A.C., and Regehr, W.G. (2001). Retrograde inhibition of presynaptic calcium influx by endogenous cannabinoids at excitatory synapses onto Purkinje cells. Neuron *29*, 717-727.

Krnjevic, K., Morris, M.E., and Reiffenstein, R.J. (1982). Stimulation-evoked changes in extracellular K+ and Ca2+ in pyramidal layers of the rat's hippocampus. Can J Physiol Pharmacol *60*, 1643-1657.

Kruk, P.J., Korn, H., and Faber, D.S. (1997). The effects of geometrical parameters on synaptic transmission: a Monte Carlo simulation study. Biophys J *73*, 2874-2890.

Kuffler, S.W., and Nicholls, J.G. (1966). The physiology of neuroglial cells. Ergeb Physiol *57*, 1-90.

Kullmann, D.M. (1999). Excitatory synapses. Neither too loud nor too quiet. Nature *399*, 111-112.

Kullmann, D.M., and Asztely, F. (1998). Extrasynaptic glutamate spillover in the hippocampus: evidence and implications. Trends Neurosci *21*, 8-14.

Lalo, U., Pankratov, Y., Kirchhoff, F., North, R.A., and Verkhratsky, A. (2006). NMDA receptors mediate neuron-to-glia signaling in mouse cortical astrocytes. J Neurosci *26*, 2673-2683.

Larkum, M.E., Waters, J., Sakmann, B., and Helmchen, F. (2007). Dendritic spikes in apical dendrites of neocortical layer 2/3 pyramidal neurons. J Neurosci *27*, 8999-9008.

Leao, R.N., Tan, H.M., and Fisahn, A. (2009). Kv7/KCNQ channels control action potential phasing of pyramidal neurons during hippocampal gamma oscillations in vitro. J Neurosci *29*, 13353-13364.

LeBeau, F.E., Towers, S.K., Traub, R.D., Whittington, M.A., and Buhl, E.H. (2002). Fast network oscillations induced by potassium transients in the rat hippocampus in vitro. J Physiol *542*, 167-179.

Lehre, K.P., Levy, L.M., Ottersen, O.P., Storm-Mathisen, J., and Danbolt, N.C. (1995).

Differential expression of two glial glutamate transporters in the rat brain: quantitative and immunocytochemical observations. J Neurosci *15*, 1835-1853.

Levy, L.M., Warr, O., and Attwell, D. (1998). Stoichiometry of the glial glutamate transporter GLT-1 expressed inducibly in a Chinese hamster ovary cell line selected for low endogenous Na+-dependent glutamate uptake. J Neurosci *18*, 9620-9628.

Li, L., Head, V., and Timpe, L.C. (2001). Identification of an inward rectifier potassium channel gene expressed in mouse cortical astrocytes. Glia *33*, 57-71.

Li, W.E., and Nagy, J.I. (2000). Activation of fibres in rat sciatic nerve alters phosphorylation state of connexin-43 at astrocytic gap junctions in spinal cord: evidence for junction regulation by neuronal-glial interactions. Neuroscience *97*, 113-123.

Lian, J., Bikson, M., Shuai, J., and Durand, D.M. (2001). Propagation of non-synaptic epileptiform activity across a lesion in rat hippocampal slices. J Physiol *537*, 191-199.

Lin, M.T., Lujan, R., Watanabe, M., Adelman, J.P., and Maylie, J. (2008). SK2 channel plasticity contributes to LTP at Schaffer collateral-CA1 synapses. Nat Neurosci *11*, 170-177.

Liu, G. (2004). Local structural balance and functional interaction of excitatory and inhibitory synapses in hippocampal dendrites. Nat Neurosci *7*, 373-379.

Liu, Q.S., Xu, Q., Kang, J., and Nedergaard, M. (2004). Astrocyte activation of presynaptic metabotropic glutamate receptors modulates hippocampal inhibitory synaptic transmission. Neuron Glia Biol *1*, 307-316.

Lozovaya, N.A., Grebenyuk, S.E., Tsintsadze, T., Feng, B., Monaghan, D.T., and Krishtal, O.A. (2004). Extrasynaptic NR2B and NR2D subunits of NMDA receptors shape 'superslow' afterburst EPSC in rat hippocampus. J Physiol *558*, 451-463.

Luque, J.M., and Richards, J.G. (1995). Expression of NMDA 2B receptor subunit mRNA in Bergmann glia. Glia *13*, 228-232.

Magee, J.C., and Johnston, D. (1997). A synaptically controlled, associative signal for Hebbian plasticity in hippocampal neurons. Science *275*, 209-213.

Major, G., Polsky, A., Denk, W., Schiller, J., and Tank, D.W. (2008). Spatiotemporally graded NMDA spike/plateau potentials in basal dendrites of neocortical pyramidal neurons. J Neurophysiol *99*, 2584-2601.

Malenka, R.C., Kocsis, J.D., Ransom, B.R., and Waxman, S.G. (1981). Modulation of parallel fiber excitability by postsynaptically mediated changes in extracellular potassium. Science *214*, 339-341.

Malenka, R.C., and Nicoll, R.A. (1999). Long-term potentiation--a decade of progress? Science *285*, 1870-1874.

Mameli, M., Carta, M., Partridge, L.D., and Valenzuela, C.F. (2005). Neurosteroid-induced plasticity of immature synapses via retrograde modulation of presynaptic NMDA receptors. J Neurosci *25*, 2285-2294.

Manabe, T., Wyllie, D.J., Perkel, D.J., and Nicoll, R.A. (1993). Modulation of synaptic transmission and long-term potentiation: effects on paired pulse facilitation and EPSC variance in the CA1 region of the hippocampus. J Neurophysiol *70*, 1451-1459.

Mangia, S., Garreffa, G., Bianciardi, M., Giove, F., Di Salle, F., and Maraviglia, B. (2003). The aerobic brain: lactate decrease at the onset of neural activity. Neuroscience *118*, 7-10.

Maravall, M., Mainen, Z.F., Sabatini, B.L., and Svoboda, K. (2000). Estimating intracellular calcium concentrations and buffering without wavelength ratioing. Biophys J *78*, 2655-2667.

Marcus, D.C., Wu, T., Wangemann, P., and Kofuji, P. (2002). KCNJ10 (Kir4.1) potassium channel knockout abolishes endocochlear potential. Am J Physiol Cell Physiol *282*, C403-407.

Mathew, S.S., and Hablitz, J.J. (2011). Presynaptic NMDA receptors mediate IPSC potentiation at GABAergic synapses in developing rat neocortex. PLoS One *6*, e17311.

Matsui, T., Sekiguchi, M., Hashimoto, A., Tomita, U., Nishikawa, T., and Wada, K. (1995). Functional comparison of D-serine and glycine in rodents: the effect on cloned NMDA receptors and the extracellular concentration. J Neurochem *65*, 454-458.

Matsuzaki, M., Ellis-Davies, G.C., Nemoto, T., Miyashita, Y., Iino, M., and Kasai, H. (2001). Dendritic spine geometry is critical for AMPA receptor expression in hippocampal CA1 pyramidal neurons. Nat Neurosci *4*, 1086-1092.

Matthias, K., Kirchhoff, F., Seifert, G., Huttmann, K., Matyash, M., Kettenmann, H., and Steinhauser, C. (2003). Segregated expression of AMPA-type glutamate receptors and glutamate transporters defines distinct astrocyte populations in the mouse hippocampus. J Neurosci *23*, 1750-1758.

Matyash, V., and Kettenmann, H. (2010). Heterogeneity in astrocyte morphology and physiology. Brain Res Rev *63*, 2-10.

Matyushkin, D.P., Krivoi, II, and Drabkina, T.M. (1995). Synaptic feed-backs mediated by potassium ions. Gen Physiol Biophys *14*, 369-381.

Mayer, M.L., and Westbrook, G.L. (1987). Permeation and block of N-methyl-D-aspartic acid receptor channels by divalent cations in mouse cultured central neurones. J Physiol *394*, 501-527.

Mayer, M.L., Westbrook, G.L., and Guthrie, P.B. (1984). Voltage-dependent block by Mg2+ of NMDA responses in spinal cord neurones. Nature *309*, 261-263.

McGuinness, L., Taylor, C., Taylor, R.D., Yau, C., Langenhan, T., Hart, M.L., Christian, H., Tynan, P.W., Donnelly, P., and Emptage, N.J. (2010). Presynaptic NMDARs in the hippocampus

facilitate transmitter release at theta frequency. Neuron *68*, 1109-1127.

McHugh, T.J., Blum, K.I., Tsien, J.Z., Tonegawa, S., and Wilson, M.A. (1996). Impaired hippocampal representation of space in CA1-specific NMDAR1 knockout mice. Cell *87*, 1339-1349.

McLaren, M.J., Inana, G., and Li, C.Y. (1993). Double fluorescent vital assay of phagocytosis by cultured retinal pigment epithelial cells. Invest Ophthalmol Vis Sci *34*, 317-326.

McNay, E.C., Fries, T.M., and Gold, P.E. (2000). Decreases in rat extracellular hippocampal glucose concentration associated with cognitive demand during a spatial task. Proc Natl Acad Sci U S A *97*, 2881-2885.

Meeks, J.P., and Mennerick, S. (2004). Selective effects of potassium elevations on glutamate signaling and action potential conduction in hippocampus. J Neurosci *24*, 197-206.

Meeks, J.P., and Mennerick, S. (2007). Astrocyte membrane responses and potassium accumulation during neuronal activity. Hippocampus *17*, 1100-1108.

Meguro, R., Ohishi, H., Hoshino, K., Hicks, T.P., and Norita, M. (1999). Metabotropic glutamate receptor 2/3 immunoreactivity in the developing rat cerebellar cortex. J Comp Neurol *410*, 243-255.

Mennerick, S., Shen, W., Xu, W., Benz, A., Tanaka, K., Shimamoto, K., Isenberg, K.E., Krause, J.E., and Zorumski, C.F. (1999). Substrate turnover by transporters curtails synaptic glutamate transients. J Neurosci *19*, 9242-9251.

Miller, R.F., Fagerson, M.H., Staff, N.P., Wolfe, R., Doerr, T., Gottesman, J., Sikora, M.A., and Schuneman, R. (2001). Structure and functional connections of presynaptic terminals in the vertebrate retina revealed by activity-dependent dyes and confocal microscopy. J Comp Neurol *437*, 129-155.

Minelli, A., Barbaresi, P., Reimer, R.J., Edwards, R.H., and Conti, F. (2001). The glial glutamate transporter GLT-1 is localized both in the vicinity of and at distance from axon terminals in the rat cerebral cortex. Neuroscience *108*, 51-59.

Mistry, D.K., and Hablitz, J.J. (1990). Nystatin-perforated patch recordings disclose NMDA-induced outward currents in cultured neocortical neurons. Brain Res *535*, 318-322.

Moody, W.J., Futamachi, K.J., and Prince, D.A. (1974). Extracellular potassium activity during epileptogenesis. Exp Neurol *42*, 248-263.

Moreno, A.P., Saez, J.C., Fishman, G.I., and Spray, D.C. (1994). Human connexin43 gap junction channels. Regulation of unitary conductances by phosphorylation. Circ Res *74*, 1050-1057.

Mori, H., and Mishina, M. (1995). Structure and function of the NMDA receptor channel.

Neuropharmacology *34*, 1219-1237.

Nagy, J.I., and Li, W.E. (2000). A brain slice model for in vitro analyses of astrocytic gap junction and connexin43 regulation: actions of ischemia, glutamate and elevated potassium. Eur J Neurosci *12*, 4567-4572.

Nakanishi, S., and Masu, M. (1994). Molecular diversity and functions of glutamate receptors. Annu Rev Biophys Biomol Struct *23*, 319-348.

Nakazawa, K., McHugh, T.J., Wilson, M.A., and Tonegawa, S. (2004). NMDA receptors, place cells and hippocampal spatial memory. Nat Rev Neurosci *5*, 361-372.

Nedergaard, M., Ransom, B., and Goldman, S.A. (2003). New roles for astrocytes: redefining the functional architecture of the brain. Trends Neurosci *26*, 523-530.

Neher, E., and Augustine, G.J. (1992). Calcium gradients and buffers in bovine chromaffin cells. J Physiol *450*, 273-301.

Neves, G., Cooke, S.F., and Bliss, T.V. (2008). Synaptic plasticity, memory and the hippocampus: a neural network approach to causality. Nat Rev Neurosci *9*, 65-75.

Nevian, T., and Sakmann, B. (2004). Single spine Ca2+ signals evoked by coincident EPSPs and backpropagating action potentials in spiny stellate cells of layer 4 in the juvenile rat somatosensory barrel cortex. J Neurosci *24*, 1689-1699.

Nevian, T., and Sakmann, B. (2006). Spine Ca2+ signaling in spike-timing-dependent plasticity. J Neurosci *26*, 11001-11013.

Newman, E.A. (1986). Regional specialization of the membrane of retinal glial cells and its importance to K+ spatial buffering. Ann N Y Acad Sci *481*, 273-286.

Newman, E.A. (1993). Inward-rectifying potassium channels in retinal glial (Muller) cells. J Neurosci *13*, 3333-3345.

Ngo-Anh, T.J., Bloodgood, B.L., Lin, M., Sabatini, B.L., Maylie, J., and Adelman, J.P. (2005). SK channels and NMDA receptors form a Ca2+-mediated feedback loop in dendritic spines. Nat Neurosci *8*, 642-649.

Nicholls, J., and Wallace, B.G. (1978). Modulation of transmission at an inhibitory synapse in the central nervous system of the leech. J Physiol *281*, 157-170.

Nicholson, C. (1980). Dynamics of the brain cell microenvironment. Neurosci Res Program Bull *18*, 175-322.

Nimmerjahn, A., Kirchhoff, F., Kerr, J.N., and Helmchen, F. (2004). Sulforhodamine 101 as a specific marker of astroglia in the neocortex in vivo. Nat Methods *1*, 31-37.

Nishi, M., Hinds, H., Lu, H.P., Kawata, M., and Hayashi, Y. (2001). Motoneuron-specific expression of NR3B, a novel NMDA-type glutamate receptor subunit that works in a dominant-negative manner. J Neurosci *21*, RC185.

Nolte, C., Matyash, M., Pivneva, T., Schipke, C.G., Ohlemeyer, C., Hanisch, U.K., Kirchhoff, F., and Kettenmann, H. (2001). GFAP promoter-controlled EGFP-expressing transgenic mice: a tool to visualize astrocytes and astrogliosis in living brain tissue. Glia *33*, 72-86.

Nowak, L., Bregestovski, P., Ascher, P., Herbet, A., and Prochiantz, A. (1984). Magnesium gates glutamate-activated channels in mouse central neurones. Nature *307*, 462-465.

Ogata, K., and Kosaka, T. (2002). Structural and quantitative analysis of astrocytes in the mouse hippocampus. Neuroscience *113*, 221-233.

Oliet, S.H., Piet, R., and Poulain, D.A. (2001). Control of glutamate clearance and synaptic efficacy by glial coverage of neurons. Science *292*, 923-926.

Olsen, M.L., Higashimori, H., Campbell, S.L., Hablitz, J.J., and Sontheimer, H. (2006). Functional expression of Kir4.1 channels in spinal cord astrocytes. Glia *53*, 516-528.

Orkand, R.K., Nicholls, J.G., and Kuffler, S.W. (1966). Effect of nerve impulses on the membrane potential of glial cells in the central nervous system of amphibia. J Neurophysiol *29*, 788-806.

Otis, T.S., and Kavanaugh, M.P. (2000). Isolation of current components and partial reaction cycles in the glial glutamate transporter EAAT2. J Neurosci *20*, 2749-2757.

Otmakhova, N.A., Otmakhov, N., and Lisman, J.E. (2002). Pathway-specific properties of AMPA and NMDA-mediated transmission in CA1 hippocampal pyramidal cells. J Neurosci *22*, 1199-1207.

Ozawa, S., Kamiya, H., and Tsuzuki, K. (1998). Glutamate receptors in the mammalian central nervous system. Prog Neurobiol *54*, 581-618.

Palacin, M., Estevez, R., Bertran, J., and Zorzano, A. (1998). Molecular biology of mammalian plasma membrane amino acid transporters. Physiol Rev *78*, 969-1054.

Palmer, L.M., and Stuart, G.J. (2006). Site of action potential initiation in layer 5 pyramidal neurons. J Neurosci *26*, 1854-1863.

Pappas, C.A., and Ransom, B.R. (1994). Depolarization-induced alkalinization (DIA) in rat hippocampal astrocytes. J Neurophysiol *72*, 2816-2826.

Paquet, M., and Smith, Y. (2000). Presynaptic NMDA receptor subunit immunoreactivity in GABAergic terminals in rat brain. J Comp Neurol *423*, 330-347.

Pelkey, K.A., Topolnik, L., Lacaille, J.C., and McBain, C.J. (2006). Compartmentalized Ca(2+)

channel regulation at divergent mossy-fiber release sites underlies target cell-dependent plasticity. Neuron *52*, 497-510.

Pellerin, L., and Magistretti, P.J. (1994). Glutamate uptake into astrocytes stimulates aerobic glycolysis: a mechanism coupling neuronal activity to glucose utilization. Proc Natl Acad Sci U S A *91*, 10625-10629.

Perea, G., and Araque, A. (2007). Astrocytes potentiate transmitter release at single hippocampal synapses. Science *317*, 1083-1086.

Perea, G., Navarrete, M., and Araque, A. (2009). Tripartite synapses: astrocytes process and control synaptic information. Trends Neurosci *32*, 421-431.

Perez-Otano, I., Schulteis, C.T., Contractor, A., Lipton, S.A., Trimmer, J.S., Sucher, N.J., and Heinemann, S.F. (2001). Assembly with the NR1 subunit is required for surface expression of NR3A-containing NMDA receptors. J Neurosci *21*, 1228-1237.

Petralia, R.S., Wang, Y.X., Hua, F., Yi, Z., Zhou, A., Ge, L., Stephenson, F.A., and Wenthold, R.J. (2010). Organization of NMDA receptors at extrasynaptic locations. Neuroscience *167*, 68-87.

Picker, S., Pieper, C.F., and Goldring, S. (1981). Glial membrane potentials and their relationship to [K+]o in man and guinea pig. A comparative study of intracellularly marked normal, reactive, and neoplastic glia. J Neurosurg *55*, 347-363.

Platt, B., and Withington, D.J. (1997). Paired-pulse depression in the superficial layers of the guinea-pig superior colliculus. Brain Res *777*, 131-139.

Polsky, A., Mel, B., and Schiller, J. (2009). Encoding and decoding bursts by NMDA spikes in basal dendrites of layer 5 pyramidal neurons. J Neurosci *29*, 11891-11903.

Polsky, A., Mel, B.W., and Schiller, J. (2004). Computational subunits in thin dendrites of pyramidal cells. Nat Neurosci *7*, 621-627.

Pongs, O. (2008). Regulation of excitability by potassium channels. Results Probl Cell Differ *44*, 145-161.

Poolos, N.P., and Kocsis, J.D. (1990). Elevated extracellular potassium concentration enhances synaptic activation of N-methyl-D-aspartate receptors in hippocampus. Brain Res *508*, 7-12.

Poolos, N.P., Mauk, M.D., and Kocsis, J.D. (1987). Activity-evoked increases in extracellular potassium modulate presynaptic excitability in the CA1 region of the hippocampus. J Neurophysiol *58*, 404-416.

Poopalasundaram, S., Knott, C., Shamotienko, O.G., Foran, P.G., Dolly, J.O., Ghiani, C.A., Gallo, V., and Wilkin, G.P. (2000). Glial heterogeneity in expression of the inwardly rectifying K(+) channel, Kir4.1, in adult rat CNS. Glia *30*, 362-372.

Pyle, J.L., Kavalali, E.T., Choi, S., and Tsien, R.W. (1999). Visualization of synaptic activity in hippocampal slices with FM1-43 enabled by fluorescence quenching. Neuron *24*, 803-808.

Qian, A., Antonov, S.M., and Johnson, J.W. (2002). Modulation by permeant ions of Mg(2+) inhibition of NMDA-activated whole-cell currents in rat cortical neurons. J Physiol *538*, 65-77.

Qiu, C., Johnson, B.N., and Tallent, M.K. (2007). K+ M-current regulates the transition to seizures in immature and adult hippocampus. Epilepsia *48*, 2047-2058.

Rabinowitch, I., and Segev, I. (2006). The interplay between homeostatic synaptic plasticity and functional dendritic compartments. J Neurophysiol *96*, 276-283.

Racca, C., Stephenson, F.A., Streit, P., Roberts, J.D., and Somogyi, P. (2000). NMDA receptor content of synapses in stratum radiatum of the hippocampal CA1 area. J Neurosci *20*, 2512-2522.

Ransom, C.B., and Sontheimer, H. (1995). Biophysical and pharmacological characterization of inwardly rectifying K+ currents in rat spinal cord astrocytes. J Neurophysiol *73*, 333-346.

Reichenbach, A., Siegel, A., Rickmann, M., Wolff, J.R., Noone, D., and Robinson, S.R. (1995). Distribution of Bergmann glial somata and processes: implications for function. J Hirnforsch *36*, 509-517.

Rhodes, P. (2006). The properties and implications of NMDA spikes in neocortical pyramidal cells. J Neurosci *26*, 6704-6715.

Rosen, A.S., and Morris, M.E. (1991). Depolarizing effects of anoxia on pyramidal cells of rat neocortex. Neurosci Lett *124*, 169-173.

Rosenmund, C., Feltz, A., and Westbrook, G.L. (1995). Synaptic NMDA receptor channels have a low open probability. J Neurosci *15*, 2788-2795.

Rothstein, J.D., Dykes-Hoberg, M., Pardo, C.A., Bristol, L.A., Jin, L., Kuncl, R.W., Kanai, Y., Hediger, M.A., Wang, Y., Schielke, J.P., *et al.* (1996). Knockout of glutamate transporters reveals a major role for astroglial transport in excitotoxicity and clearance of glutamate. Neuron *16*, 675-686.

Rudy, B., and McBain, C.J. (2001). Kv3 channels: voltage-gated K+ channels designed for high-frequency repetitive firing. Trends Neurosci *24*, 517-526.

Rutecki, P.A., Lebeda, F.J., and Johnston, D. (1985). Epileptiform activity induced by changes in extracellular potassium in hippocampus. J Neurophysiol *54*, 1363-1374.

Sabatini, B.L., Oertner, T.G., and Svoboda, K. (2002). The life cycle of Ca(2+) ions in dendritic spines. Neuron *33*, 439-452.

Saez, J.C., Nairn, A.C., Czernik, A.J., Fishman, G.I., Spray, D.C., and Hertzberg, E.L. (1997). Phosphorylation of connexin43 and the regulation of neonatal rat cardiac myocyte gap junctions.

J Mol Cell Cardiol *29*, 2131-2145.

Samson, R.D., and Pare, D. (2005). Activity-dependent synaptic plasticity in the central nucleus of the amygdala. J Neurosci *25*, 1847-1855.

Sandhiya, S., and Dkhar, S.A. (2009). Potassium channels in health, disease & development of channel modulators. Indian J Med Res *129*, 223-232.

Schell, M.J., Brady, R.O., Jr., Molliver, M.E., and Snyder, S.H. (1997). D-serine as a neuromodulator: regional and developmental localizations in rat brain glia resemble NMDA receptors. J Neurosci *17*, 1604-1615.

Schneggenburger, R., and Neher, E. (2000). Intracellular calcium dependence of transmitter release rates at a fast central synapse. Nature *406*, 889-893.

Schousboe, A., Westergaard, N., Sonnewald, U., Petersen, S.B., Yu, A.C., and Hertz, L. (1992). Regulatory role of astrocytes for neuronal biosynthesis and homeostasis of glutamate and GABA. Prog Brain Res *94*, 199-211.

Schumacher, M.A., Rivard, A.F., Bachinger, H.P., and Adelman, J.P. (2001). Structure of the gating domain of a Ca2+-activated K+ channel complexed with Ca2+/calmodulin. Nature *410*, 1120-1124.

Scimemi, A., Tian, H., and Diamond, J.S. (2009). Neuronal transporters regulate glutamate clearance, NMDA receptor activation, and synaptic plasticity in the hippocampus. J Neurosci *29*, 14581-14595.

Shah, M.M., and Haylett, D.G. (2002). K+ currents generated by NMDA receptor activation in rat hippocampal pyramidal neurons. J Neurophysiol *87*, 2983-2989.

Sheng, M. (2001). The postsynaptic NMDA-receptor--PSD-95 signaling complex in excitatory synapses of the brain. J Cell Sci *114*, 1251.

Sheng, M., and Kim, M.J. (2002). Postsynaptic signaling and plasticity mechanisms. Science *298*, 776-780.

Sheng, M., Liao, Y.J., Jan, Y.N., and Jan, L.Y. (1993). Presynaptic A-current based on heteromultimeric K+ channels detected in vivo. Nature *365*, 72-75.

Sheng, M., Tsaur, M.L., Jan, Y.N., and Jan, L.Y. (1992). Subcellular segregation of two A-type K+ channel proteins in rat central neurons. Neuron *9*, 271-284.

Shepherd, G.M., and Harris, K.M. (1998). Three-dimensional structure and composition of CA3-->CA1 axons in rat hippocampal slices: implications for presynaptic connectivity and compartmentalization. J Neurosci *18*, 8300-8310.

Shigetomi, E., Bowser, D.N., Sofroniew, M.V., and Khakh, B.S. (2008). Two forms of astrocyte

calcium excitability have distinct effects on NMDA receptor-mediated slow inward currents in pyramidal neurons. J Neurosci *28*, 6659-6663.

Sik, A., Tamamaki, N., and Freund, T.F. (1993). Complete axon arborization of a single CA3 pyramidal cell in the rat hippocampus, and its relationship with postsynaptic parvalbumin-containing interneurons. Eur J Neurosci *5*, 1719-1728.

Silver, I.A., and Erecinska, M. (1994). Extracellular glucose concentration in mammalian brain: continuous monitoring of changes during increased neuronal activity and upon limitation in oxygen supply in normo-, hypo-, and hyperglycemic animals. J Neurosci *14*, 5068-5076.

Singer, W., and Lux, H.D. (1973). Presynaptic depolarization and extracellular potassium in the cat lateral geniculate nucleus. Brain Res *64*, 17-33.

Sjostrom, P.J., and Hausser, M. (2006). A cooperative switch determines the sign of synaptic plasticity in distal dendrites of neocortical pyramidal neurons. Neuron *51*, 227-238.

Sjostrom, P.J., and Nelson, S.B. (2002). Spike timing, calcium signals and synaptic plasticity. Curr Opin Neurobiol *12*, 305-314.

Skopinskaia, S.N., Iarkov, S.P., Khramov, E.N., and Zlobin, V.N. (2000). [Sulforodamine 101: novel effective marker in liposomal immunoassay]. Vestn Ross Akad Med Nauk, 19-24.

Skov, J., Andreasen, M., Hablitz, J.J., and Nedergaard, S. (2011). Baclofen and adenosine inhibition of synaptic transmission at CA3-CA1 synapses display differential sensitivity to K+ channel blockade. Cell Mol Neurobiol *31*, 587-596.

Smirnov, S., Paalasmaa, P., Uusisaari, M., Voipio, J., and Kaila, K. (1999). Pharmacological isolation of the synaptic and nonsynaptic components of the GABA-mediated biphasic response in rat CA1 hippocampal pyramidal cells. J Neurosci *19*, 9252-9260.

Somjen, G.G. (1979). Extracellular potassium in the mammalian central nervous system. Annu Rev Physiol *41*, 159-177.

Somjen, G.G. (2001). Mechanisms of spreading depression and hypoxic spreading depression-like depolarization. Physiol Rev *81*, 1065-1096.

Somjen, G.G. (2002). Ion regulation in the brain: implications for pathophysiology. Neuroscientist *8*, 254-267.

Somjen, G.G., Aitken, P.G., Czeh, G.L., Herreras, O., Jing, J., and Young, J.N. (1992). Mechanism of spreading depression: a review of recent findings and a hypothesis. Can J Physiol Pharmacol *70 Suppl*, S248-254.

Sorra, K.E., and Harris, K.M. (1993). Occurrence and three-dimensional structure of multiple synapses between individual radiatum axons and their target pyramidal cells in hippocampal area CA1. J Neurosci *13*, 3736-3748.

Spruston, N., Jonas, P., and Sakmann, B. (1995). Dendritic glutamate receptor channels in rat hippocampal CA3 and CA1 pyramidal neurons. J Physiol *482 (Pt 2)*, 325-352.

Stackman, R.W., Hammond, R.S., Linardatos, E., Gerlach, A., Maylie, J., Adelman, J.P., and Tzounopoulos, T. (2002). Small conductance Ca2+-activated K+ channels modulate synaptic plasticity and memory encoding. J Neurosci *22*, 10163-10171.

Steinhauser, C., Berger, T., Frotscher, M., and Kettenmann, H. (1992). Heterogeneity in the Membrane Current Pattern of Identified Glial Cells in the Hippocampal Slice. Eur J Neurosci *4*, 472-484.

Stern, P., Edwards, F.A., and Sakmann, B. (1992). Fast and slow components of unitary EPSCs on stellate cells elicited by focal stimulation in slices of rat visual cortex. J Physiol *449*, 247-278.

Stibitz, G.R. (1969). Calculating diffusion in biological systems by random walks with special reference to gases diffusion in the lung. Respir Physiol *7*, 230-262.

Stuart, G., Schiller, J., and Sakmann, B. (1997). Action potential initiation and propagation in rat neocortical pyramidal neurons. J Physiol *505 (Pt 3)*, 617-632.

Stuart, G.J., and Hausser, M. (2001). Dendritic coincidence detection of EPSPs and action potentials. Nat Neurosci *4*, 63-71.

Sutton, M.A., Ito, H.T., Cressy, P., Kempf, C., Woo, J.C., and Schuman, E.M. (2006). Miniature neurotransmission stabilizes synaptic function via tonic suppression of local dendritic protein synthesis. Cell *125*, 785-799.

Suzuki, S.S., and Smith, G.K. (1985). Single-cell activity and synchronous bursting in the rat hippocampus during waking behavior and sleep. Exp Neurol *89*, 71-89.

Svoboda, K., and Yasuda, R. (2006). Principles of two-photon excitation microscopy and its applications to neuroscience. Neuron *50*, 823-839.

Tamas, G., Szabadics, J., and Somogyi, P. (2002). Cell type- and subcellular position-dependent summation of unitary postsynaptic potentials in neocortical neurons. J Neurosci *22*, 740-747.

Tanaka, K., Watase, K., Manabe, T., Yamada, K., Watanabe, M., Takahashi, K., Iwama, H., Nishikawa, T., Ichihara, N., Kikuchi, T., *et al.* (1997). Epilepsy and exacerbation of brain injury in mice lacking the glutamate transporter GLT-1. Science *276*, 1699-1702.

Tang, X., Taniguchi, K., and Kofuji, P. (2009). Heterogeneity of Kir4.1 channel expression in glia revealed by mouse transgenesis. Glia *57*, 1706-1715.

Thompson, C.L., Drewery, D.L., Atkins, H.D., Stephenson, F.A., and Chazot, P.L. (2002). Immunohistochemical localization of N-methyl-D-aspartate receptor subunits in the adult murine hippocampal formation: evidence for a unique role of the NR2D subunit. Brain Res Mol Brain Res *102*, 55-61.

Tong, G., and Jahr, C.E. (1994). Block of glutamate transporters potentiates postsynaptic excitation. Neuron *13*, 1195-1203.

Torres, G.E., and Amara, S.G. (2007). Glutamate and monoamine transporters: new visions of form and function. Curr Opin Neurobiol *17*, 304-312.

Tovar, K.R., and Westbrook, G.L. (1999). The incorporation of NMDA receptors with a distinct subunit composition at nascent hippocampal synapses in vitro. J Neurosci *19*, 4180-4188.

Triller, A., and Korn, H. (1982). Transmission at a central inhibitory synapse. III. Ultrastructure of physiologically identified and stained terminals. J Neurophysiol *48*, 708-736.

Tsien, J.Z., Huerta, P.T., and Tonegawa, S. (1996). The essential role of hippocampal CA1 NMDA receptor-dependent synaptic plasticity in spatial memory. Cell *87*, 1327-1338.

Tsien, R.Y. (1981). A non-disruptive technique for loading calcium buffers and indicators into cells. Nature *290*, 527-528.

Turecek, R., and Trussell, L.O. (2000). Control of synaptic depression by glutamate transporters. J Neurosci *20*, 2054-2063.

Tzounopoulos, T., and Stackman, R. (2003). Enhancing synaptic plasticity and memory: a role for small-conductance Ca(2+)-activated K+ channels. Neuroscientist *9*, 434-439.

VanderMeulen, D.L., Misra, P., Michael, J., Spears, K.G., and Khoka, M. (1992). Laser mediated release of dye from liposomes. Photochem Photobiol *56*, 325-332.

Vanhoutte, P., and Bading, H. (2003). Opposing roles of synaptic and extrasynaptic NMDA receptors in neuronal calcium signalling and BDNF gene regulation. Curr Opin Neurobiol *13*, 366-371.

Vargas-Caballero, M., and Robinson, H.P. (2003). A slow fraction of Mg2+ unblock of NMDA receptors limits their contribution to spike generation in cortical pyramidal neurons. J Neurophysiol *89*, 2778-2783.

Veh, R.W., Lichtinghagen, R., Sewing, S., Wunder, F., Grumbach, I.M., and Pongs, O. (1995). Immunohistochemical localization of five members of the Kv1 channel subunits: contrasting subcellular locations and neuron-specific co-localizations in rat brain. Eur J Neurosci *7*, 2189-2205.

Ventura, R., and Harris, K.M. (1999). Three-dimensional relationships between hippocampal synapses and astrocytes. J Neurosci *19*, 6897-6906.

Vervaeke, K., Gu, N., Agdestein, C., Hu, H., and Storm, J.F. (2006). Kv7/KCNQ/M-channels in rat glutamatergic hippocampal axons and their role in regulation of excitability and transmitter release. J Physiol *576*, 235-256.

Voglis, G., and Tavernarakis, N. (2006). The role of synaptic ion channels in synaptic plasticity. EMBO Rep *7*, 1104-1110.

Wallraff, A., Kohling, R., Heinemann, U., Theis, M., Willecke, K., and Steinhauser, C. (2006). The impact of astrocytic gap junctional coupling on potassium buffering in the hippocampus. J Neurosci *26*, 5438-5447.

Wallraff, A., Odermatt, B., Willecke, K., and Steinhauser, C. (2004). Distinct types of astroglial cells in the hippocampus differ in gap junction coupling. Glia *48*, 36-43.

Walz, W. (2000). Controversy surrounding the existence of discrete functional classes of astrocytes in adult gray matter. Glia *31*, 95-103.

Wang, D.D., and Bordey, A. (2008). The astrocyte odyssey. Prog Neurobiol *86*, 342-367.

Wang, H., Kunkel, D.D., Martin, T.M., Schwartzkroin, P.A., and Tempel, B.L. (1993). Heteromultimeric K+ channels in terminal and juxtaparanodal regions of neurons. Nature *365*, 75-79.

Wang, H., Kunkel, D.D., Schwartzkroin, P.A., and Tempel, B.L. (1994). Localization of Kv1.1 and Kv1.2, two K channel proteins, to synaptic terminals, somata, and dendrites in the mouse brain. J Neurosci *14*, 4588-4599.

Wang, X., Lou, N., Xu, Q., Tian, G.F., Peng, W.G., Han, X., Kang, J., Takano, T., and Nedergaard, M. (2006). Astrocytic Ca2+ signaling evoked by sensory stimulation in vivo. Nat Neurosci *9*, 816-823.

Wang, Y.L., and Goren, M.B. (1987). Differential and sequential delivery of fluorescent lysosomal probes into phagosomes in mouse peritoneal macrophages. J Cell Biol *104*, 1749-1754.

Warn-Cramer, B.J., Lampe, P.D., Kurata, W.E., Kanemitsu, M.Y., Loo, L.W., Eckhart, W., and Lau, A.F. (1996). Characterization of the mitogen-activated protein kinase phosphorylation sites on the connexin-43 gap junction protein. J Biol Chem *271*, 3779-3786.

Watase, K., Hashimoto, K., Kano, M., Yamada, K., Watanabe, M., Inoue, Y., Okuyama, S., Sakagawa, T., Ogawa, S., Kawashima, N., *et al.* (1998). Motor discoordination and increased susceptibility to cerebellar injury in GLAST mutant mice. Eur J Neurosci *10*, 976-988.

Wilson, R.I., and Nicoll, R.A. (2001). Endogenous cannabinoids mediate retrograde signalling at hippocampal synapses. Nature *410*, 588-592.

Winship, I.R., Plaa, N., and Murphy, T.H. (2007). Rapid astrocyte calcium signals correlate with neuronal activity and onset of the hemodynamic response in vivo. J Neurosci *27*, 6268-6272.

Winterer, J., Stanton, P.K., and Muller, W. (2006). Direct monitoring of vesicular release and uptake in brain slices by multiphoton excitation of the styryl FM 1-43. Biotechniques *40*, 343-351.

Xia, X.M., Fakler, B., Rivard, A., Wayman, G., Johnson-Pais, T., Keen, J.E., Ishii, T., Hirschberg, B., Bond, C.T., Lutsenko, S., *et al.* (1998). Mechanism of calcium gating in small-conductance calcium-activated potassium channels. Nature *395*, 503-507.

Yaari, Y., Konnerth, A., and Heinemann, U. (1986). Nonsynaptic epileptogenesis in the mammalian hippocampus in vitro. II. Role of extracellular potassium. J Neurophysiol *56*, 424-438.

Yang, J., Woodhall, G.L., and Jones, R.S. (2006). Tonic facilitation of glutamate release by presynaptic NR2B-containing NMDA receptors is increased in the entorhinal cortex of chronically epileptic rats. J Neurosci *26*, 406-410.

Yang, Y.C., Lee, C.H., and Kuo, C.C. (2010). Ionic flow enhances low-affinity binding: a revised mechanistic view into Mg2+ block of NMDA receptors. J Physiol *588*, 633-650.

Yasuda, R., Nimchinsky, E.A., Scheuss, V., Pologruto, T.A., Oertner, T.G., Sabatini, B.L., and Svoboda, K. (2004). Imaging calcium concentration dynamics in small neuronal compartments. Sci STKE *2004*, pl5.

Yu, S.P., Yeh, C., Strasser, U., Tian, M., and Choi, D.W. (1999). NMDA receptor-mediated K+ efflux and neuronal apoptosis. Science *284*, 336-339.

Yuan, L.L., and Chen, X. (2006). Diversity of potassium channels in neuronal dendrites. Prog Neurobiol *78*, 374-389.

Yue, C., and Yaari, Y. (2006). Axo-somatic and apical dendritic Kv7/M channels differentially regulate the intrinsic excitability of adult rat CA1 pyramidal cells. J Neurophysiol *95*, 3480-3495.

Zhang, W., and Linden, D.J. (2003). The other side of the engram: experience-driven changes in neuronal intrinsic excitability. Nat Rev Neurosci *4*, 885-900.

Zhang, Y., and Barres, B.A. (2010). Astrocyte heterogeneity: an underappreciated topic in neurobiology. Curr Opin Neurobiol *20*, 588-594.

Zhou, M., and Kimelberg, H.K. (2001). Freshly isolated hippocampal CA1 astrocytes comprise two populations differing in glutamate transporter and AMPA receptor expression. J Neurosci *21*, 7901-7908.

Zhou, M., Schools, G.P., and Kimelberg, H.K. (2006). Development of GLAST(+) astrocytes and NG2(+) glia in rat hippocampus CA1: mature astrocytes are electrophysiologically passive. J Neurophysiol *95*, 134-143.

Zhu, Y., and Auerbach, A. (2001). K(+) occupancy of the N-methyl-d-aspartate receptor channel probed by Mg(2+) block. J Gen Physiol *117*, 287-298.

Zorumski, C.F., Yang, J., and Fischbach, G.D. (1989). Calcium-dependent, slow desensitization distinguishes different types of glutamate receptors. Cell Mol Neurobiol *9*, 95-104.

Zucker, R.S., and Regehr, W.G. (2002). Short-term synaptic plasticity. Annu Rev Physiol *64*, 355-405.

Zuckermann, E.C., and Glaser, G.H. (1968). Hippocampal epileptic activity induced by localized ventricular perfusion with high-potassium cerebrospinal fluid. Exp Neurol *20*, 87-110.